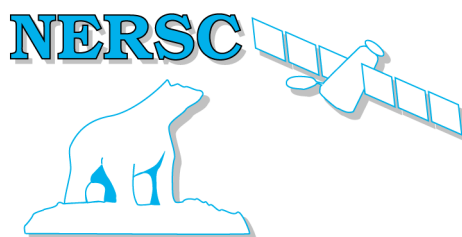


# Nansen Environmental and Remote Sensing Center

*A non-profit  
Research institute affiliated  
With the University of  
Bergen*



*Thormøhlensgate 47  
N-5006 Bergen,  
Norway  
<http://www.nersc.no>*

## NERSC Technical Report no. 270



## Sea Ice thickness Observation System

**Project funded by the European Community's Fifth Framework Programme under  
Environment and Sustainable Development**

**Key Action: Global Change, Climate and Biodiversity**

**Contract Number: EVK2-CT-2002-00146**







**Period: 01 December 2002 – 30 November 2005**

## Final Scientific Report

**February 2006**

### Partners:

Nansen Environmental and Remote Sensing Center (NERSC), Norway  
Alfred Wegener Institute for Polar and Marine Research (AWI), Germany  
Scottish Association for Marine Science (SAMS), UK  
University College London, Centre for Polar Observation and Modelling (CPOM), UK  
National Survey and Cadastre (KMS), Denmark  
Christian Michelsen Research A/S, Conmar (CMR), Norway

					
<b>Nansen Environmental and Remote Sensing Center,</b> Thormøhlensgt 47, 5006 Bergen, Norway Tel: +47 55205800, Fax: +47 55205801 <a href="http://www.nersc.no">http://www.nersc.no</a> Stein Sandven e-mail: <a href="mailto:stein@nersc.no">stein@nersc.no</a>	<b>Alfred Wegener Institute for Polar and Marine Research</b> Bussestrasse 24 D-27570 Bremerhaven Germany T. 49-471-4831-1128, F.49-471-4831-1797 <a href="http://www.awi-bremerhaven.de">http://www.awi-bremerhaven.de</a> Christian Haas. E-mail: <a href="mailto:chaas@awi-bremerhaven.de">chaas@awi-bremerhaven.de</a>	<b>Scottish Association for Marine Science</b> Dunstaffnage Marine Laboratory Dunbeg, Argyll, PA37 1QA, UK Tel. 44 1631 559215, Fax 44 1631 559001 <a href="http://www.sams.ac.uk">http://www.sams.ac.uk</a> Peter Wadhams, e-mail: <a href="mailto:pw11@cam.ac.uk">pw11@cam.ac.uk</a>	<b>University College London,</b> Centre for Polar Observation and Modelling, Pearson Building, Gower St., London WC1H 6BT, UK tel :+44 2076 793932 fax: +44 2076 797883 <a href="http://www.cpom.ucl.ac.uk">http://www.cpom.ucl.ac.uk</a> Seymour Laxon, e-mail: <a href="mailto:swl@cpom.ucl.ac.uk">swl@cpom.ucl.ac.uk</a>	<b>KMS (National Survey and Cadastre)</b> Geodynamics Dept., Rentemestervej 8, DK-2400 Copenhagen NV Denmark T. +45-3587-5319, F +45-3587-5052, <a href="http://www.kms.dk">http://www.kms.dk</a> Rene Forsberg E-mail: <a href="mailto:rf@kms.dk">rf@kms.dk</a>	<b>Christian Michelsen Research A/S</b> Conmar N-5892 Bergen Norway Tel 47 5557 4040 Fax 47 5557 4041 <a href="http://www.cmr.no/">http://www.cmr.no/</a> conmar David Peddie e-mail: <a href="mailto:davidp@cmr.no">davidp@cmr.no</a> ,

<b>TITLE:</b> <b>Sea Ice thickness Observation System BSITHOS</b>	<b>REPORT IDENTIFICATION</b>  <b>Final Scientific Report</b>  <b>NERSC Technical Report no. 270</b>
<b>CLIENT</b>  EU DG Environment  Environment and Sustainable Development Programme	<b>CONTRACT</b>  Contract Number: EVK2-CT-2002-00146
<b>CLIENT REFERENCE</b>  Riccardo Casale	<b>AVAILABILITY</b>  Open
<b>INVESTIGATORS</b> (in alphabetic order) Vitaly Alexandrov, NIERSC Martin Doble, SAMS Rene Forsberg, KMS Katherine Giles, UCL Christian Haas, AWI Kjell Kloster, NERSC Seymour Laxon, UCL Jan Lieser, AWI Tor Olaussen, NERSC David Peddie, CMR Andy Ridout, UCL Hanne Sagen, NERSC Stein Sandven, NERSC (co-ordinator) Peter Wadhams, SAMS Jeremy Wilkinson, SAMS	<b>AUTHORISATION</b>  Bergen, 27 February 2006  Stein Sandven



## Contents

<b>EXECUTIVE SUMMARY .....</b>	<b>3</b>
<b>1. INTRODUCTION .....</b>	<b>6</b>
1.1 RATIONALE AND BACKGROUND.....	6
1.2 OVERVIEW OF THE FIELD EXPERIMENTS AND MEASUREMENT TECHNIQUE.....	8
<b>2. REQUIREMENTS AND FIELD WORK PLANNING.....</b>	<b>8</b>
<b>3. RESULTS FROM THE POLARSTERN EXPEDITIONS ARK19 &amp; 20.....</b>	<b>10</b>
3.1 INTRODUCTION .....	10
3.2 SEA ICE THICKNESS ANALYSIS TOOLS BASED ON EM MEASUREMENTS .....	10
3.2.1 Helicopter-borne EM thickness sounding.....	11
3.2.2 Laser profiling of surface roughness and ridge distributions .....	12
3.2.3 Surface elevation measurements using laser altimetry and DGPS.....	14
3.3 MEASUREMENT CAMPAIGNS .....	16
3.3.1 Ark 19: March/April 2003.....	16
3.3.2 Ark 20: August 2004 - Ice thickness in the Transpolar Drift, 1991-2004.....	17
<b>4. RESULTS OF BUOY MEASUREMENTS .....</b>	<b>19</b>
4.1 INTRODUCTION TO WAVE MEASUREMENTS IN ICE .....	19
4.2 THE AIS SYSTEM DEVELOPED BY SAMS.....	20
4.3 THE AIS DEVELOPED BY CMR AND NERSC .....	22
4.4 EXPERIMENTS IN 2003.....	23
4.5 RESULTS FROM THE FRAM STRAIT EXPERIMENTS.....	26
4.6 CONSTRUCTION OF THE SITHOS I AUTONOMOUS WAVE BUOY .....	26
4.7 SITHOS I DEPLOYMENT AND DATA ACQUISITION.....	27
4.8 PRELIMINARY CONCLUSION ON THE SITHOS I BUOY.....	29
<b>5. RESULTS FROM AIRCRAFT SURVEYS .....</b>	<b>30</b>
5.1 OVERVIEW OF THE FIELD EXPERIMENTS.....	30
5.2 METHOD DESCRIPTION .....	31
5.3 RESULTS FROM THE LASER SCANNER SURVEYS .....	32
5.3.1 Laser scanning thickness images.....	32
5.3.2 Comparison of laser scanner and ICESat observations .....	33
5.3.3 Comparison of laser scanner and HEM observations .....	35
5.3.4 Discussion of results.....	36
<b>6. RESULTS FROM ULS MEASUREMENTS.....</b>	<b>37</b>
6.1 THE SUBMARINE MISSION IN APRIL 2004 .....	37
6.2 AUTONOMOUS UNDERWATER VEHICLES.....	39
6.2.1 The Vehicle.....	39
6.2.2 The surveys.....	40
6.2.3 Data .....	41
6.2.4 Conclusions.....	43
<b>7. RESULTS FROM RADAR ALTIMETER MEASUREMENTS.....</b>	<b>43</b>
7.1 INTRODUCTION TO RADAR ALTIMETRY FOR ICE THICKNESS RETRIEVAL .....	43
7.2 DATA AVAILABILITY .....	44
7.3 METHOD DESCRIPTION .....	44
7.4 VALIDATION WITH IN SITU DATA .....	46
7.5. DISCRIMINATION CHECKING WITH ATSR IMAGES .....	47
7.6. DISCUSSION OF THE RESULTS.....	49
7.7 CONCLUDING REMARKS .....	53

---

<b>8. RESULTS FROM ICE MODELLING.....</b>	<b>54</b>
8.1 INTRODUCTION .....	54
8.2 ICE MODELS AT NERSC .....	54
8.3 ICE THICKNESS VARIABILITY FROM THE NORTH ATLANTIC MODEL .....	55
8.4 COMPARISON BETWEEN MODELED AND OBSERVED ICE THICKNESS .....	56
8.5 COMPARISON WITH AIRBORNE LASER DATA NORTH OF GREENLAND .....	60
8.6 AWI SEA ICE MODEL WITH FAST ICE PARAMETERIZATION .....	62
8.7. MODELLING OF SEA ICE RIDGING.....	63
8.8 FINITE ELEMENT MODEL.....	66
8.9 CONCLUSION ON THE MODELLING WORK .....	68
<b>9. SYNTHESIS OF RESULTS AND CONCLUSIONS.....</b>	<b>69</b>
9.1 LOCAL AND REGIONAL SCALE.....	69
9.2 LARGE SCALE.....	69
9.3 OVERALL RESULTS OF THE THICKNESS MEASUREMENTS.....	70
9.4 BASIC PHYSICAL MEASUREMENTS OF SNOW AND ICE .....	70
9.5 FURTHER WORK .....	71
<b>10. REFERENCES.....</b>	<b>72</b>

## Executive Summary

The focus of the SITHOS project has been to develop and test new observing systems for sea ice thickness and related parameters for climate change detection, support to sea transport, offshore operations as well as environmental monitoring in polar regions. The project has collected and analysed new data sea ice sets from several field experiments, analyzed satellite altimeter data and conducted model simulations of sea ice in the Arctic. Sea-ice thickness is one of the most difficult ice parameters to measure, because it requires use of platforms which can operate in the ice environment. Today, most data have been gathered by upward-looking sonar measurements from military nuclear submarines. These data are normally released only years after they had been acquired, and with a poor geographic reference. Cruise tracks are designed for military interests, and not for scientific purposes. After the end of the cold war, even scientifically motivated cruises like the Scientific Ice Expeditions SCICEX will be performed only sporadically. Echo sounders deployed on oceanographic moorings can monitor ice thickness only at fixed locations. To obtain synoptic measurements of ice thickness is a real challenge, and several observing methods including use of satellites are required.

In the SITHOS project the following methods have been used:

- **use of electromagnetic induction** and laser (EM) mounted on helicopters which can operate up to 100 km from an icebreaker.
- **aircraft surveys with laser and GPS**. Scanning laser and GPS positioning can provide data on surface topography, freeboard and thickness from aircraft over distances from a few hundred to thousand km depending on type of aircraft (AL)
- **use of Upward Looking Sonars (from submarines and AUVs)** for mapping of ice draft along tracks (ULS)
- time series of ice thickness from **automatic ice stations** (AIS) deployed on ice floes in the interior of the Arctic
- **satellite altimeter** data providing regular data on ice freeboard and thickness averaged to typically 100 by 100 km grid cells
- **sea ice modelling** for comparison with the new data sets and validation of the modelled ice thickness and other sea ice parameters.

Use of electromagnetic induction (EM method) has become a well-established technique for measuring ice thickness. The method has been validated by in situ drilling during many field experiments before and during SITHOS. In SITHOS AWI has used a standalone system consisting of the EM device in combination with a laser, which is tailored to be operated from helicopters. Large data sets representative for certain ice regimes have been gathered. The comparison with in situ drilling shows very good agreement, except for the thickest ridges and ice keels, where the EM method tends to underestimate the thickness. In a series of field experiments from 1991 to 2004, AWI has found the mean modal ice thickness in the European sector of the Arctic to decrease from 2.5 m to about 2.0 m for the summer period. For the winter period there are not any repeated measurements of ice thickness by this method.

Aircraft laser scanning and GPS surveys (the AL method) have been conducted by KMS during several of the SITHOS experiments. The basic idea is to use kinematic GPS in combination with laser to map the surface of the ice at few cm accuracy over longer distances which includes variations of geoid and sea surface topography. The height difference between geoid and laser/GPS is sea-surface topography plus ice freeboard. Through the SITHOS flight campaigns it has been demonstrated that the airborne lidar measurements are an effective way to measure sea ice thickness and freeboard over large scales (100 to 1000 km). Comparison with simultaneous EM measurements shows that the mean ice thickness measurements from the laser data are within 10 – 20 % of the EM data over 100 km distances. The method requires input data on ice

and snow density in order to retrieve thickness from freeboard. In future sea ice observing systems it is recommended to use airborne scanning laser surveys, representing an important "bridging" of sea ice scales between locally based ground- and helicopter work and the large-scale coverage by satellites and occasional basin-wide surveys by submarines and icebreakers.

An interesting technique to derive spatially averaged ice thickness has been demonstrated using directional surface elastic-gravity wave measurements from Russian *North Pole* drifting stations. Measurements of ice surface oscillations were carried out regularly in the Eurasian Basin from 1972-91. The ice thickness obtained varied between 3.02 m and 2.8 m. In SITHOS two types of wave measurement buoys (Automatic Ice Station - AIS) have been developed and tested by SAMS and CMR/NERSC. The wave data collection is in progress and continues after the end of the SITHOS contract. The wave spectra derived from the buoys so far have been analysed, but retrieval of ice thickness has not yet been obtained. It is therefore too early to validate ice thickness retrieval by the wave method. The plan is to deploy a cluster of AIS 's which can measure wave spectra and retrieve ice thickness over the whole Arctic. This plan is included in the DAMOCLES project for 2006 – 2009.

Autonomous Underwater Vehicles (AUV) which are small unmanned submarines operated from a ship, have been developed in recent years as part of the offshore technology. In SITHOS one successful experiment was conducted in the Fram Strait where an AUV equipped with an upward-looking multibeam bathymetric mapping system measured ice draft along sections, each were a few tens km long. The system, which was called Autosub, operated highly successfully under sea ice, obtaining 458 km of high quality upward looking swath sonar data and accompanying oceanographic data. It undertook necessary avoidance manoeuvres for obstacles, and the acoustic homing system ensured that the vehicle could be returned with confidence to an area covered with loose moving pack ice. The combination of an unmanned under-ice vehicle and a multibeam sonar gives, literally, a new dimension to under-ice studies, and is important for work on ice thickness changes, the disappearance of deep ridges from the Arctic, navigability in ice, and many other studies critical to the role of ice in polar climate change.

It is hoped that this successful ice profiling mission will be a precursor to larger-scale missions with AUVs which will develop into a major monitoring effort for Arctic sea ice changes. Also ice thickness results from future AUV runs can be used to validate freeboard estimates from the satellite altimeters, in order to allow mean ice thickness to be estimated throughout the Arctic. The AUV has many advantages, notably the high resolution which is possible by sailing close to the ice bottom, a possibility which manned submarines cannot enjoy for safety reasons; and the possibility of a closely controlled tight or overlapping grid of imaging tracks. The main drawback of the present AUV is lack of range when compared to nuclear submarines.

Satellite radar altimetry has a potential to provide estimates of sea ice thickness for the whole Arctic area from direct measurement of ice freeboard. Preliminary results from the ERS radar altimeter show good agreement with in-situ submarine observations and reveal that Arctic ice thickness is highly variable and largely controlled by the length of the summer melt season [Laxon, et al., 2003]. Since September 2003 CPOM has been developing a processing system to extract sea ice thickness from Envisat altimetry data. The system can now produce ice freeboard and thickness maps within a short time after reception of the satellite data. The result of the work has been to produce monthly ice freeboard maps for the winter seasons 2002-03, 2003-04 and 2004-05. The freeboard data have been averaged to 1 deg latitude and 5 deg longitude cells. The maps show characteristic maximum freeboard in the Canadian archipelago where the thickest ice in the Arctic is found. The in situ data from the SITHOS field experiments have too small scale to be useful for validation of the altimeter maps. Other large-scale validation data for the altimeter results are not available.

The failure of the Cryosat launch in October 2005 has increased the importance of the Envisat altimeter for monitoring sea ice thickness, and work will continue to try to improve on the current results. One of the highest priorities is to improve the performance of the retracking algorithms.

The waveforms should be properly corrected for the antenna response to remove the bias in the observed floe elevations. The tracking of the sea surface in leads is believed to be working well, but work is planned on developing a retracker specifically designed for this purpose which could make use of a larger number of the specular returns than can currently be used. Hand in hand with this, further work is planned on more accurately separating leads from floes and data filtering by looking at satellite imagery. Finally, further validation with in situ data is highly desirable.

Sea ice modelling work have been conducted by NERSC and AWI to support the observational work from the field expeditions. The main purpose of demonstrating sea ice modeling results is to compare observed ice thickness by the different methods used in the other SITHOS tasks with modelled ice fields. The observations can be used to validate the model results, but the validation is of limited value when the observations are on a different scale compared to the models. The comparison can also be used to define scales of observations that are needed in the future for model validation. The AWI modeling activities show interesting results of ridge simulations and ice age simulations. This is complementary to the results provided by the NERSC models. The modelling systems are producing large-scale sea ice thickness fields which need to be validated on similar scales. This is a real challenge because most ice thickness measurements are obtained on regional and local scale. The large-scale observations by radar altimetry provide interesting data for comparison with large-scale model results. In this case the scale of observations matches the scale of the models. But the radar altimeter method needs further validation before it can be a useful tool for model validation. Another limitation is that sea ice models can only be expected to be as good as the atmospheric forcing fields and the ocean models coupled to the ice models. It is therefore important to provide improved atmospheric fields in the Arctic where the meteorological observation network is sparse.

The main achievements in SITHOS have been the field experiments where several methods of observing ice thickness have been successfully used to collect observations of ice thickness and related parameters. These methods have clearly complementary roles and should be used regularly in future observing systems. The main problem of most observing systems is that they cover local and regional scale, while for climate studies it is necessary to obtain data for the whole Arctic. Satellites has the capability to observe thickness on large scale and should be implemented as part of a global observing system with support from aircraft and in situ measurements.

# 1. Introduction

## 1.1 Rationale and background

Sea ice is an important component of the earth system and of geophysical and practical importance on global, regional and local scales. The most important aspects of the sea-ice cover are its: 1) Spatial coverage or extent, 2) Composition, in terms of ice types within the ice cover, 3) Drift and deformation, and 4) Thickness distribution. Except for the first aspect, the spatial-temporal variability of these key parameters is neither well quantified nor adequately understood.

Among the many apparent changes in the Arctic during the recent decades [e.g., *Serreze et al.*, 2000; *Moritz et al.*, 2002], sea-ice 'extent' (area within the ice–ocean margin) is the one parameter whose variability and trends are most firmly established. Several independent analyses [e.g., *Johannessen et al.*, 1995; *Bjørge et al.*, 1997; *Cavalieri et al.*, 1997; *Vinnikov et al.*, 1999] have led to the consensus that the annual sea-ice extent decreased ~3% per decade from the late 1970s to the late 1990s. Seasonal and monthly analyses have found the negative trends to be greatest in summer [*Chapman and Walsh*, 1993; *Maslanik et al.*, 1996; *Parkinson et al.*, 1999], as exemplified by the record-low summer ice minimum in September 2002 [*Serreze et al.*, 2003]. Furthermore, summer 2003, 2004 and 2005 showed consistent large negative ice anomaly, setting a new record for sea-ice 'area' (extent weighted by mean ice concentration), with unusually low ice concentration [*Stroeve et al.*, 2005].

*Serreze et al.*'s [2003] diagnostic study found that the 2002 record-low probably resulted from anomalous warmth and atmospheric circulation in spring and summer. However, neither the 2002 nor 2003 sea-ice anomaly appear to be strongly linked to the Arctic Oscillation (AO) / North Atlantic Oscillation (NAO), which in the current view is a primary driver of arctic sea-ice variability and trends [*Deser et al.*, 2000; *Dickson et al.*, 2000; *Rigor et al.*, 2003]. The AO/NAO index values in winter 2001/02 were only modestly positive, less than one standard deviation, while during winter 2002/03 they were strongly negative. *Serreze et al.* [2003, p. 1113] suggest that in order to explain such large negative ice anomalies during weakly positive and negative AO years, it may be necessary to invoke factors internal to the ice cover, e.g., "it is reasonable to expect that a general decrease in ice thickness accompanying warming would manifest itself as greater sensitivity of the ice pack to wind forcing and albedo feedbacks." The same line of reasoning was proposed more than a decade ago [*Walsh and Zwally*, 1990] and following the then-record summer ice minima in 1990, 1993 and 1995, when a NERSC research team suggested that a decrease in the amount of 'multi-year' (MY) ice – ice that has survived at least one summer melt – in the Arctic and attendant changes in the ice-thickness could in turn pre-condition the ice cover to further reductions in the subsequent summers.

Recent observational evidence appears to corroborate the predicted decreases in perennial ice area [*McPhee et al.*, 1998; *Johannessen et al.* 1999; *Comiso*, 2002; *Belchansky et al.*, 2005] and ice thickness [e.g., *Rothrock et al.* 1999; *Wadhams and Davis*, 2000]. However, there remain large uncertainties about these ice parameters, requiring advancements towards: 1) Accurate, error-constrained measurements and improved retrieval algorithms, e.g., regarding MY ice concentration, 2) Spatial and temporal sampling improvements and accurate satellite retrievals, regarding ice thickness, and 3) Seamless, reliable integration with new satellite sensor data in a sea-ice monitoring and analysis system. Each of these requires improved testing and validation with independent data, including *in situ* data from field experiments, such the newest Russian North Pole Drifting Station and expeditions with ice-going ships planned under the International Polar Year (IPY) programme in 2007–08.

The significance of the observed reductions in MY ice area [*Johannessen et al.*, 1999] in terms of the ice cover's mass balance could be quantitatively assessed if there were spatially- and



temporally-coincident data on the ice thickness distribution. Sea ice thickness is a key diagnostic parameter; however, its variability is poorly known, due largely to spatial-temporal sampling deficiencies in data from submarines carrying upward-looking sonar. According to the Rothrock *et al.*, [1999] analysis of data from the summers in the 1950s/1970s and the 1990s, the mean ice thickness decreased from 3.1 m to 1.8 m or a 40% reduction over 3-4 decades – if indeed representative. However, analyses of sonar data from different transects, years and seasons yield a wide range of estimates. The large variability inherent in the arctic system, coupled with the scarcity of data, renders the evaluation of ice thickness trends from sonar and *in situ* data an open question. A promising new technique to retrieve sea-ice thickness from satellite-borne altimeter data has been developed and tested on archival ERS-1/2 altimeter data, e.g., Laxon *et al.* [2003]. This technique is further explored in this project.

Sea ice thickness is a key parameter which is a real challenge to observe and there is an urgent need for improved measurement techniques. Results from global climate models indicate that global warming in the next decades will be most pronounced in the Arctic region, causing a net melting of the sea ice. Ice area and thickness are the two fundamental parameters for estimation of ice mass balance, which shows the response of sea to climate change. In addition to the climate aspect, sea ice thickness is also important to observe for practical operations such as ice navigation, sea transportation and offshore drilling. There are several measurement techniques for ice thickness, but few of them are developed into regular monitoring systems. The most important data for ice thickness in the Arctic are provided by US and British submarines through the SCICEX Programme (e.g. Rothrock *et al.*, 1999), however the future access to submarine data is expected to decline.

The European Space Agency is developing a new satellite, CRYOSAT, which will have sea ice thickness measurement as a main objective. CRYOSAT was launch in October 2005, but the launched failed. A CryoSat-2 will be built and launched by ESA in 2009. For sea ice the principle is to observe freeboard height and translate this to ice thickness. Specific studies on this problem are urgently needed to validate if basin-scale thickness distributions can be derived from freeboard data provided by CRYOSAT. In addition to satellite data, it is important to have robust and cost-effective *in situ* measurement systems to be operated from platforms such as drifting buoys, fixed-wing aircraft, helicopters and ice-going vessels. SITHOS will develop and test techniques which are feasible for use on automatic buoys, fixed-wing aircraft, helicopter and ice-going vessels. These systems will be important for acquisition of ice thickness data in the Arctic as well as the Antarctic. There are several user groups which need ice thickness data. The most important are:

- **polar climate research and monitoring programmes (CliC)**, new data on ice thickness can have significant contributions to these programmes
- **operational oceanography and met-ocean services**, sea ice measurements techniques are needed which can be implemented in regular monitoring and net-ocean forecasting for the Arctic Ocean and adjacent seas
- **climate modellers**, ice thickness data are needed for validation of coupled ice-ocean models for the Arctic and Antarctic
- **sea transportation** including ice navigation and use of icebreakers in ice-covered areas in the Northern hemisphere: the Baltic Sea, Greenland waters, the Svalbard area including the Fram Strait and the Barents Sea, the Northern Sea Route, the Canadian Arctic, the Bering Sea and the Beaufort Sea.
- **offshore operations** in Arctic waters which are planned in the Barants/Pechora/Kara Seas and other Arctic regions. Exploitation of oil, gas and mineral resources on land as well as offshore is expected to increase in coming years, which require much better sea ice observation methods both for the operators and for environmental monitoring and protection
- **design criteria for ships and offshore structures**, data on ice thickness is important input to these criteria

- **rules and regulations**, ice thickness data are needed to develop the regulations for operations in Arctic waters
- **environmental monitoring and ecosystem protection**. Sea ice extent and thickness has important impact on ecosystems in the Arctic. Furthermore, pollution from rivers, offshore activities and ships can be captured and conserved in sea ice and be transported across the Arctic Ocean

## 1.2 Overview of the field experiments and measurement technique

The main activities in SITHOS was planning, coordination and implementation of a series of field experiments in the Arctic between March 2003 and May 2005. An overview of the field experiments and measurement techniques is given in Table 1 a and b.

**Table 1a.** Overview of the summer and winter experiments of SITHOS

Exp. no	Acronym	Platform	Time	Experiment area	Methods*
1	ARK 19	Polarstern	March – April 2003	Greenland Sea, Fram Strait, Barents Sea	EM, AIS, in situ
	CryoVex	Twin Otter		Fram Strait	AL
2	GreenIceCamp**	Ice camp & Twin Otter	April – May 2004	North Greenland	AL, AIS
3	ARK 20	Polarstern	Aug. – Sept. 2004	Fram Strait /Arctic	EM, AIS, in situ
4		James Clarke Ross with Autosub	August 2004	Fram Strait	Upward multibeam sonar - UMS
5	ICEX-04	UK submarine	March 2004	Fram Strait – North Pole	ULS + sidescan sonar
6	GreenIce Camp*	Ice camp & Twin Otter	May 2005	North Greenland	AL, AIS

\* The methods are summarized in Table 2

\*\* coordinated with GreenIce camp

**Table 1b.** Summary of non-space methods of ice thickness measurements used in SITHOS

Acronym	Characterization of the method	Partners
EM	Electromagnetic induction combined with laser altimeter, mounted on helicopter or from a beam mounted in the bow of an ice-going vessel.	AWI
AIS	Automatic ice station which can measure ice thickness using surface wave information or other techniques and send data via ARGOS or IRIDIUM	CMR, SAMS and NERSC
ULS	Upward-Looking Sonar and sidescan sonar data from submarines	SAMS
AUV	Autosub: Autonomous Underwater Vehicle with several instruments including Upward Multibeam Sonar	SAMS
AL	Airborne laser profiling and scanning combined with kinematic GPS from aircraft.	KMS
IN SITU	In situ measurement of ice thickness, freeboard, snow cover, etc. from expeditions including ice camps	all

The field experiments and their main results are presented in chapters 3 – 6.

## 2. Requirements and field work planning



The planning of the first field experiment started a year before the SITHOS contract started, since this experiment was part of the ESA pre-launch cal-val experiment for CryoSat. This experiment was called Cryovex and was co-funded by European Space Agency. The general requirement in this experiment was to collect various snow and ice data for validation of the ice thickness retrieval algorithm to be used for CryoSat. The parameters and method of observation are summarized in Table 2.1. The specific requirement for the Cryovex experiment was to have coincident aircraft flights with airborne laser and D2P radar (Delayed Doppler Phase monopulse) and helicopter-borne ice thickness measurements. The D2P radar mounted onboard the Twin Otter aircraft operated by KMS was a similar radar altimeter as the SIRAL altimeter on CryoSat. The radar altimeter data will in principle penetrate the snow cover on top of the sea ice while the laser altimeter data is reflected at the snow surface. This will give different height measurements which can be used to derive snow thickness. The results of the joint aircraft and helicopter measurements of ice freeboard and thickness are presented in chapter 3 and 5. The analysis of the D2P radar data was not a part of the SITHOS project.

*Table 2.1 Validation parameters and method of observation*

	<i>Volumetric Measurements</i>	<i>Drilling holes</i>	<i>Surveying</i>	<i>Scanning Laser</i>	<i>EM Sounding</i>	<i>Video Records</i>
Platform	In situ & ships	In situ & ships	In situ, sledge, ships	Aircraft	Helicopter, ships	Aircraft, helicopter, ships
Snow Density	X	X				
Snow Thickness		X				
Ice Density	X	X				
Freeboard		X	X	X	X	
Surface Topography			X	X	X	
Ice Thickness		X			X	
Floe Size				X	X	X
Role of partners	AWI, NERSC,	AWI, NERSC	AWI	KMS	AWI	KMS

In addition to the data listed in Table 2.1, satellite data, in particular Synthetic Aperture Radar (SAR) images were obtained during the experiment and used to map ice types, leads, floes and ice drift. By collocating ice type information from SAR with freeboard and thickness profiles from laser and other data collected in the experiment, the laser and D2P data can be studied in relation to ice properties observed in the SAR images.

The fundamental relations between the main ice, snow and ocean parameters are illustrated in Fig. 2.1 where isostatic equilibrium is assumed for ice floating on water. Sea ice thickness can be retrieved from ice freeboard using the relation  $H=(R+1)h_f$ , where  $R= \rho_m/(\rho_w-\rho_m)$ ,  $\rho_m$  is the mean density of the snow and ice layer. The variability of  $R$  needs to be established for different seasons and areas. The density ratio,  $R$ , which is determined by the density of ice, snow and water, can be used to retrieve thickness from freeboard. The variability of  $R$  needs to be established. From literature, the following estimates are given:  $R = 9.1$  under the assumption of no snow layer on top of the ice;  $R = 8.7$  from the Beaufort Sea in spring (Bourke, Paquette, 1989);  $R = 7.8$  using direct measurements of draft and freeboard (Wadhams, 1991).  $R$  is also dependent on ice thickness. For  $H = 2$  m, the freeboard is typically 20 - 30 cm, depending on snow cover and density. For more accurate calculation of ice thickness from freeboard, taking into account varying snow depth and density, a similar factor,  $K$ , can be used based on the isostatic equilibrium assumption shown in Fig. 2.1.  $K$  is defined as  $K = 1 + (\rho_i H + \rho_s h_s)/[H(\rho_w-\rho_i) + h_s(\rho_w-\rho_s)]$ , where  $\rho_{w,i,s}$  is density of water, ice and snow, respectively.

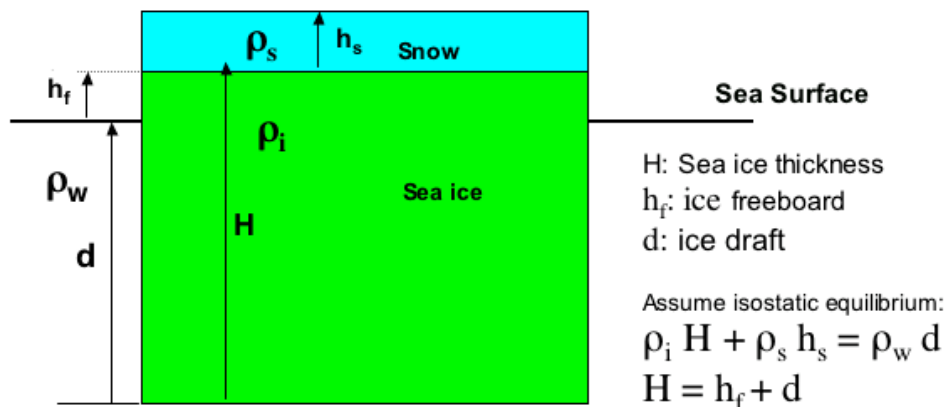


**Figure 2.1.** The relation between ice thickness, freeboard and density for snow-covered ice

The basic method of computing sea ice thickness by altimetry is to measure freeboard (that is the height of the ice or of the snow surface above water) from the difference between: a) the surface height of the larger ice floes, and b) the height of the thin ice or water surface in the major leads. Both heights may be referred to a common fixed surface (ellipsoid or geoid), but with sufficient small distance between major leads, this is not necessary to get the difference. In this context, an ice floe is a reasonably thick and old piece of ice, usually MY (multiyear) ice. In the winter season, almost all leads are covered with thin ice, while in summer the leads are mostly open. The freeboard estimates are translated into thickness by use of the K-factor defined above.

In conclusion, a number of requirements for field observations can be stated. These are related to which parameters should be observed, what should the spatial and temporal sampling be, which geographical areas should be covered, and under what snow and ice conditions should the data be collected. In practice, field experiments can only satisfy very few requirements at the time. Besides, working with Arctic field experiments always involves risks that planned observations are not achieved due to for example bad weather and other constraints which limit use of helicopters and fixed-wing aircraft. In addition to the experiments conducted in the SITHOS project, it is also very important to use results from previous field experiments in other projects.

### 3. Results from the Polarstern expeditions ARK19 & 20

#### 3.1 Introduction

The main contribution from AWI was the development and application of an electromagnetic induction and laser system (EM) for sea ice thickness measurements. Data of regional scale were acquired on expeditions of the German icebreaker RV Polarstern to investigate and demonstrate the potential of an EM system as a component of a future sea ice thickness observation system. In this chapter we summarize the method, present the main results and give an estimate of the ice thickness accuracy. Applications of the EM + laser measurements for surface roughness studies and retrieval of surface elevation by means of an additional DGPS receiver are shown. Finally, a summary of observations of ice thickness from Polarstern expeditions from 1991 to 2004 is presented.

#### 3.2 Sea ice thickness analysis tools based on EM measurements

### 3.2.1 Helicopter-borne EM thickness sounding

During the SITHOS project we have optimized the helicopter-borne EM instrument, the EM-bird as shown in Figure 3.1, and based on the good experience built a second sensor. The EM-bird operates at 3.68 and 112 kHz. The size of the bird is relatively small (length 3.4 m, weight 100 kg), and therefore operable from icebreakers and any helicopter with an external load hook. Within SITHOS, we have improved the calibration and the ice thickness retrieval algorithms (Figure 3.2).

The ice thickness retrieval is based on an electromagnetic measurement of the height of the EM-Bird above the water surface, which coincides with the ice underside. From this distance, the height of the bird above the ice surface is subtracted to obtain total (ice plus snow) thickness. The latter is measured with a laser altimeter in the bird. Key to an accurate estimate of ice thickness is the transformation of the EM signal to a distance to the water surface. This can be either performed by means of fitting a negative-exponential function to measurements over open water, which always exist, or by inverting a model curve computed from knowledge of the sea water conductivity (Figure 3.2). The good agreement with the model curve shows the almost perfect calibration of our EM Bird.

The data processing applied here assumes that the ice conductivity is negligible, and that the sea water conductivity is roughly known. It has been shown that those assumptions are mostly valid. Figure 3.2 suggests that under these assumptions and with a proper signal calibration, the accuracy of each measurement depends only on signal noise and flying altitude. Experience gathered during SITHOS shows that the EM thickness estimates are generally accurate to within  $\pm 0.1$  m relative to drill hole measurements (Figure 3.3). However, the analysis also assumes that the ice is a uniform horizontal slab, and that conductivity varies only one-dimensionally with depth. Over pressure ridges, the accuracy can be much worse, with maximum keel depths underestimated by up to 60%. This underestimation results from the three-dimensional and block structure of the keels. The water in the voids and to both sides of the keel leads to an increase of the EM signal compared to the one-dimensional case, and therefore to an underestimate of ice thickness (Figure 3.2). However, we believe that the EM thickness estimate is a good measure of the ice volume contained in ridges, and in fact SITHOS shows that thicker ridges can be distinguished from thinner ridges.

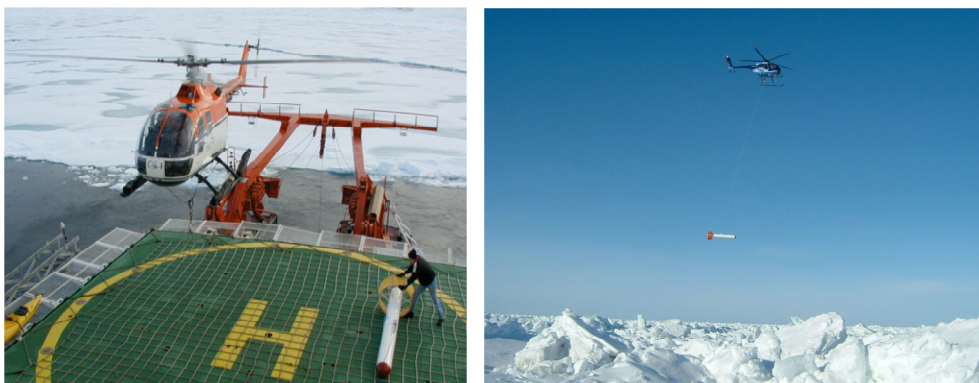


**Figure 3.1** AWI HEM bird during take-off from the helicopter deck of RV Polarstern, and during operation at 15 to 20 m above the ice surface (right photo courtesy J. Wilkinson).

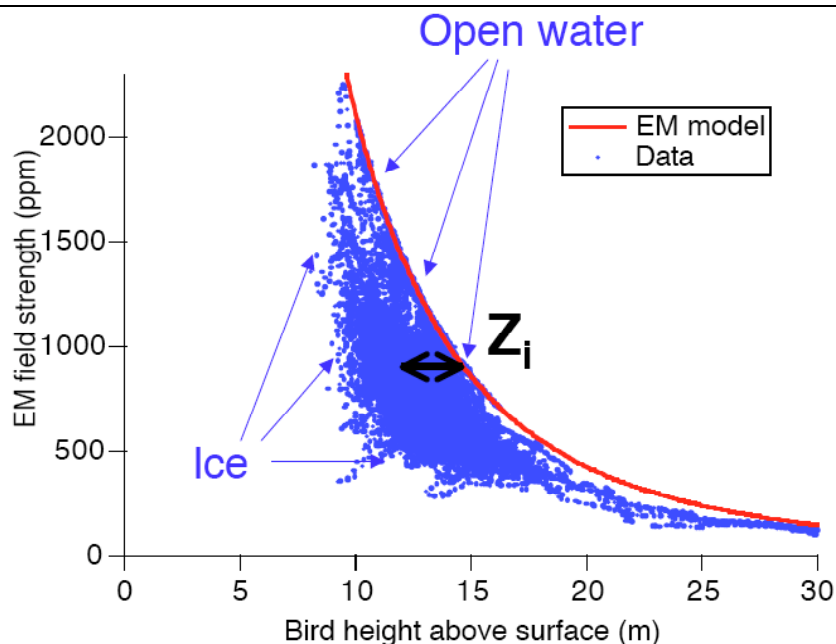


**Figure 3.2** EM data presented as relative secondary field in-phase component plotted versus bird height, measured with a laser altimeter. Measurements over open water line up along a negative exponential curve, which agrees well with a model curve of EM signal versus bird height. This is used to transform the EM signal into a height above the water. Ice thickness  $Z_i$  is obtained by subtracting the measured bird height from each EM derived height. This corresponds to the horizontal distance between each point in the plot and the model curve.

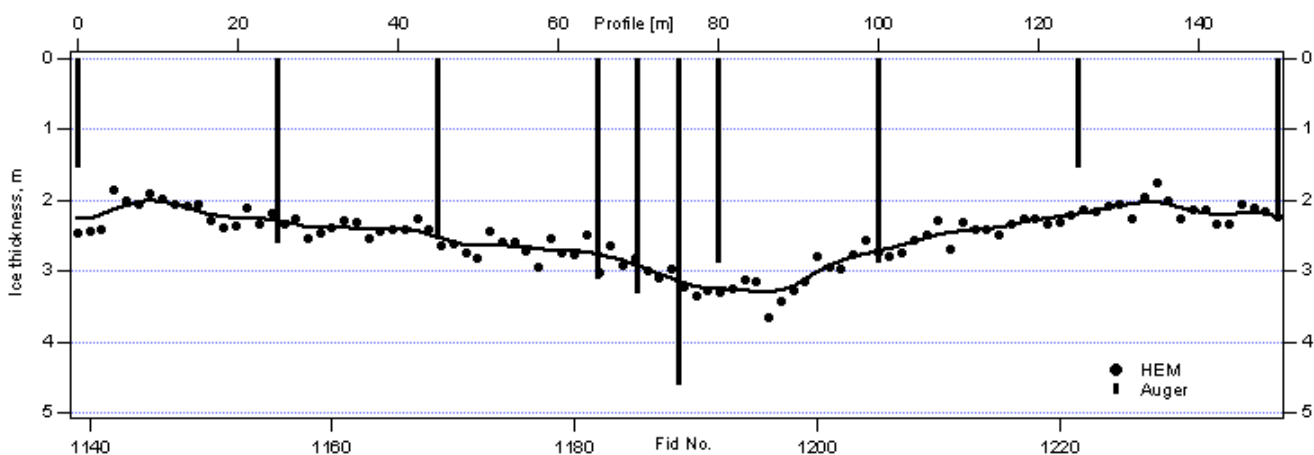


**Figure 3.3** Comparison of helicopter EM thickness estimates with drill-hole measurements obtained during SITHOS experiment 2, Polarstern cruise Ark 20.

### 3.2.2 Laser profiling of surface roughness and ridge distributions

The laser altimeter included in the EM Bird can be used independently of the EM measurements to obtain information on surface roughness and ridge statistics. Originally, there was no DGPS

receiver in the EM Bird to obtain measurements of bird altitude variations, which is necessary to extract the surface roughness profiles. However, the bird altitude variations can also roughly be removed by a combination of different high- and low-pass filters. While this does not allow computation of absolute values of surface elevation, the small scale roughness on scales of some ten meters remains unaffected. Figure 3.4 shows typical roughness profiles for characteristically different ice types based on the WMO sea ice classification.

Within SITHOS, we have developed classification algorithms based on the laser data to distinguish between different ice types, and to relate them to ice thickness. A results of a clustering algorithm is shown in Figure 3.5, where the region around Svalbard is grouped into different degrees of deformation. Unfortunately, there was only weak agreement between roughness and thickness classes. The two thickest ice classes (Thick FY and Old ice) could be discriminated best with the classification technique, and it was also possible to distinguish these thicker classes from the three thinner classes. The three thinner ice classes could not be separated.

The surface roughness profiles can also be used to identify pressure ridges. This is routinely done with all EM Bird data, as it provides additional information on the amount and thickness of deformed ice, which is underestimated from the EM thickness data alone. Figure 3.6 summarizes the results obtained during the experiment in August 2004 in the Transpolar Drift north of Fram Strait.

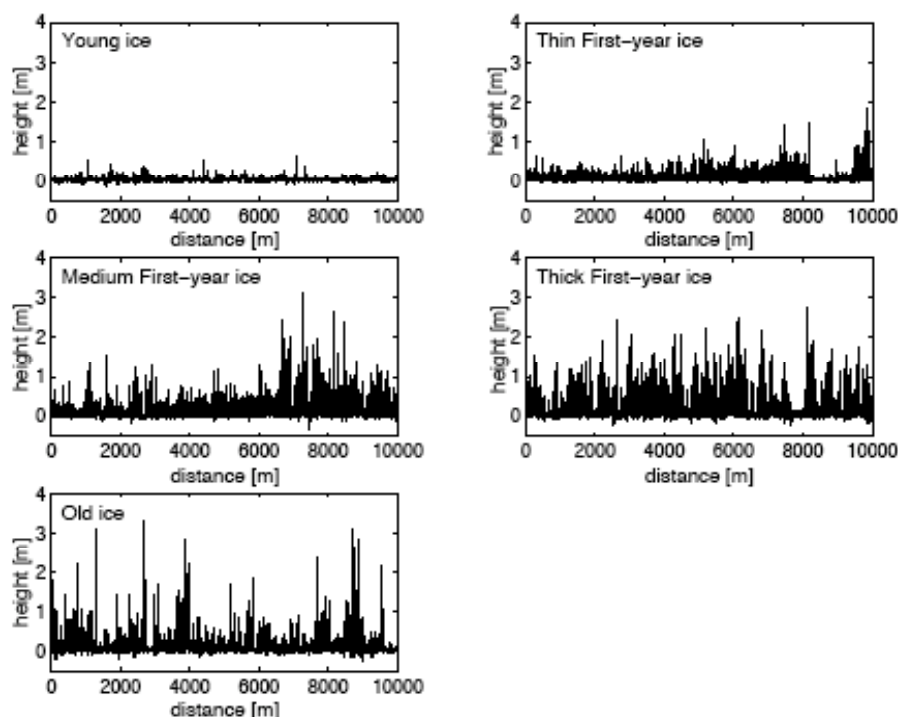


**Figure 3.4** Surface roughness profiles of different ice types, which have been used to develop algorithms for their objective classification.

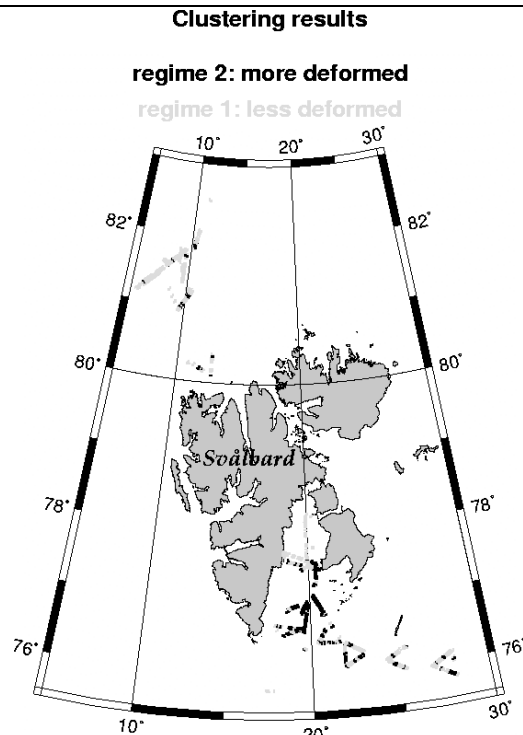


**Figure 3.5** Geographical distribution of two roughness regimes around Svalbard in March and April 2003, in Storfjord and the Barents Sea, and in Fram Strait.

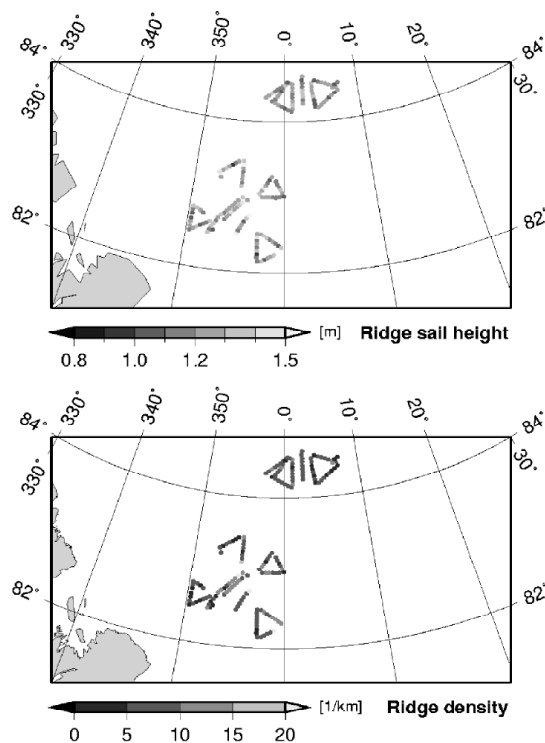


**Figure 3.6** Ridge sail heights and ridge density in the Transpolar drift north of Fram Strait in August 2004, as derived from EM-Bird laser data.

### 3.2.3 Surface elevation measurements using laser altimetry and DGPS



In 2004, we included a DGPS receiver in the EM Bird for accurate determination of surface elevation from laser and DGPS data. With the DGPS data, the bird altitude variations can be accurately removed from the laser measurements. Therefore, the EM Bird now acquires coincident profiles of ice thickness and surface elevation (Figure 3.7), allowing to test the concept of ICESat and CryoSat ice thickness retrievals.

Key to an accurate thickness retrieval is the transformation of surface elevation to ice thickness by multiplying it with a factor  $R$ , which is a function of snow depth and the densities of snow and ice. While these are generally not known with sufficient accuracy, the situation is even more complicated if different ice and snow thickness classes are present. Figure 3.8 shows an example from the Lincoln Sea, where thick MY ice and thinner FY ice were present. The histogram of surface elevation can be transformed into a thickness distribution matching the EM-derived data, if varying  $R$ -factors are assumed for different surface elevations. From the varying  $R$ -factors, snow thickness can be calculated. Results show that there is generally a good agreement between derived snow thicknesses and few direct measurements on the ground. However, our results show that  $R$  varies widely between values of 5 and 8, and that functions of  $R$  versus surface elevation have to be tuned for any different ice type.

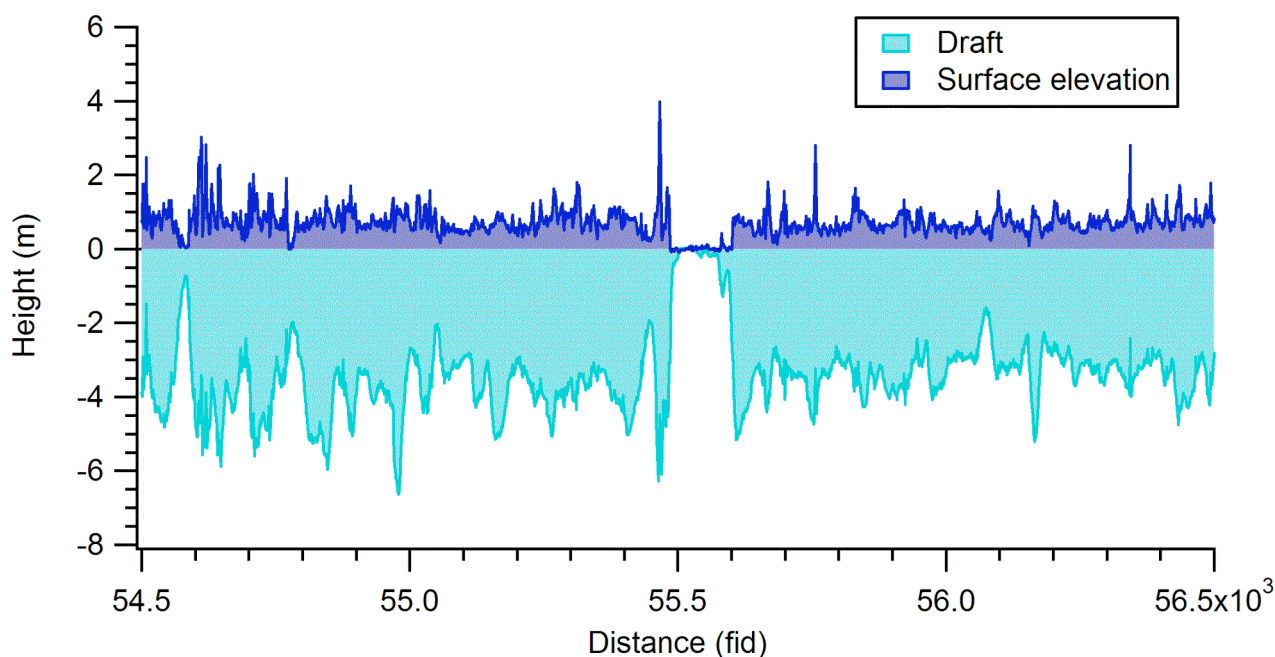


**Figure 3.7** Comparison of DGPS/laser-derived surface elevation and EM ice thickness.

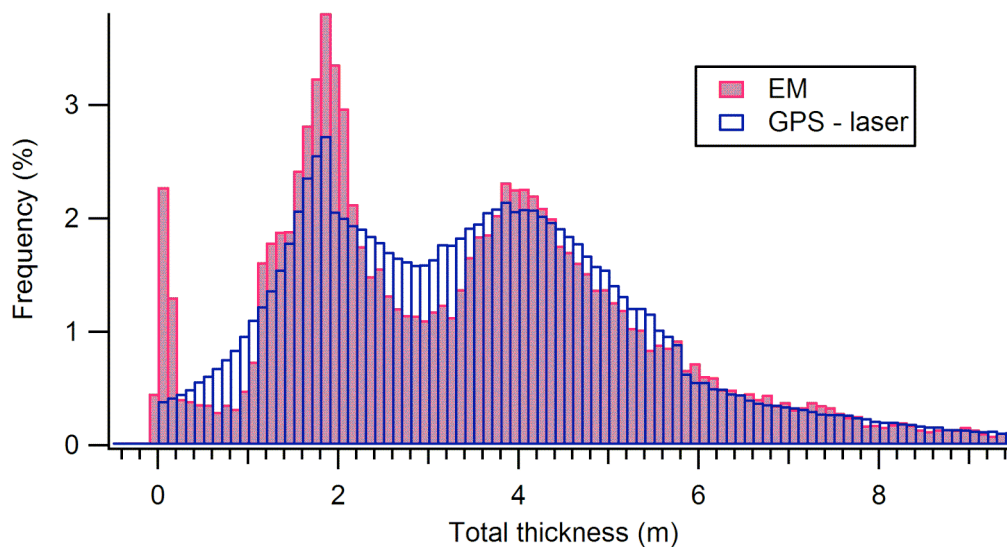


**Figure 3.8** Comparison of the calculated total thickness based on laser/DGPS measured surface elevation with the EM thickness distribution.

### 3.3 Measurement campaigns

Two expeditions were performed within SITHOS with RV Polarstern, one in winter and one in summer. The results demonstrate the applicability of EM measurements in different seasons.

#### 3.3.1 Ark 19: March/April 2003

Ark 19 was a winter cruise of RV Polarstern to investigate atmosphere-ice-ocean interaction around Svalbard, in the Barents Sea including Storfjord and in Fram Strait. Therefore, a wide range of different ice types and conditions were met, optimal for testing the performance of the EM-Bird under winter conditions. Some of the flights were also performed together with KMS as part of the 2003 campaign. KMS obtained simultaneously laser scanner and D2P radar altimeter for CryoSat pre-launch validation studies.

Figure 3.9 shows the ice thickness distributions along the flight tracks of all HEM flights performed during the cruise. In Storfjord, very thin grey ice formed in the recurring polynya was observed. However, the entrance of Storfjord was covered by very thick and deformed ice with thicknesses of 2-3 m, which was MY ice originating from the Arctic Ocean and was advected with the East Spitzbergen Current. Further to the Southeast, thinner FY ice formed in the Barents Sea was observed, with thicknesses between 0.5 and 1 m.

In contrast, the ice thickness in the Fram Strait was very large and ranging between 3 and 4 m. Figure 3.10 shows an ice thickness distribution obtained on April 11, the first CryoVex 2003 flight, where a prominent mode of 2.7 m can be seen representing the MY ice of the region (mean thickness  $2.46 \pm 1.37$  m). However, it can also be seen that the ice in Fram Strait also comprised thinner FY ice resulting from refreezing of leads in a divergent ice regime. The figure also shows the snow thickness distribution obtained by in-situ measurements on the main ice station (Tomato Island), with a modal thickness between 5 and 10 cm, and a mean of  $11 \pm 8$  cm.



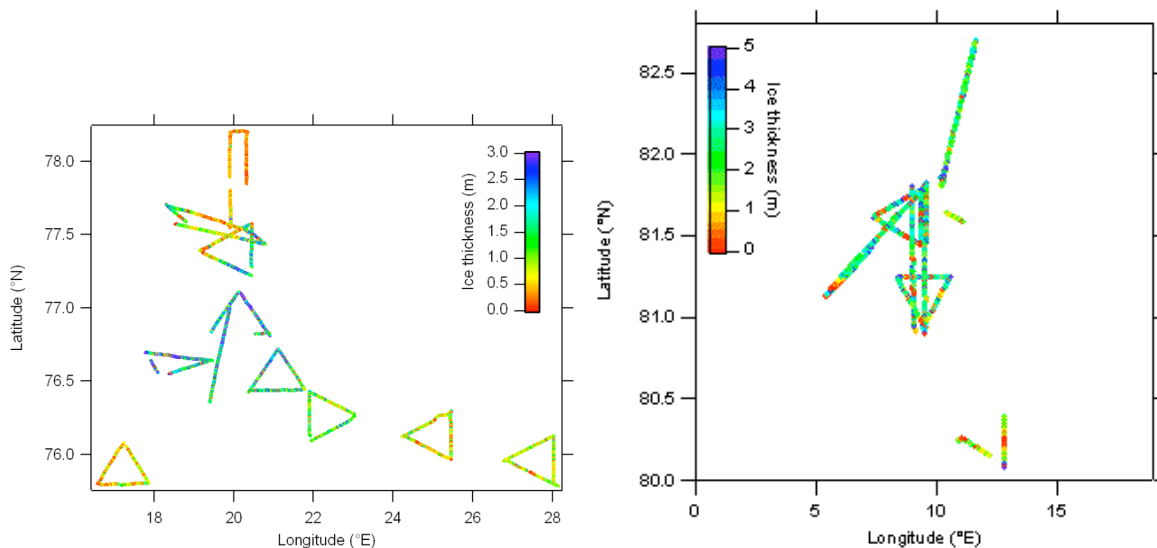


**Figure 3.9** Ice thickness along all HEM flight tracks performed during Ark 19, in the Storfjord/Barents Sea region (left) and Fram Strait (right).

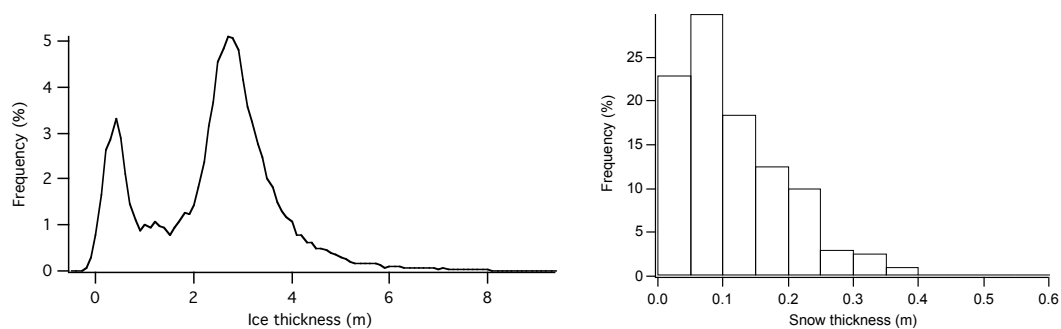


**Figure 3.10** Ice (left) and snow (right) thickness histograms obtained in Fram Strait on April 11, 2003, during the first CryoVex flight.

### 3.3.2 Ark 20: August 2004 - Ice thickness in the Transpolar Drift, 1991-2004

Ark 20 was performed in the region north of Fram Strait (Figure 3.11). It offered the unique opportunity to extend observations of the temporal sea ice thickness variability of the Transpolar Drift, which AWI has irregularly performed since 1991.

The conducted EM-Bird flights during Ark 20/2 provide an outstanding regional ice thickness dataset for the area (Figure 3.11). The observed sea ice was second-/multiyear ice, mostly heavily deformed. There was only a thin, weathered ice layer on the sea ice. Melt ponds were occasionally of huge size, having a diameter of several hundred meters. Ice concentration was typically high, mostly more than 80%.

Eleven out of all flights were performed over the inner pack to retrieve the thermodynamic state of the sea ice and compare the results to findings from the summers of 1991, '96, '98 and 2001.

Besides this regional study, two flights (2<sup>nd</sup> and 11<sup>th</sup> August) were laid across the marginal sea ice zone to investigate the ice thickness and concentration gradient approaching the inner pack.

To compare the results of ARK 20/2 to the observed decrease in ice thickness from 1991 to 2001, the thickness distribution was computed using the thickness profiles acquired on the 28<sup>th</sup> July and 3<sup>rd</sup>, 4<sup>th</sup>, 6<sup>th</sup>, 12<sup>th</sup> and 14<sup>th</sup> August (Figure 3.12). Measurements over the marginal sea ice zone were not included in the histogram. As the profiles on the 4<sup>th</sup> and 9<sup>th</sup> as well as on the 6<sup>th</sup> and 7<sup>th</sup> August were over the same region, only data from the 4<sup>th</sup> and 6<sup>th</sup> were considered respectively.

It can be seen that the observed modal ice thickness of 2.0 m was only 0.05 m thicker than in 2001. Thus, there was no further thinning observed between 2001 and 2004. However, we do not know how ice thickness has varied in the meantime.

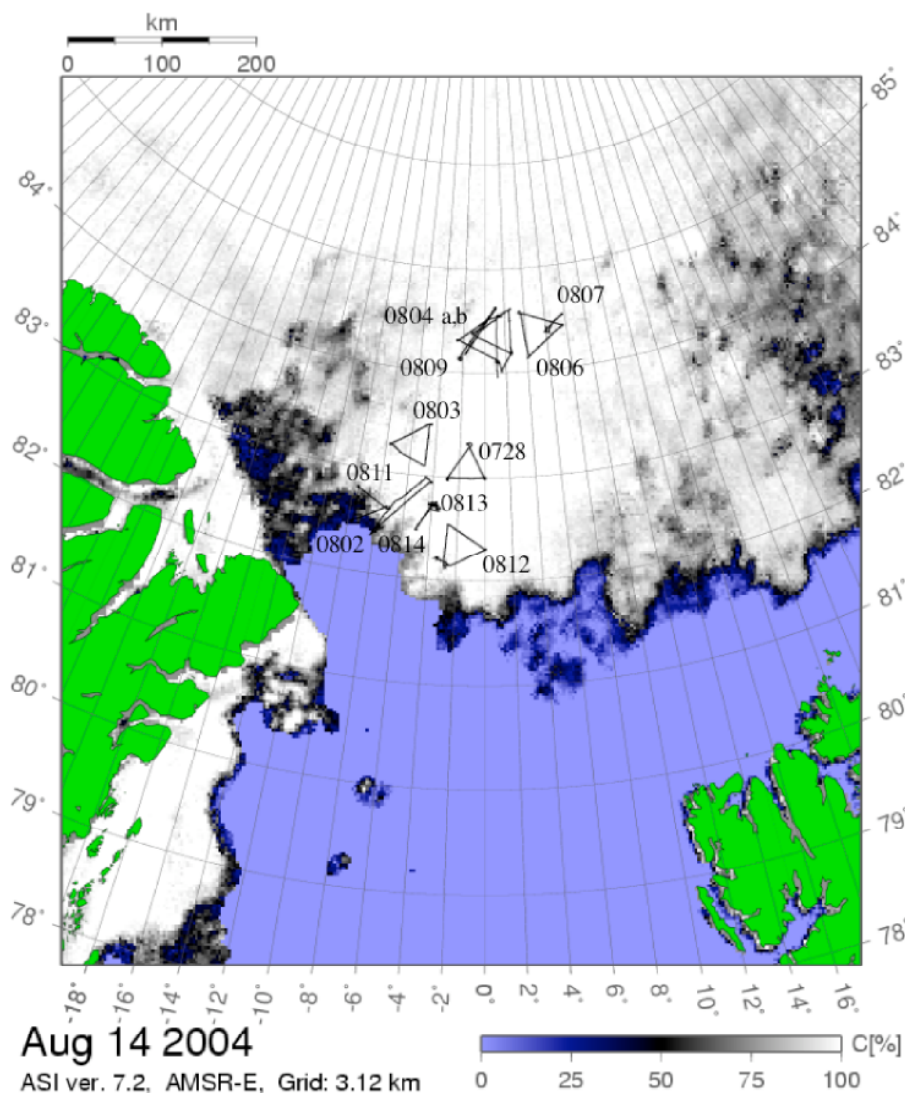


**Figure 3.11** Ice chart of the study region during Ark 20, with all flight tracks covered to obtain ice thickness profiles.

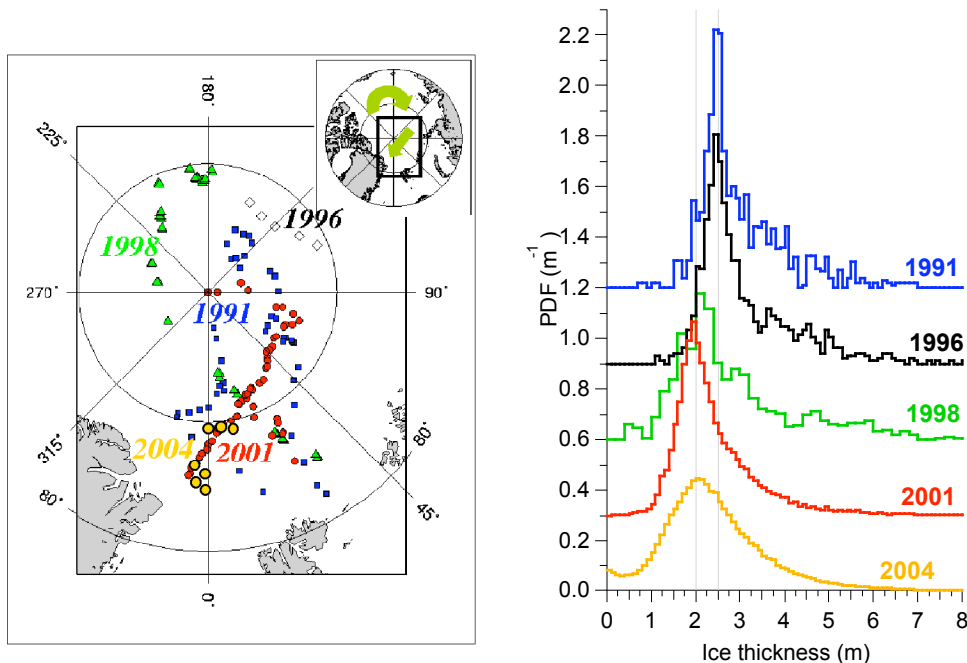


**Figure 3.12:** Map of ice thickness measurements performed between 1991 and 2004 in the Transpolar Drift (left). In 2004, all measurements were performed with the EM Bird for the first time. Earlier measurements have been performed by ground-based EM profiling on single floes. Observed ice thickness distributions from the years 1991, '96, '98, 2001 and 2004 denoted by their modal thickness of 2.5, 2.5, 2.1, 1.95 and 2.0 m respectively (right).

## 4. Results of buoy measurements

### 4.1 Introduction to wave measurements in ice

Over the past few decades powerful evidence has been acquired from satellite, submarine and modelling that the thickness and extent of sea ice is diminishing (Wadhams and Davis, 2000; Rothrock et al., 1999). At present direct ice thickness mapping, over large regions, is most accurately carried out by sonar profiling, but this is dependent on the availability of submarines. With the end of the Cold war the number of submarines obtaining ice thickness data from the Arctic has diminished to the point where we are no longer acquiring enough data to show us what trends are occurring in time and also in space.

Recently developed theory suggests that the propagation of flexural-gravity waves in ice (originating from open ocean waves) involves a spectral peak at a frequency which is a function of modal ice thickness along the path of the wave. In other words, if we measure the oscillation spectrum on the ice surface, we can learn about the ice thickness. These tiny oscillations can be detected in the central Arctic by very sensitive instruments such as tiltmeters and strainmeters. These waves originate as long swell in the distant Greenland Sea but evolve as they cross the ice into a spectrum where the peak energy is concentrated at longer periods, usually around 30 seconds.

The measurement of waves in sea ice formed an important component of the large drifting-floe field experiments in the 1970s and 1980s. Groups involved in these studies used a wide variety of devices, most commonly wire strainmeters (Squire 1978; Squire and Allan 1978), adapted from

earlier research on earth tides and glaciers.. Attempts were made to improve their design by incorporating three smaller strainmeters in a single “delta” frame (Duckworth and Westermann 1989) which required only three anchorage points instead of six. Other practitioners went ‘low tech’, freezing wooden posts into the ice and using a stainless steel rod as the sensing element during the AIDJEX experiments. Mechanical rezeroing mechanisms were introduced, either manual (Moore and Wadhams 1981) or automatic (Haskell and Robinson 1994).

Later measurements used highly sensitive accelerometers (seismographs, gravimeters) and tide gauges, though these were similarly delicate to transport, maintain and install. Tiltmeters offered a less troublesome installation procedure, being simply placed onto a bare ice surface. The Arctic Internal Waves Experiment (AIWEX) and Co-ordinated Eastern Arctic Experiment (CEAREX) used biaxial tiltmeters (Czipott and Podney 1989; Menemenlis *et al.* 1995), sufficiently sensitive to measure the long period waves of interest, though they had a limited dynamic range. The instruments were also rather sensitive to temperature effects, repeatedly going out of range with temperature fluctuations, sometimes at the cost of large gaps in the measurements (Czipott and Podney 1989). All these instruments were connected to an *in situ* recording device; variously analogue or digital tape, hard disk or paper roll, and required constant attention during the course of a manned experiment.

With the renewed interest in obtaining ice thickness from propagation of flexural-gravity waves in ice, which has the potential to measure the modal multiyear ice thickness along the whole wave propagation path from the open ocean to the measurement site (Nagurny *et al.* 1994; Menemenlis *et al.* 1995), there is a need to develop a robust, autonomous system to measure and transmit wave information.

The requirements called for a more sophisticated device, able to maintain its sensors in the desired range despite large secular changes, either real – from movement of the floe or box – or induced by the very large temperature variations encountered over an annual cycle. Additionally, long data timeseries would need to be transmitted over a satellite link to the laboratory, since initial investigations suggested that data reduction by on-board calculation of wave spectra would not allow a robust evaluation of the method.

## 4.2 The AIS system developed by SAMS

A pilot experiment between strainmeters and tilt meters on the sea ice in the Beaufort Sea March 2003, staged from the APLIS ice camp, demonstrated that tiltmeters provided good results and were more robust and easier to install than the strainmeters. Tiltmeters were therefore chosen as the sensing element, providing sufficient sensitivity while being the most robust and easy to deploy (Fig 4.1).

The low-Earth orbit *Iridium* system provided a high-bandwidth, two-way connection to the tiltmeter buoys or Automatic Ice Station (AIS). The AIS were initially configured to transmit around 70 minutes of tilt data (9216 samples at 2 Hz), taking measurements every 12 hours. The sampling strategy was designed to provide enough samples to localise the spectral peaks with sufficient accuracy. The data were analysed using a ‘Welch’ scheme to give the smallest possible variance per data point (Emery and Thomson 1998). The record was divided into 8 segments of 2048 samples each, overlapped by half their width (1024 samples). Each segment was windowed to reduce leakage and preserve its statistical independence before performing a 2048-point FFT. The eight FFTs were then averaged together, to produce a single spectrum with 16 degrees-of-freedom. The resolution given by the 2048-point FFT was  $1.1 \times 10^{-3}$  Hz.



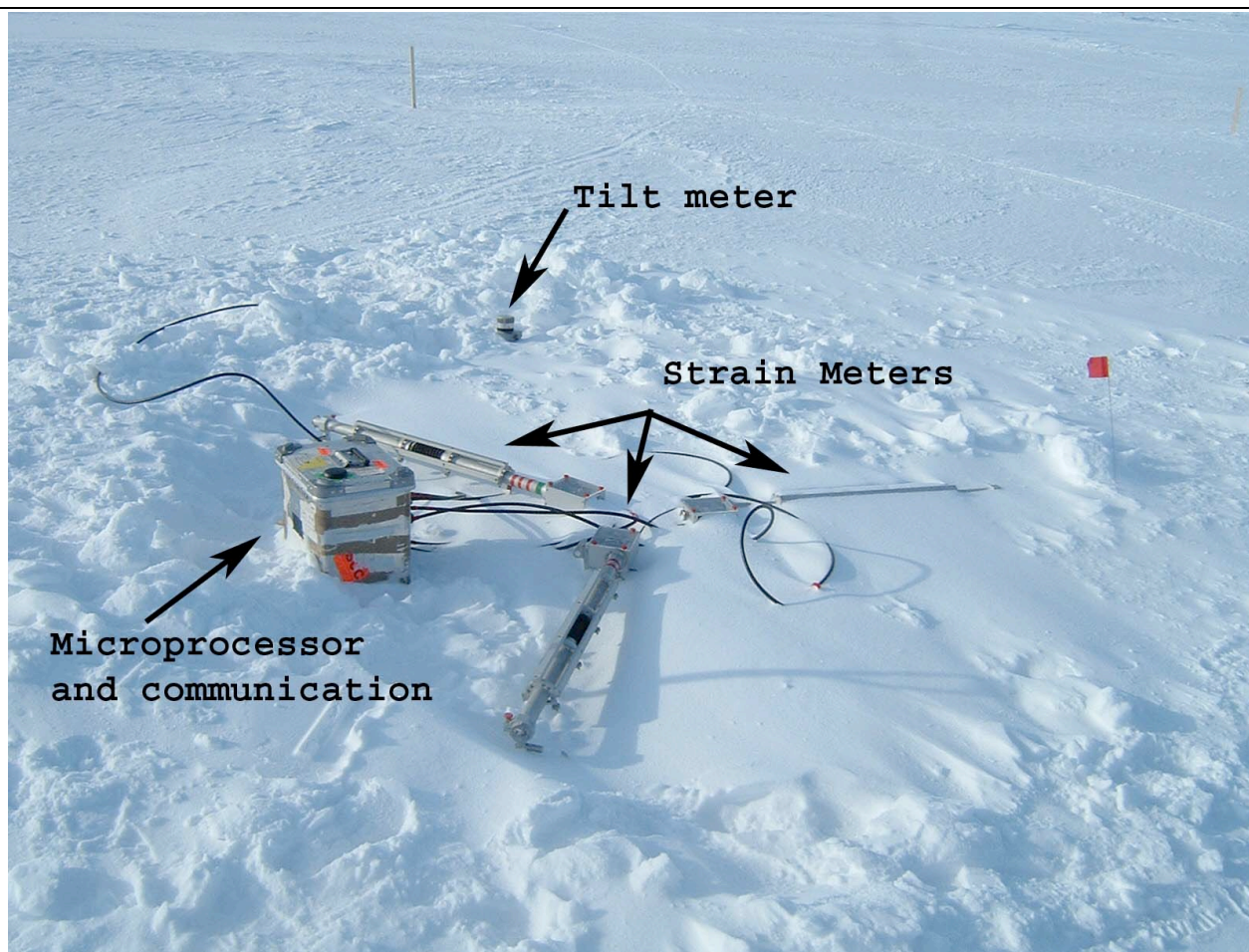


**Figure 4.1.** The setup of the tiltmeter and strain meter array experiments performed during the APLIS ice camp.

GPS positions were determined every hour and packaged with the rest of the data. Data were transmitted across a "dial up" connection to a server within the laboratory and consisted of 30 kB files sent twice daily. The two-way capability of the *Iridium* system was also used to implement at various times, alternative sampling strategies; discontinuing transmission of the tilt data once the water depth became too shallow to allow the propagation of the long-period (i.e. long wavelength) waves. GPS positions, surface temperature and diagnostic data continued to be sent, though the interval between messages was increased to one week, minimising ongoing *Iridium* transmission charges.

Figure 4.2 shows an example winter spectrum, with an ice swell peak at 31 seconds and a secondary peak at 19 seconds. The ice thickness implied by these values, using the wave-based method, is 3.6 m – a believable value – though there is currently considerable scatter in the results.

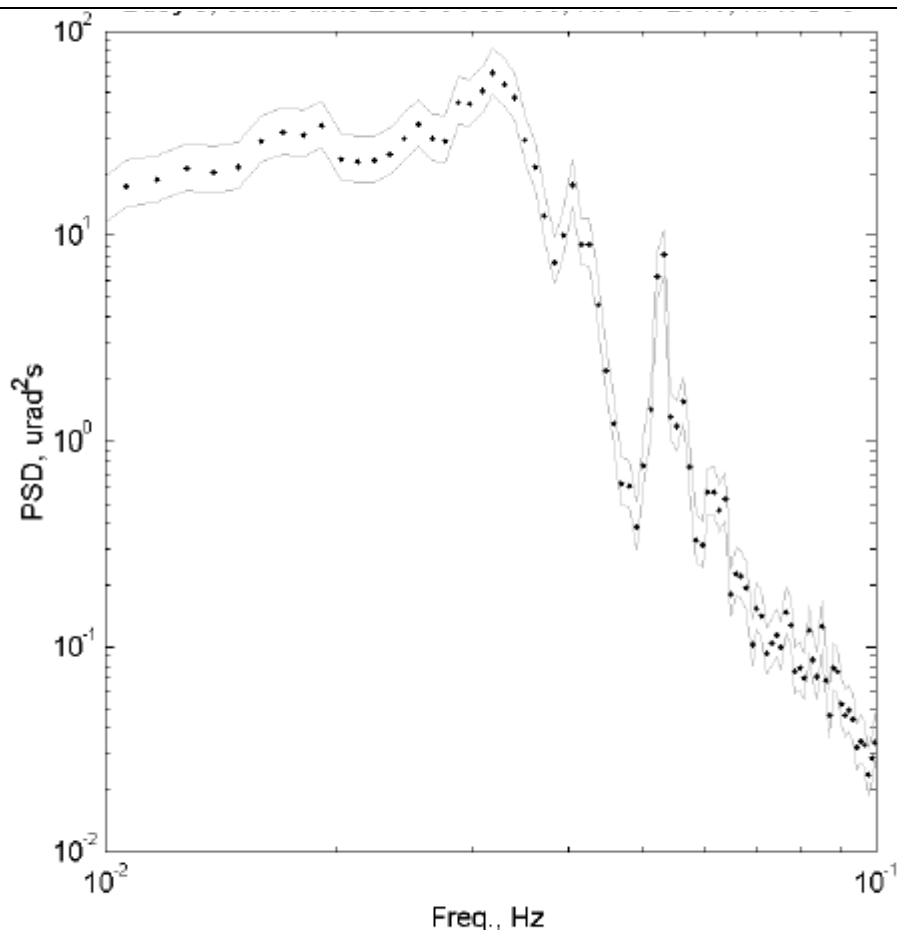


**Figure 4.2.** An example tilt spectrum, averaged from five consecutive time series. The values are marked as dots, with the 95% confidence interval plotted as a continuous envelope in grey. The ice swell peak can be seen at 0.032 Hz (31 seconds period), with significant secondary peaks at 0.041 Hz (24 seconds) and 0.053 Hz (19 seconds).

We have designed a robust, autonomous system which measures and transmits information on the flexural gravity waves within the Arctic Ocean. If the theory is correct it is envisaged that one approach to monitoring ice thickness in the Arctic would be to have a number of these systems or AISs throughout the Arctic all transmitting their data back by satellite.

#### 4.3 The AIS developed by CMR and NERSC

Our aim was to develop a wave buoy which could potentially be dropped from aircraft. Therefore, an accelerometer was selected in the first experiment, as this is more a robust technology than the more sensitive tilt-meters. Technical details of the BM01 are shown in Fig. 4.3.

The instrument was constructed to measure the accelerations related to the ice vibrations in three directions: x representing the acceleration in North/South direction, y representing acceleration in the East/West direction and z acceleration in representing the vertical component. Data were sampled with a resolution of 0.2 s (5.0 Hz). The sampled data was first converted from integer values to g (gravitation). All further data processing is performed using MATLAB program language and functions.

The amplitude of the vibrations in ice floes due to the impact of swell propagation is decaying with distance from the ice edge. Vibrations occurring more than 100 km into the ice pack will have

small amplitudes, and requires sensitive sensors, to be measured. Correspondingly, to test the accelerometer, measurements were obtained at locations 0 - 100 km away from the ice edge.

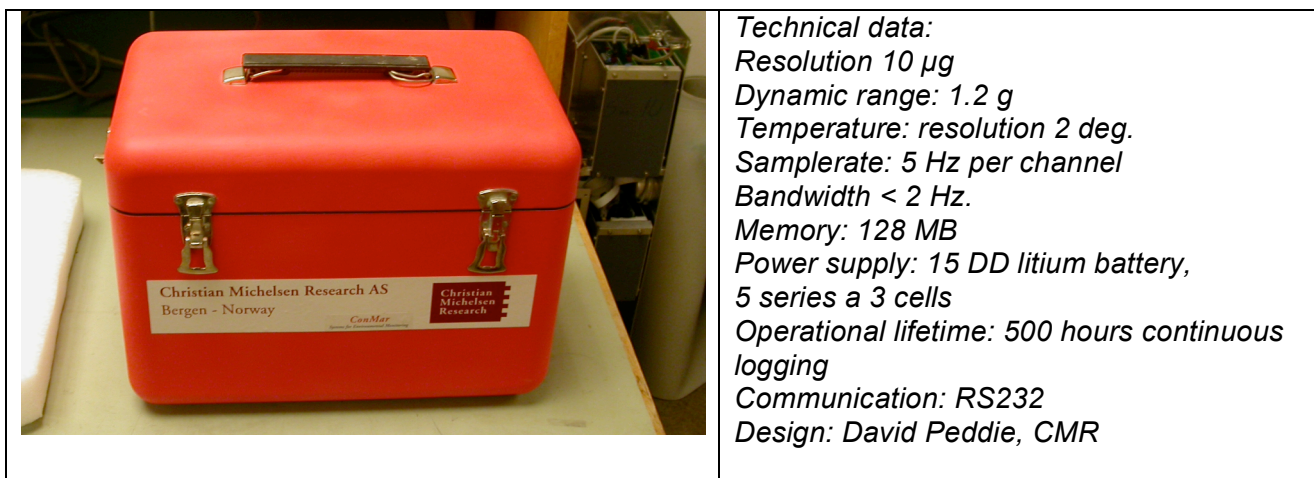


**Figure 4.3** BM01 Sensors 3 axis servo accelerometer produced by CMR

#### 4.4 Experiments in 2003

During the first phase of SITHOS experiment, March 7-March 25 2003, the BM01 buoy was recording ice oscillations at 10 different locations in Barents Sea south of Svalbard. A total of 2.5 day of data was recorded in this region. During the next phase the wave recordings were first performed close to ice edge zone northwest Svalbard, and then recordings were made, almost continuously, during a ice drift phase from April 7 to April 17. The wave recording was made during a period where the drift and wind direction first shift from southward direction to northward direction. Then, during a period with very low wind the drift is still towards north, thereafter, both the wind and the drift is directed southward until the end of the wave recording.

In Figure 4.4 we present a 100 s segment of data from the wave buoy obtained on March 15. The upper triplet of plots show that signals from each component have a strong low frequent ( $O(20s)$ ) periodic component and a significant component at a significantly higher frequency ( $O(1s)$ ). It is also clearly seen that the vertical component (z) arrives later than the horizontal components (x&y). The x and y component are close in phase. To test the stability of the filters, two different Butterworth filters have been used. In the upper plot a filter of order 5 have been used while the middle plot a filter of order 1 have been used. Changing the order of the filter only influences the higher frequency components of the vibration signals, which are less interesting in our forthcoming analysis.

Cross-correlations between the three components are plotted in the lower plot of the upper triplet (Fig. 4.4). Both the correlations between x and z and y and z have a positive time lag of around 6 s, which reflects that x and y arrives 6 s earlier than the vertical z signal. It is also seen that the lag between x and y component is positive, but very close to zero, so x and y are almost in phase. The cross-correlations have a strong maximum correlation, around 0.8, and a very clear periodic behavior with respect to time lag. The same analysis has been carried out at a later time in the wave recording, and the results are shown in the lower triplet of plots in Figure 4.4. First of all we see that the low frequent component of the three signals are much weaker, and correspondingly the high frequency component dominates more in this period. This is also observed as a clear



reduction of the maximum amplitude of the cross-correlation, with maximum amplitudes less than 0.5. The periodic character of the cross-correlation function is also significantly reduced.

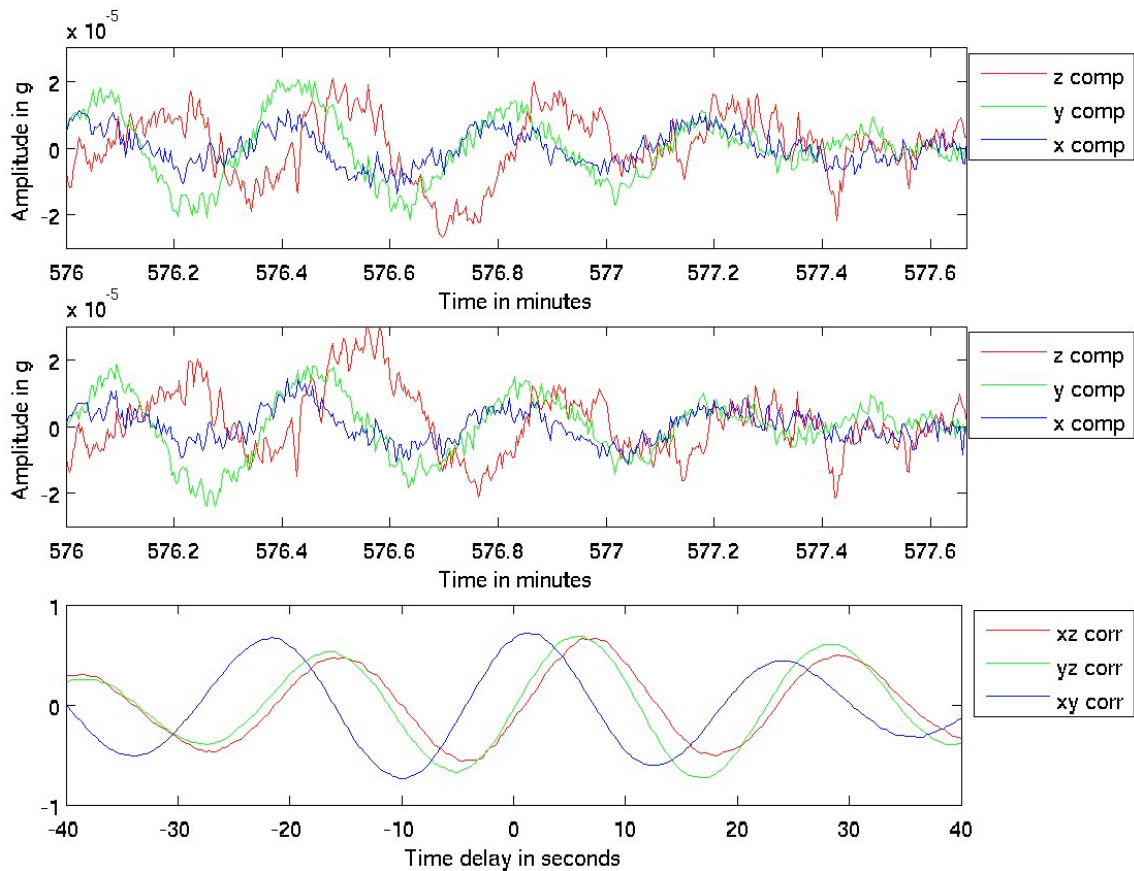


**Figure 4.4** Comparison of  $x$ ,  $y$  and  $z$  recorded signals at two different times during the recordings made on 15 April. The upper triplets of plots is taken at a time when the signals have a significant low frequency component, whereas the lower plot is taken at a time when the signals are more dominated by vibrations at higher frequencies. In each triplet of plots, the two upper plots the  $x$ ,  $y$  and  $z$  components are plotted using two different filters, Butterworth of order 5 and Butterworth of order 1, in the upper and middle plot, respectively. In both cases a band-pass filter stopping frequencies below 0.01 Hz and above 2 Hz has been employed. In the lowest plot the cross-correlation using the order 1 filtered signal.

The spectrogram have been calculated for each of the components using 4096 long time segments covering the full time of recording without overlap. The spectra are plotted as function of time and frequency in Figure 4.5. The similarity between the  $z$  component and the  $y$  component is very clear. Both signals have a strong contributions wave components from a relatively narrow band of frequencies centered at 0.047 Hz and a width of 0.02Hz. The energy in the  $x$  component is significantly less than the two other components, but the energy come from the same frequency band. The width of the frequency band seems to be relatively stable with time, but a small drift towards higher frequencies can be seen in the spectrogram plots. Several peaks can be observed within the frequency band at different times.



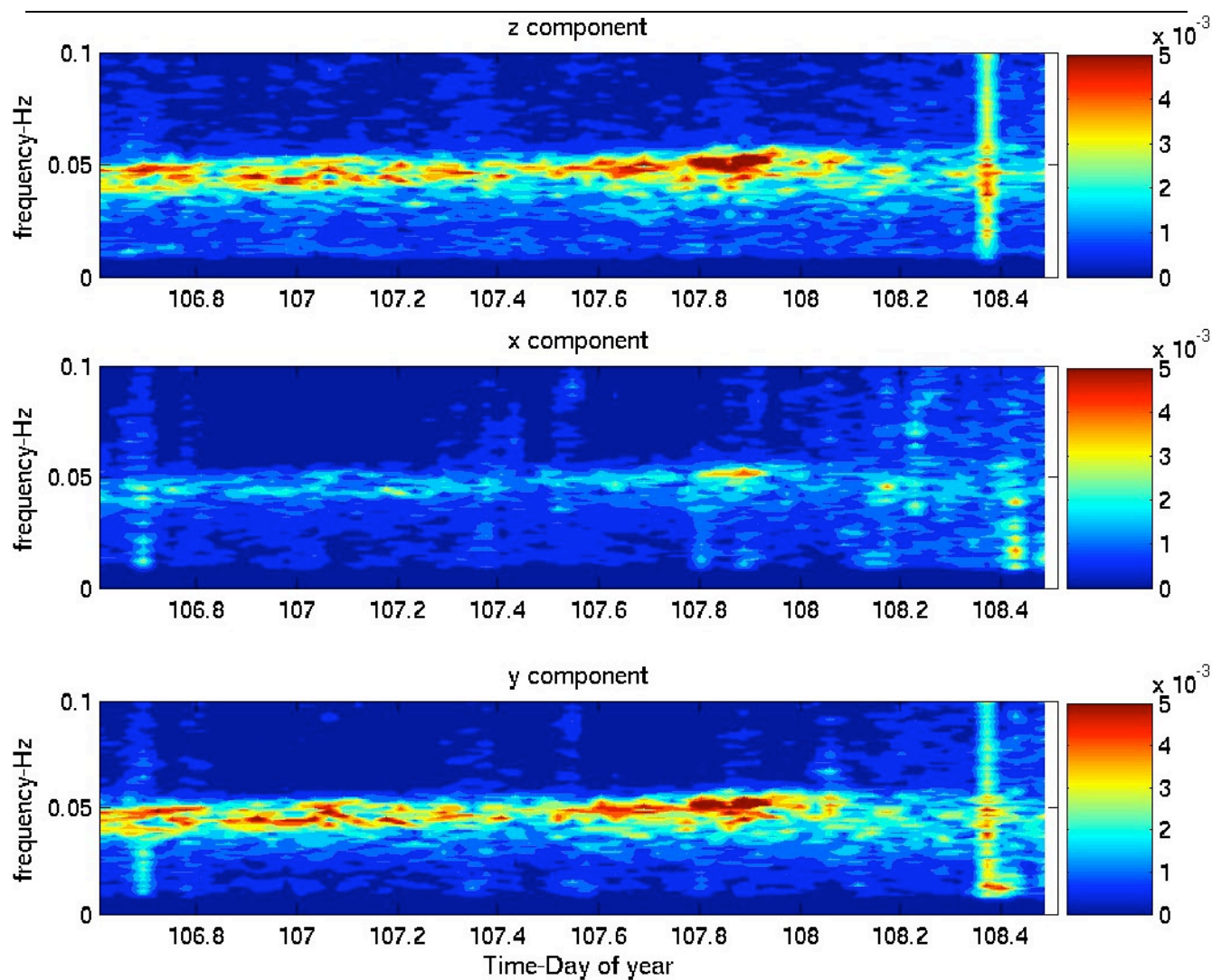


**Figure 4.5** Spectrogram calculated and plotted as function of time and frequency (range: 0- 0.1 Hz). Each time segment consists of 4096 samples. The data started on 15 April 2003 and covers the entire period of recording, a total of 46 hours and 25 minutes.

## 4.5 Results from the Fram Strait experiments

In this study we have successfully demonstrated the use of accelerometer to characterize the vibrations decomposed in three components both in the Barents Sea and in the Fram Strait. A major finding was that the vertical acceleration component of the vibrations induced by swell propagation is three-six seconds out of phase with the horizontal components corresponding to tilt. The two horizontal components are more or less in phase. Also, we are able to extract reasonable directions from the two tilt components.

Another finding is that the thinner ice in Barents Sea causes shorter periods (14-17 s) than in the thicker ice regions at the ice station well within the ice pack in the Fram Strait (20-22 s). These differences in periods may be due to differences sea ice parameters, mainly thickness, and distance to the open ocean. The variation in periods found at the ice station, with constant local ice conditions, is most likely due to changes in the distance from the ice edge caused by ice drift and/or to changes in the incoming open ocean wave field. The explanation of these observations will be addressed more in detail in forthcoming work by two approaches (1) compare the results to modeled incoming directional wave spectrum data from ECMWF (WAM model) and (2) in wave propagation modeling experiments, using models which are able to handle the changing ice conditions found by crossing the MIZ into the ice pack.

A local broad, but weak, maximum lobe between 0.01-0.02 Hz is observed in the recordings obtained during the ice station. This may indicate the presence and development of the 30 s resonant wave observed in the interior Arctic. However, this is quite speculative and needs further investigation. The conclusion is therefore that the Nagurny method can not be used in the Fram Strait or in the Barents Sea. As in other inversion problems, the quality of the inversion of vibration observations to ice thickness relies on the validity of the underlying forward wave models. The assumption of a infinite thin elastic plate, as used in the Nagurny method, is not realistic for the MIZ or in regions close to the MIZ. In future work we will start use more complex models including inhomogeneous ice fields (f.ex Williams, 2005) to understand the wave propagation, and potentially develop new inversion schemes with better validity also in the Fram Strait region.

## 4.6 Construction of the SITHOS I autonomous wave buoy

The second prototype wave buoy (SITHOS I) was based on the ICEX product made at CMR and the previous CMR SITHOS prototype BM01 (prototype 1). An illustration of the SITHOS I buoy is shown in Fig. 4.6 a. SITHOS I uses an accurate 2-axis tilt meter to measure the waves and an IRIDIUM™ phone to communicate. Custom made electronics was used to collect and control the instrument. The 2-axis tilt meter was placed on a specially designed auto levelling system so the tilt meter could be levelled to within  $\pm 0.046$  degrees, which is the dynamic range of the tilt meter. SITHOS I is an autonomous buoy that sends back data at regular intervals. The configuration can be changed at any time by sending new parameters to the buoy. When the buoy wakes up from sleep state it immediately initiates a acquisition cycle. First the auto-levelling system starts up to level the tilt-meter to within  $\pm 0.0046^\circ$  of the horizontal. Once this is achieved the acquisition starts and continues for a predefined period (typical 1 hr). At last the data is sent using the Iridium modem. Before going to sleep the buoy checks to see if new configuration parameters have been received. The buoy stays in sleep state until next wake up defined by the log rate.

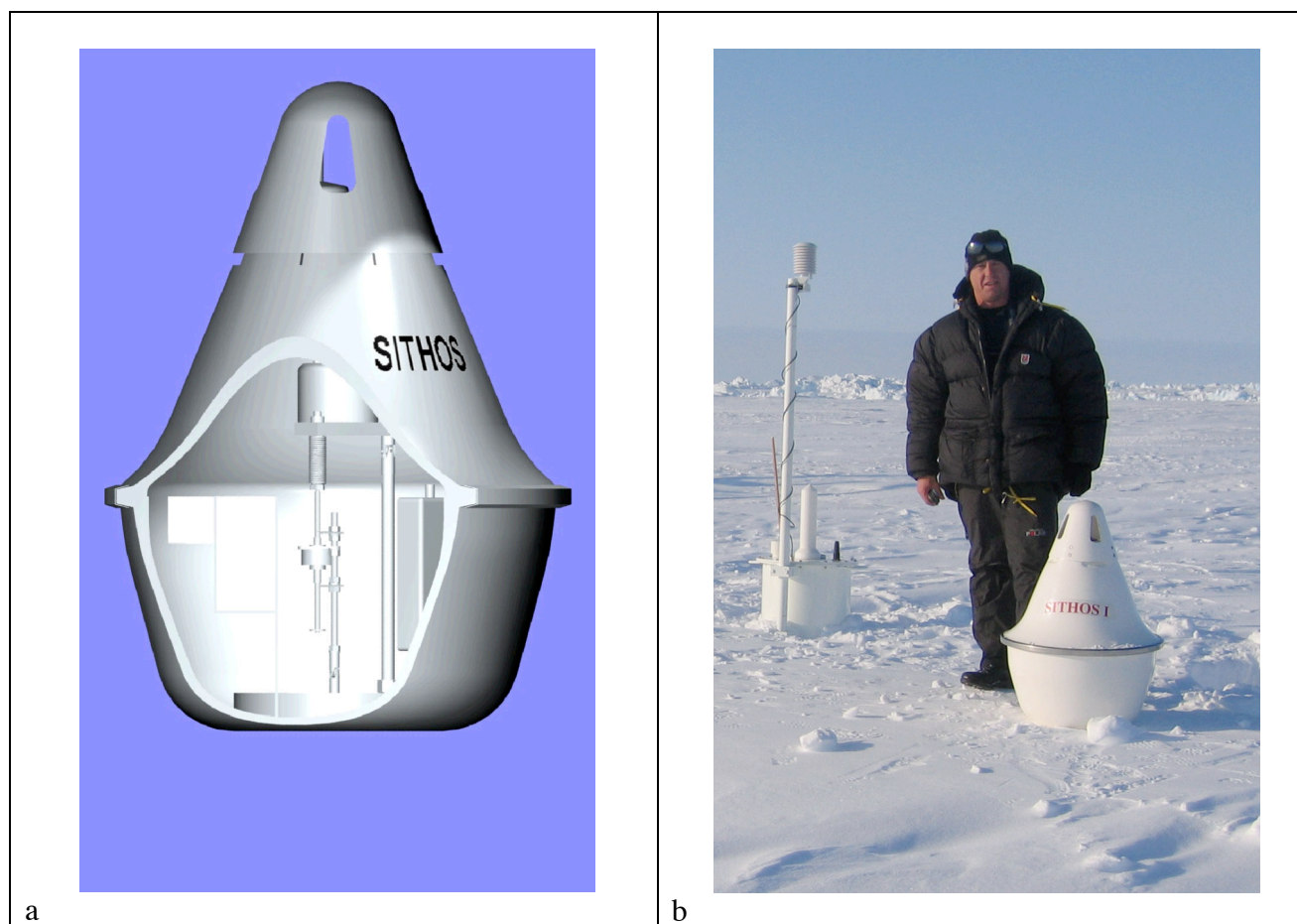


**Figure 4.6.** a) Design of SITHOS I; b) deployment of SITHOS I at 84N on 13 May 2005 by David Peddie. The AWI buoy (behind David) was deployed close to the SITHOS I.

#### 4.7 SITHOS I deployment and data acquisition

The automatic ice station SITHOS I was transported to Greenland in April 2005 and onwards to Alert in Canada. Here the buoy was assembled and tested until deployment. After several attempts the buoy was deployed the 13<sup>th</sup> of May 2005 at N 84.00 ° W64.00 ° on a multiyear ice flow of about 0.5 sq. km. The SITHOS I was deployed together with an ARGOS buoy from AWI (Fig. 4.6 b).

Since the deployment the buoy has been working without problems for more that 6 months. By 23 January 2006 the buoy has collected 150 hours of tiltmeter data. Each measurement contains 1 hour of data, and the sample rate is set to 2 Hz. The wave amplitudes varied from a maximum of 5  $\mu$ rad to a minimum of 0.1  $\mu$ rad over the total acquired data. Remote configuration of the buoy has worked perfectly as well as the data transmission. The Iridium system gives the position of the buoy and buoy track is shown in Fig. 4.7. It is seen that the buoy is drifting into Baffin Bay and not further into the Arctic Basin as we hoped when we dropped the buoy.

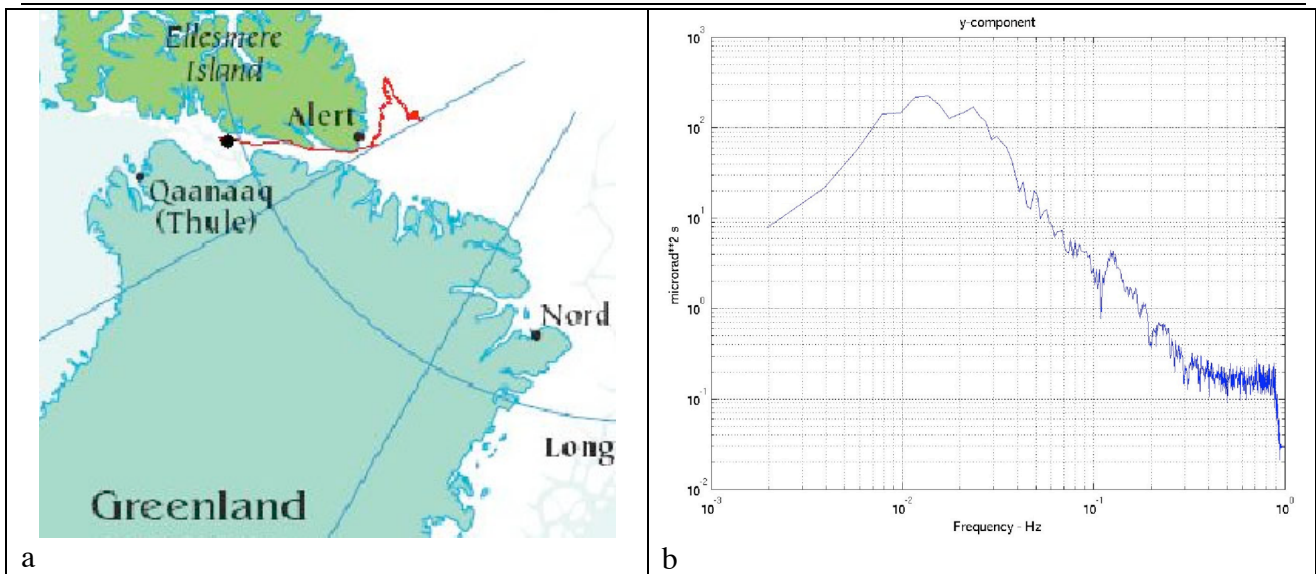


**Figure 4.7.** a) Drift track of SITHOS I from May 2005 to January 2006, and b) Mean spectrum representing the y-component of the data obtained the 25 September 2005. FFT has been carried out by 1024 sample in each segment, and thereafter a mean has been taken over all the spectra. Maximum peaks are observed at 73.0 s for 42.73 s.

The data analysis has just started and results are expected during 2006. The mean spectra are calculated for each component (example of y-component is shown in Fig. 4.7.b), and both of them have two spectral peaks at frequencies corresponding to periods of 42 s and 73 s. Furthermore, the same analysis will be carried out and summarized for the rest of the data and correlated to other environmental data. Figure 4.8 shows a short extract of data, and it is seen that the amplitude for both axes is around 3-4  $\mu\text{rad}$ . Furthermore, each component behaves as a modulated periodic signal. By comparing the two components, it is seen that they are in general out of phase.

Cross-correlation, as function of time lag and recording time, has been calculated between x and y and is shown in Figure 4.9. The very strong periodic characteristics observed in the cross-correlation function in the Fram Strait and Barents Sea is not present for the selected recording segment. However, some very strong anomalies in the cross-correlation function is observed at several times for example at lags around 20 s at clock time 13.8. The lack of systematic characteristics in the correlation function lacks systematic characteristics, this shows that the signal characteristics are not stable with time. A more detailed analysis of the correlation function at other time segments of the SITHOS-1 data is needed to understand how the signal characteristics are.



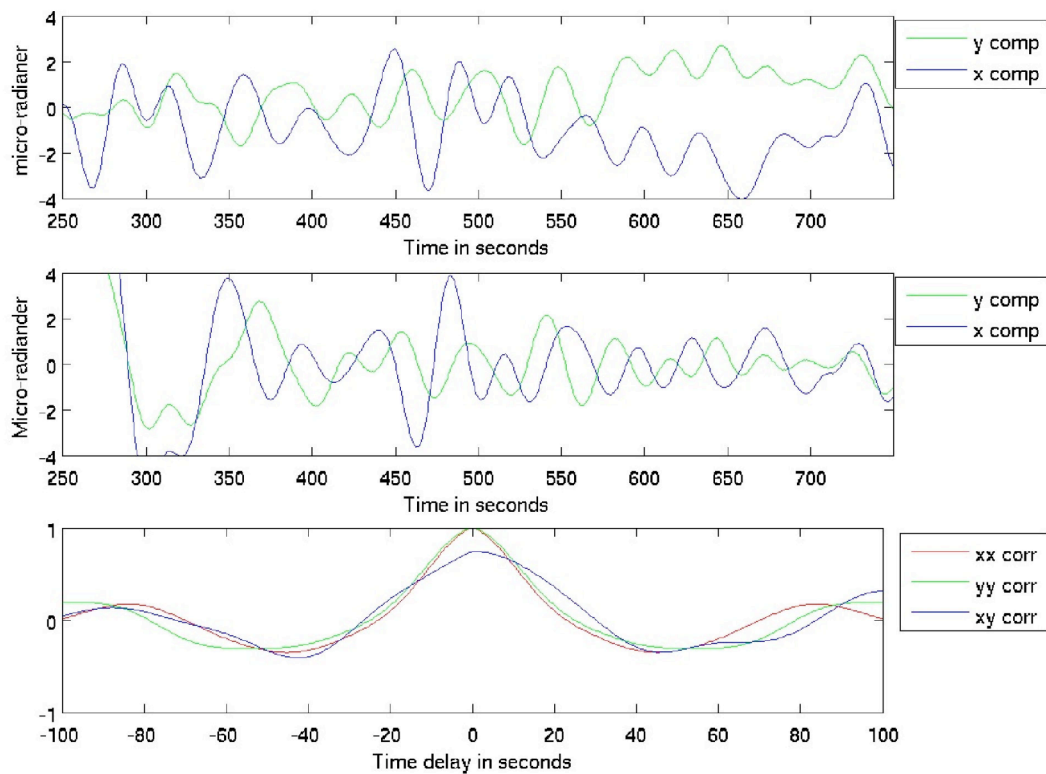


**Figure 4.8.** A first display of data from 25 September 2005. The two upper plots show time series of wave data (in s), using two different Butterworth filters (order 1 in the upper plot and order 5 in the lower plot)

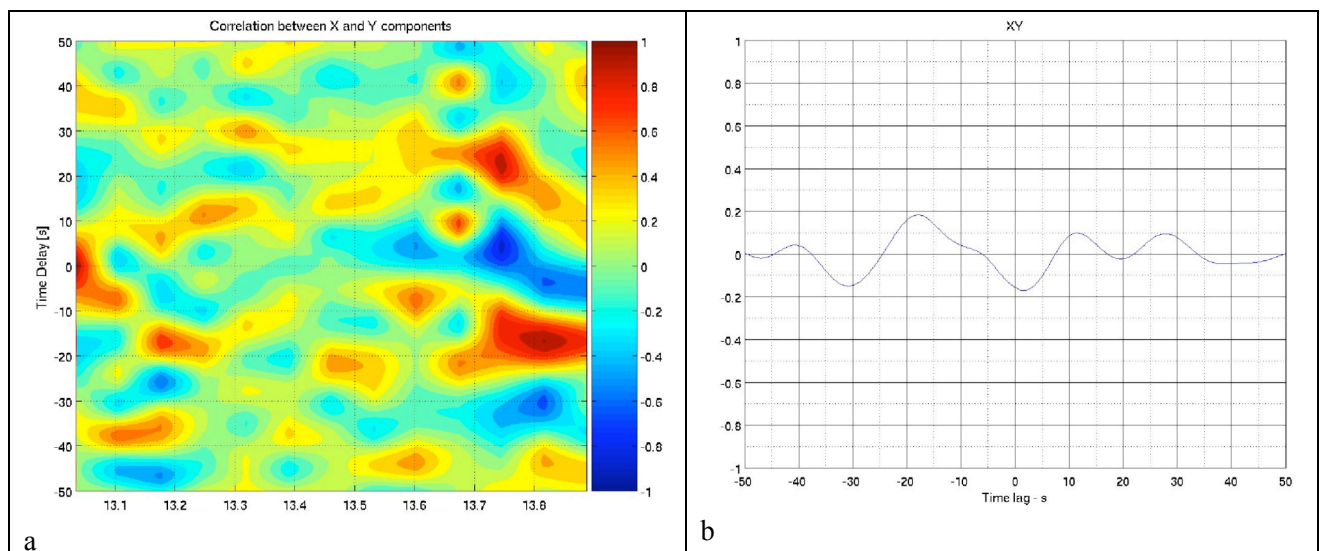


**Figure 4.9** (a) cross-correlation of 512 long (256 s) segment pairs of x component and y component as function of time, given as hours on the 25 September 2005, and time delay. (b) the time averaged cross-correlation function.

#### 4.8 Preliminary conclusion on the SITHOS I buoy

The design and the deployment of the buoy was successfully performed. However, it would have been better to deploy the buoy further north to facilitate drift further into the Arctic. This was not possible due to the limited range of the helicopter.

In future designs a system to determine the orientation of the buoy should be added. This was omitted in the SITHOS I buoy to keep the design simple and robust. The resolution at the lowest frequencies are not so good when it comes to decide the dominant frequencies accurately. According to this it is recommended to sample more than one hour, at least two hours, to get a smoother mean frequency spectrum, calculated by FFTs of longer individual time segments.

The pre-liminary analysis of data obtained with SITHOS-1 in north of Greenland indicate that the vibrations here are very different from the vibrations observed in the Fram Strait and Barents Sea during the 2003 experiments. In the selected data segment (September 2005) there are two dominant periods of 42s and 73 s, present and both of them significantly longer than the periods observed in Barents Sea and the Fram Strait which were all less than 25 s.

## 5. Results from aircraft surveys

### 5.1 Overview of the field experiments

The SITHOS project contributed to three aircraft laser scanner (lidar) measurement campaigns. These were carried out in April 2003, May 2004, and May 2005. The survey flight tracks are shown in Figure 5.1. The long-range flight lines were SITHOS designated flights, aimed at study of sea ice freeboard at large scales; the flights were shared with the GreenIce project, which has primary focus on inter-comparison of methods around the 2003 Polarstern ice mooring and the 2004 GreenIce ice camp north of Alert.

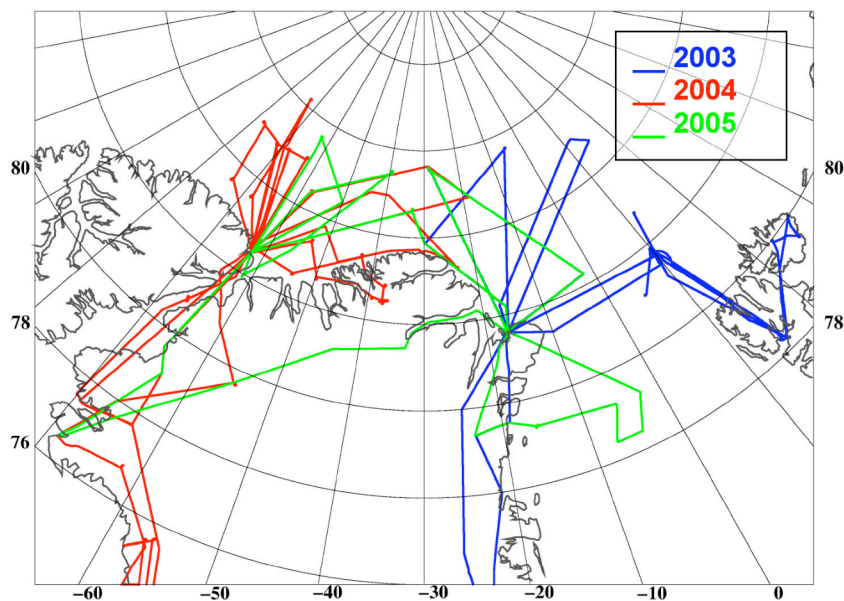


**Figure 5.1.** Airborne laser scanner survey flight tracks in the SITHOS project

The 2003 campaign was coordinated with observations from the German Research vessel Polarstern. Polarstern was anchored to an ice floe in the Fram Strait for about one week where both helicopter EM measurements and groundwork were carried out. Coincident HEM and airborne laser scanner data were sampled on to 100 km lines north and southwest of Polarstern. In addition to the flights near Polarstern long flights north of Greenland were performed to sample different sea ice in that region.

The SITHOS flights in 2004 was part of a larger field campaign based out of the Canadian Forces Station Alert and an ice camp established at approximately 85N and 65W on the sea ice in the Arctic Ocean. The SITHOS flights were the long-range tracks north of Greenland aimed at repeating previously surveyed lines and under-flying the ICESat satellite.

The primary goal of the 2005 campaign was to perform coincident laser scanner and helicopter flights of the thick sea ice in the Lincoln Sea and along with this also to re-survey previously measured areas north of Greenland.

## 5.2 Method description

The DNSC laser scanner system was installed in and operated from a Twin-Otter from Air Greenland. The system consists of the laser scanner, several precise geodetic GPS receivers and inertial navigation instrument (INS). Basic observation by the laser scanner is the range between the instrument and the surface of the snow layer on top of the sea ice. From this the surface elevation is found using information about the instrument platform (in the aircraft) position and attitude measured by the GPS and INS equipment. The measurement method is illustrated in Figure 5.2 and 5.3.

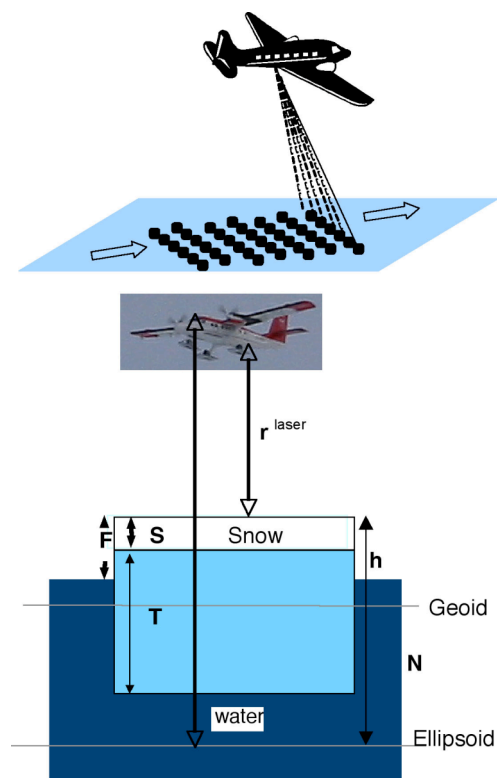


**Figure 5.2.** Airborne laser scanner measurement principle.

From the observed surface elevations the sea ice freeboard,  $F$ , is determined by lowest-level-filtering where the elevations are referred to the local sea level [Hvidegaard and Forsberg, 2002]. The sea ice thickness can then be estimated from the freeboard observations using a ratio,  $K$ , between the freeboard and the thickness expressed as,

$$T = K \cdot F$$

With total ice and snow thickness  $T$ . The formula for  $K$  is shown in Fig. 5.3. It depends on the snow depth, densities of snow, ice and seawater and varied with season.  $K$  can also be determined from

local measurements of the snow and ice density and thickness. A description of the K-factor is also given in chapter 2.

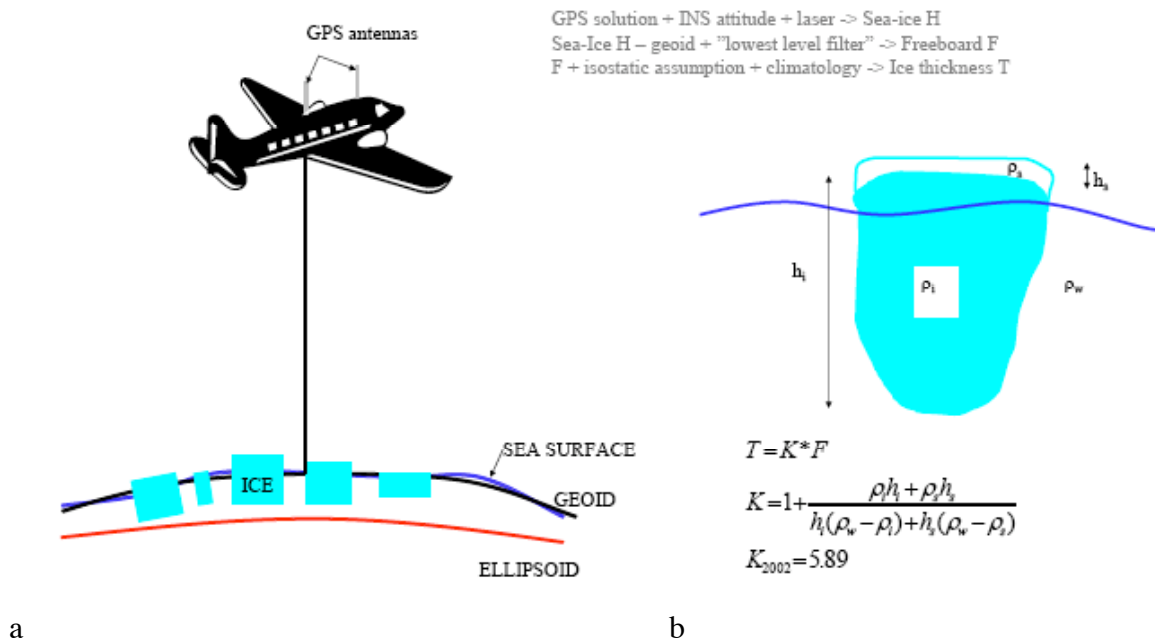


**Figure 5.3** a) The scanning laser measures the distance to the surface of the snow layer on top of the sea ice and to the open water between the ice floes. The distance is relative a reference geoid. b) the translation for freeboard to thickness requires knowledge of snow and ice density and snow thickness.

## 5.3 Results from the laser scanner surveys

### 5.3.1 Laser scanning thickness images

The sea ice thickness is estimated from the airborne laser scanner observations from the three campaigns as described above. A sample of the results is shown in Figure 5.4 where an image of thickness estimates are generated along the flight track. The scanned images show detailed thickness of the ice floes, the ridges and the thin ice between the floes. Figure 5.5. gives an overview of the thickness results from the complete 2003-5 flight tracks, using averaged, thinned-out results.

It is seen that the sea ice north of Greenland is exceptionally thick, and with large inter-annual variations. It is clear that the airborne lidar method is very efficient, and allows large areas to be covered in a relatively economical way. The method needs, however, to be externally validated; this is outlined in the next section.



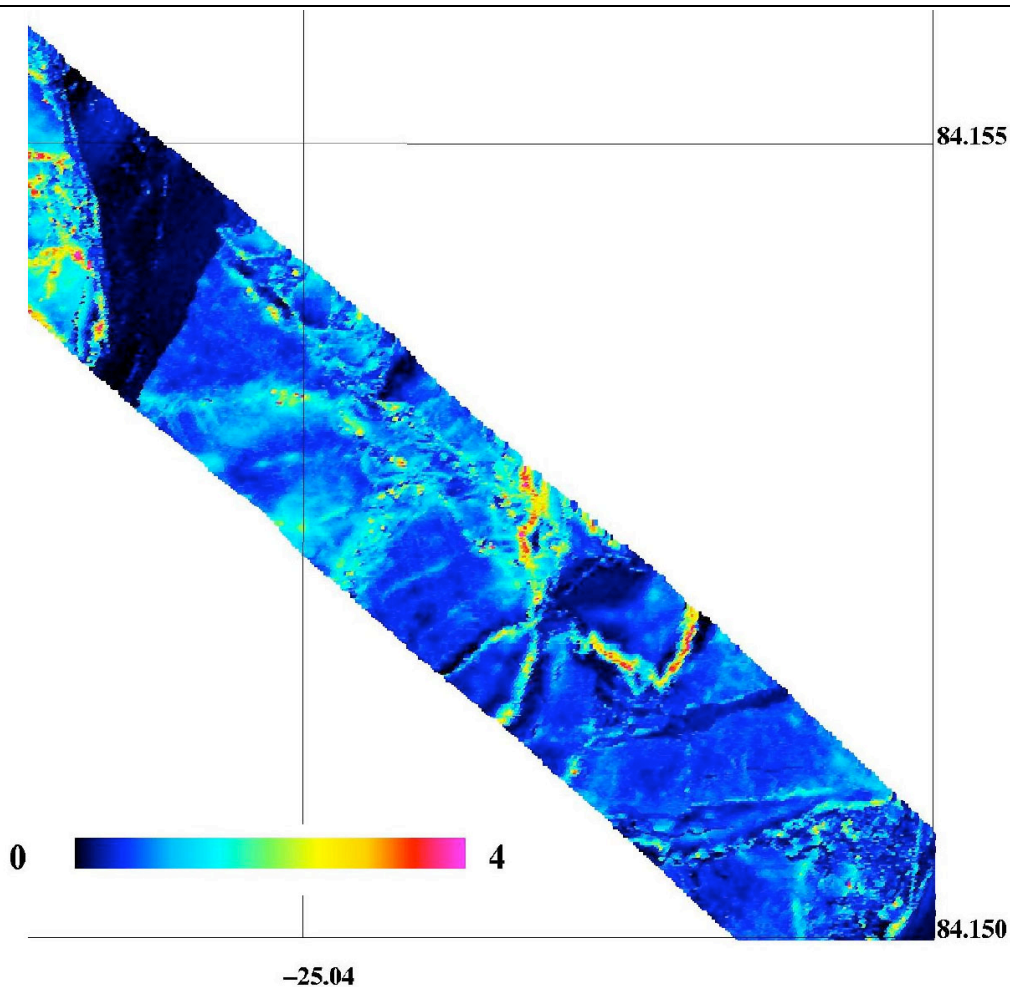


**Figure 5.4.** Laser scanner freeboard height data example (m). 150 m swath width. Ridges in the floes are clearly seen, as are a major thin-ice lead (top).

### 5.3.2 Comparison of laser scanner and ICESat observations

During the 2004 campaign two flight lines were flown nearly coincident with ICESat sub-tracks. Figure 5.6 shows an example of the laser scanner derived and ICESat freeboard data. To the left laser swath data is overlaid with ICESat point measurements and to the right a longer profile of freeboard elevations from laser scanner, in blue, and ICESat, in black, is seen. Good correlation is found but with an average difference of approximately 25 cm. The reasons for this are likely the lower resolution and larger footprint of ICESat, giving inaccurate lowest-level-fitting of the ICESat data.

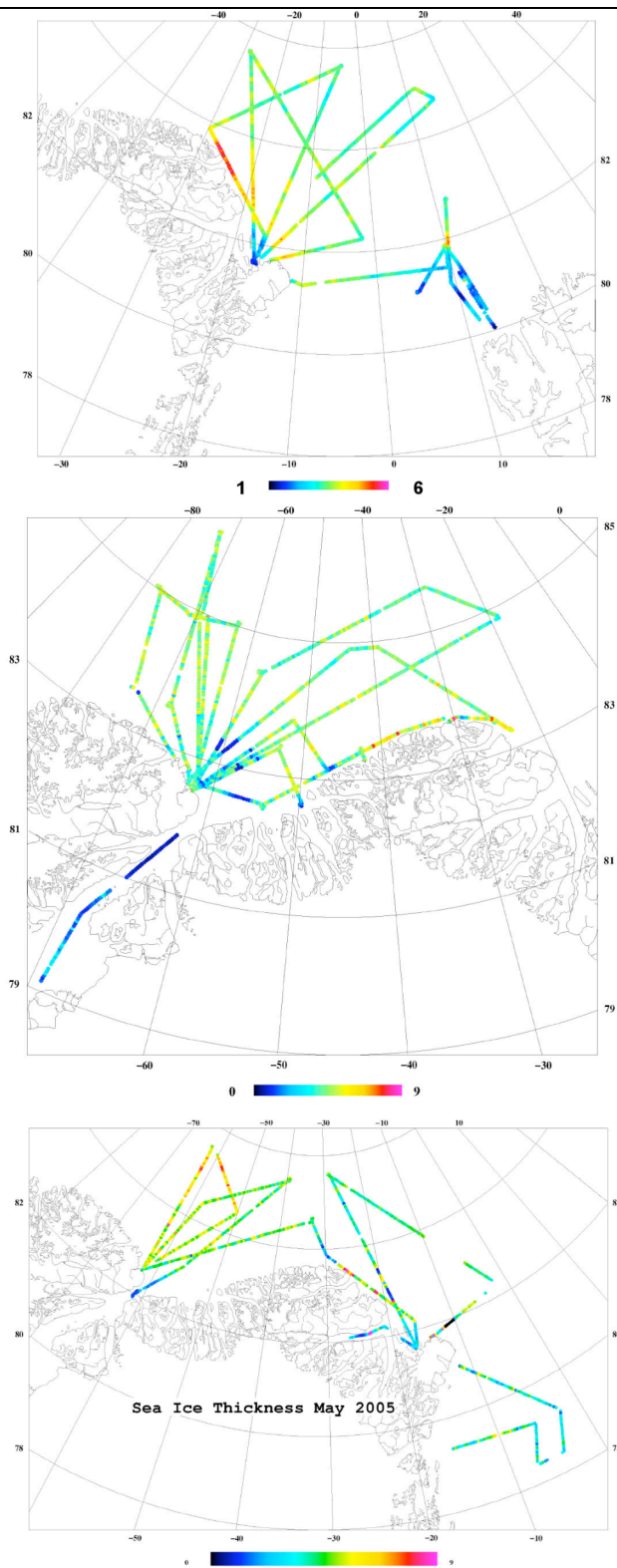


**Figure 5.5.** Sea ice thickness results from 2003 (top), 2004 (middle) and 2005 (bottom).

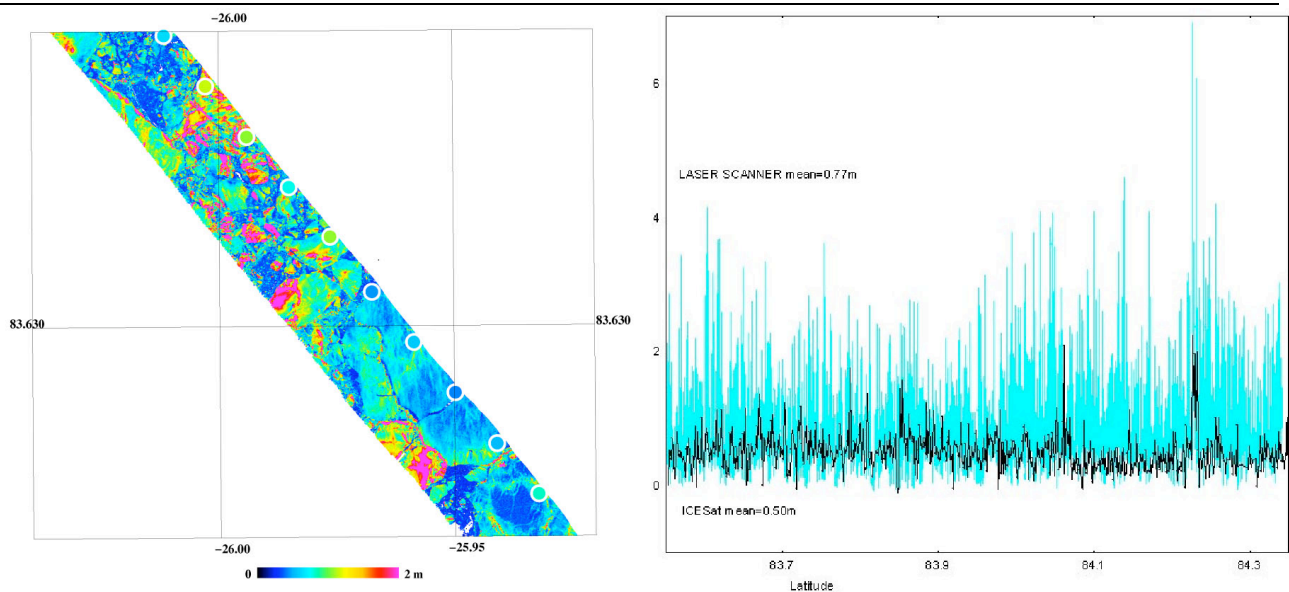


**Figure 5.6** Laser scanning swath example of freeboard heights north of Greenland with coincident ICESat heights (left: ICESat shown with dots; right: airborne lidar in blue, ICESat in black).

### 5.3.3 Comparison of laser scanner and HEM observations

Both in 2003 and 2005 laser scanner and helicopter EM measurements were coordinated. The coincident data sets from the two campaigns are shown in Figure 5.7. The results of the comparison between the two data sets are shown in Tables 5.1 and 5.2.

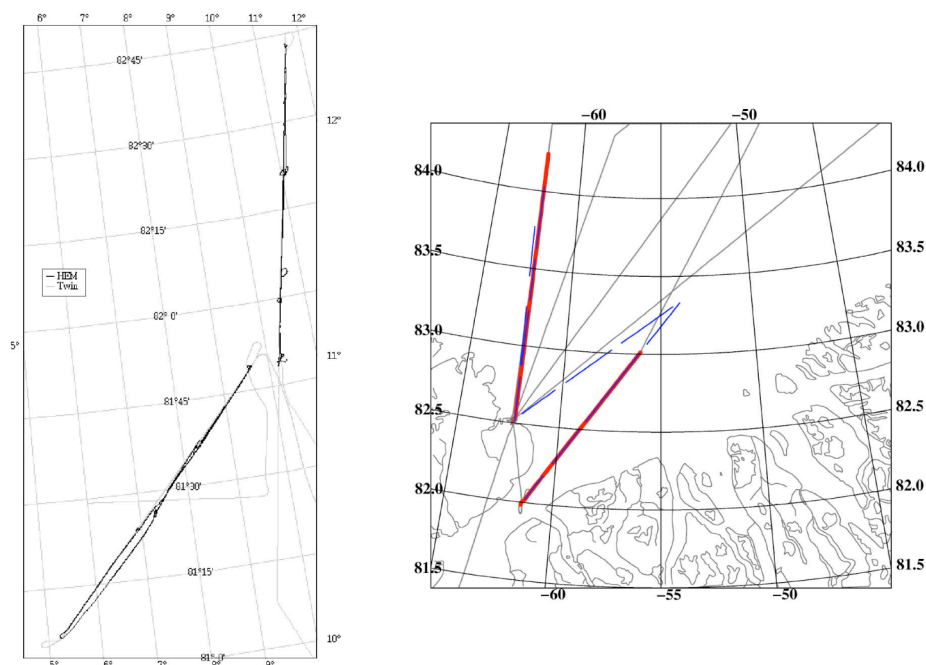


**Figure 5.7.** Location of coincident tracks in 2003 (left) and 2005 (right).

The two data sets have been matched and only coincident observation points have been compared. Fairly good agreement between the data sets are found, with generally higher thickness values estimated by the laser scanner system. This may be caused by underestimation

of the thickest ice, especially ridges, by the HEM system. Though, the differences are within the accuracy of the laser scanner method of 0.5-1 metres depending of the accuracy of the ratio between sea ice freeboard and thickness. Examples of the match of features observed by the two systems are seen in Figure 5.8.

*Table 5.1. Comparison of the 2003 data*

Data type	Mean Thickness (m)	Modal Thickness (m)	Std. dev. (m)
Laser scanner 11 April 2003	2.12	1.3	1.56
HEM 11 April 2003	2.05	2.5 (0.4/1.3)	1.24
Laser scanner 15 April 2003	3.83/3.67*	3.3/3.1	1.77/1.66
HEM 15 April 2003	3.40	2.5	1.44

*Table 5.2. Comparison of the 2005 data*

Data type	Mean Thickness (m)	Modal Thickness (m)	Std. dev. (m)
Laser scanner 13 May 2005	5.94	1.0/4.8	2.95
HEM 13 May 2005	5.20	0.0/4.2	2.52
Laser scanner 14 May 2005	3.73	2.4/4.8	2.04
HEM 14 May 2005	2.90	1.8/3.8	1.75

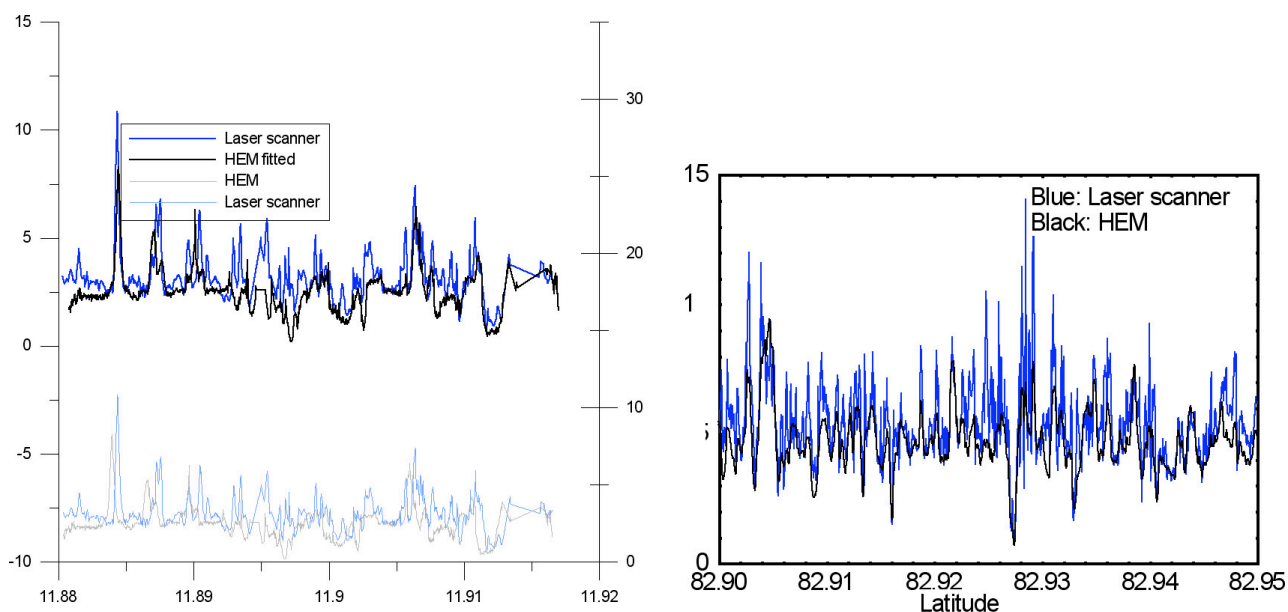


**Figure 5.8** Examples of matched laser scanner derived sea ice thickness, blue, and HEM thickness, black. Left is an example from April 2003 in the Fram Strait and right, an example from measurements in the Lincoln Sea in May 2005.

### 5.3.4 Discussion of results

Through the SITHOS flight campaigns it has been demonstrated that the airborne lidar measurements are an effective way to measure sea ice thickness and freeboard over large scales

(100 to 1000 km). It would therefore be a logical step that a future sea ice observing system incorporates a component of regular airborne lidar flights, which performs an import “bridging” of sea ice scales between locally based ground- and helicopter work and satellites, and the more sparse information from submarines and icebreakers. Further description of the results are presented in the reports by Keller et al., 2004, Dal  et al., 2005, Hvidegaard et al., 2006.

The relatively low costs of the airborne operations, and potential possibilities to carry these out in different seasons of the years, would mean a major supplement to satellite measurements, such as with the future Cryosat-2. Coincident EM measurements, and in-situ measures of the K-factor, will continue to be useful to quantify the inherent errors in the freeboard to thickness conversion.

## 6. Results from ULS measurements

### 6.1 The submarine mission in April 2004

In April 2004 *HMS Tireless* conducted an Arctic operational voyage (ICEX-04) during which upward-looking sonar profiling of the ice canopy was carried out. During this cruise over 9,000 km of data was obtained of which about > 3,000 km was ice draft and accompanying oceanographic data. In addition sidescan sonar imaging and along-track oceanographic measurements were carried out. Nicholas Hughes (SAMS) was on board as mission scientist and advisor. Two sonar systems were in simultaneous use for the scientific legs of the voyage. The first of these was an Admiralty-pattern 780 system recording on paper chart. This was identical to the system used by *HMS Superb* in May 1987 (Wadhams, 1990 and 1992) and *HMS Trafalgar* in September 1996 (Wadhams and Davis, 2001), as well as other UK submarine voyages of the 1980s and early 1990s. The second was a narrow-beam digital system, the 2077, which is better at resolving the structure of individual pressure-ridge keels.

In 2003 preparations began for a Royal Navy return to the Arctic with civilian scientific involvement. *HMS Tireless* sailed for the Arctic in late March 2004 with Nicholas Hughes at the scientific advisor. Work included:

- a) Oceanographic survey of the central Greenland Sea
- b) Oceanographic survey of the Molloy Deep and sea ice survey in the Fram Strait.
- c) Ice draft surveys along 5 E to the North Pole.
- d) Ice draft surveys along the line of latitude 85 N to replicate surveys done in 1976 and 1987.
- e) Ice draft survey of the Lincoln Sea.

The route of *Tireless* covered a large area of the European sector of the Arctic from 5 E to 62 W (Figure 6.1). Transects were carried out from the Marginal Ice Zone (MIZ) in Fram Strait up to the North Pole and along the 85 N parallel north of Greenland. Sites investigated included the Molloy Deep and eddying along the MIZ, the site of warm Bering Sea Water (BSW) incursion at the Morris Jessup Plateau and sea ice over the Lincoln Sea. A total of 9 days of dedicated submarine time was achieved.



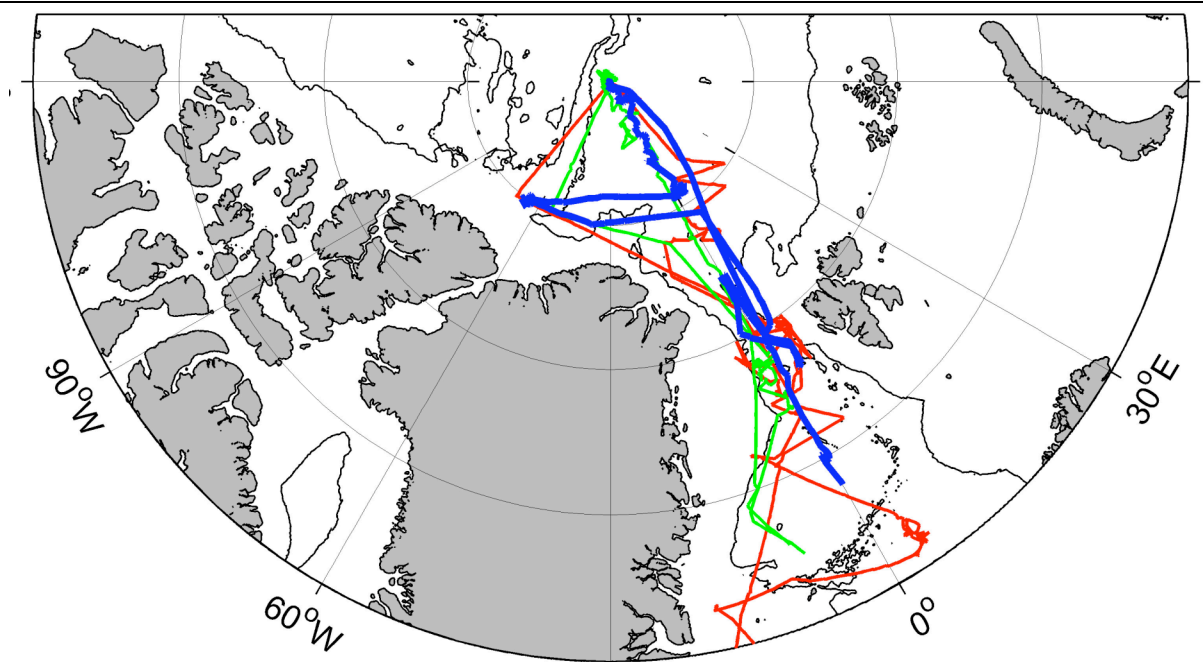


**Fig. 6.1.** Submarine tracks; 1976 (red), 1987 (green) and 2004 (blue). The 2000 m isobath is also shown as a thin solid line.

Whilst sea ice in the Arctic is observed to be decreasing in extent and thickness there would still appear to be regions where large scale ice circulation patterns maintain near similar thicknesses to those observed in the 1980's. In the late 1990's it was believed that the Beaufort Gyre had weakened reducing ice thicknesses north of Greenland. The situation almost 10 years later would appear that this thick ice draft seen in the late 1980's has re-established itself in 2004. Figure 6.2 shows the ice draft in degree bins along the 85°N with maximum observed keel depths per degree longitude also shown in the depth of the Atlantic Water, AW, defined as the depth of the 0°C isotherm) depths as well as the bathymetry as seen by the submarine.

The ICEX-04 demonstrates that manned submarines still have a role to play in scientific exploration of the Arctic Ocean. Whilst most Autonomous Underwater Vehicle (AUV) technology has advanced the battery technology to power them has not thus limiting the range over which they can operate. The use of a full-size submarine provides scope for pan-Arctic monitoring and a flexibility to reverse course and carry out a detailed survey of an area of interest as it is encountered.

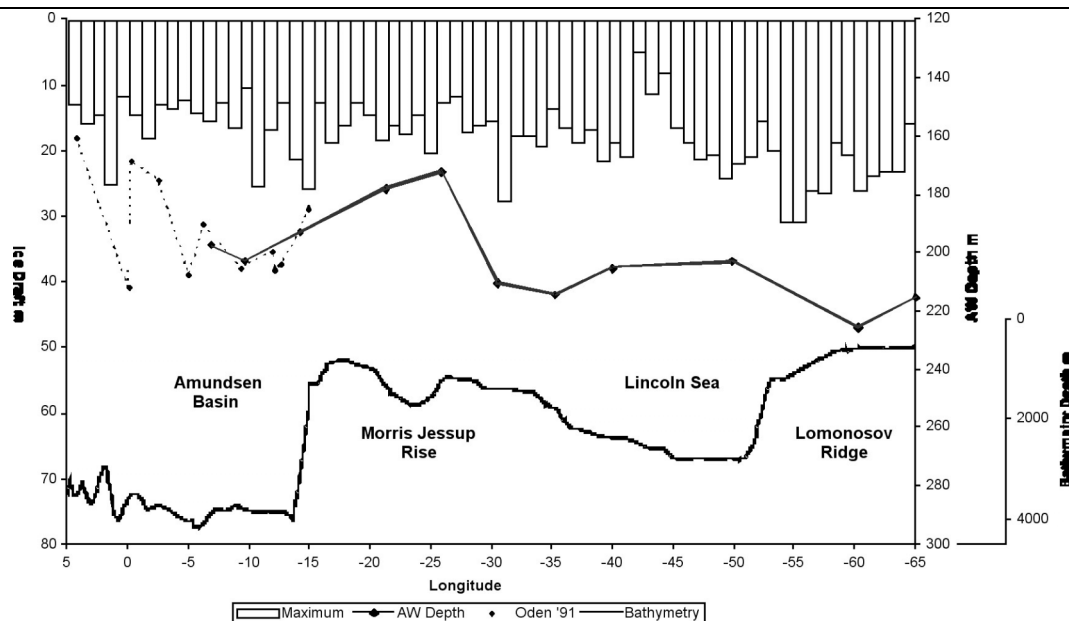


**Figure 6.2.** Section along 85°N with maximum observed keel depths per degree longitude, Atlantic Water, AW, (0°C isotherm) depths and bathymetry

## 6.2 Autonomous Underwater Vehicles

At present only submarines can provide true direct ice thickness mapping over large regions of the ice covered seas. The continued availability of submarines (US and British) is therefore essential to the task of monitoring Arctic ice thickness through the present period of rapid change. Since the end of the Cold War, however, the deployment of British submarines in the Arctic has become more sporadic (the previous mission before 2004 occurred in 1996), and the US civilian Scientific Ice Expeditions (SCICEX) programme, which also produced much valuable data on Arctic sea ice from submarines, ended in 2000. Given the probable continued shortage of submarine availability, the use of autonomous underwater vehicles (AUVs) under sea ice is clearly an attractive option which allows scientifically controlled missions.

### 6.2.1 The Vehicle

The Autosub AUVs are built and operated by National Oceanography Centre, UK. They are 7 m long, 3.6 tonne AUVs which are powered by 500 kg of primary manganese alkaline batteries, and have a range of 300 km at a speed of 1.8 m s<sup>-1</sup>. The depth limit for the vehicle used in this campaign was 1600 m. The navigation system relied on a Doppler sonar system, able to track the seabed at ranges of up to 500 m, and an Ixas-Oceano PHINS, a fibre optic gyro -based inertial navigation system, which together are able to give dead reckoned positional accuracies of 0.1% of distance travelled. Dual conductivity, temperature and depth (SBE-911 CTD) systems as well as a dissolved oxygen sensor (SBE-43) were installed in the nose section. Upward (300kHz) and downward (150 kHz) looking RD Instruments Acoustic Doppler Current Profilers were used for navigation, current profiling, collision avoidance and bathymetric and low resolution ice draft measurements. For high resolution mapping of the ice underside the Simrad EM-2000 swath multibeam bathymetric mapping system was mounted looking upwards; this produces a swath equivalent to 111 independent beams equally spaced on a horizontal plane. Data obtained from the EM-2000 was processed using software developed in-house and projected on to a 2 m by 2 m grid.

### 6.2.2 The surveys

More than 450 km of under-ice data were obtained during the 11 missions performed in the region between 17<sup>th</sup> August and the 26<sup>th</sup> August 2004 (M358 – M368, Figure 6.3). After five successful test missions under the drifting ice of Fram Strait and the western edge of Belgica Bank (M358 – M362) we were ready to perform the first exploratory runs under the NØIB (Norske Øer Ice Barrier). On 19<sup>th</sup> August the RRS *James Clark Ross* reached the western extremity of the NØIB and at 17:23 mission M363 was released: a 24 hour mission running in an easterly direction under the NØIB towards the coast of Greenland. Autosub's collision avoidance system was triggered during this mission and she aborted the mission and returned back to the ship early.

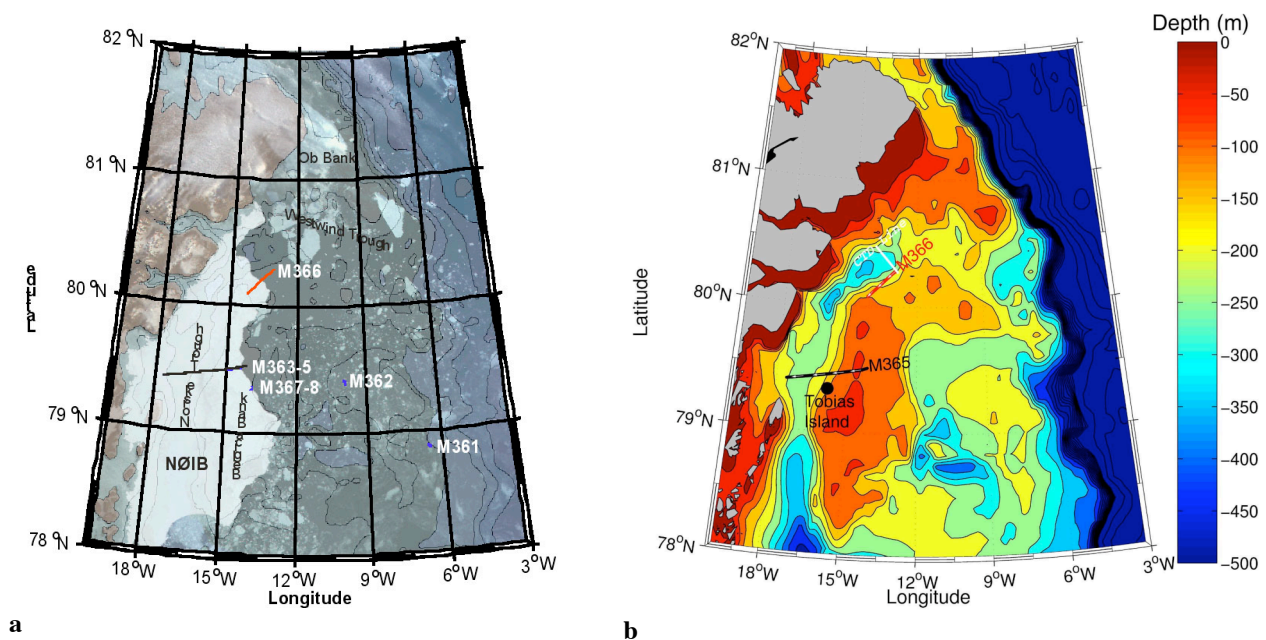


**Figure 6.3 (a)** MODIS TERRA visual image showing ice extent on NEG shelf, 12 August 2004 18:50. Bathymetric features mentioned in the text are shown, and the locations of Autosub-II missions., **(b)** Bathymetry of the NE Greenland shelf, according to IBCAO. Tracks of missions M365 (black) and M366 (red) are shown.

In order to avoid the same obstacle that tripped the collision avoidance system during M363 the angle of the run was slightly altered and Autosub was released again (M364). However the collision avoidance system was activated in the same vicinity and she returned to the ship. The angle of the mission was again modified and this time she completed the mission (M365) and obtained 150 km of data. During the return leg of M365, the Autosub collision avoidance system was activated when the forward-looking sonar detected a deep ice keel ahead. After successful manoeuvring around this obstacle, the recovery of Autosub was hampered by ice which had drifted over the intended recovery position, necessitating the use of a acoustic homing system to shepherd the AUV to a safe ice-free area for surfacing and recovery. This mission proved the total autonomy of this vehicle as well as its problem solving capability by successfully avoiding obstacles that were in its path. We know that the reason for the triggering of the collision avoidance system during these missions was a ridge extending over 30 m in depth. The 3-dimensional image of this ridge from the multibeam sonar can be seen in figure 6.4.

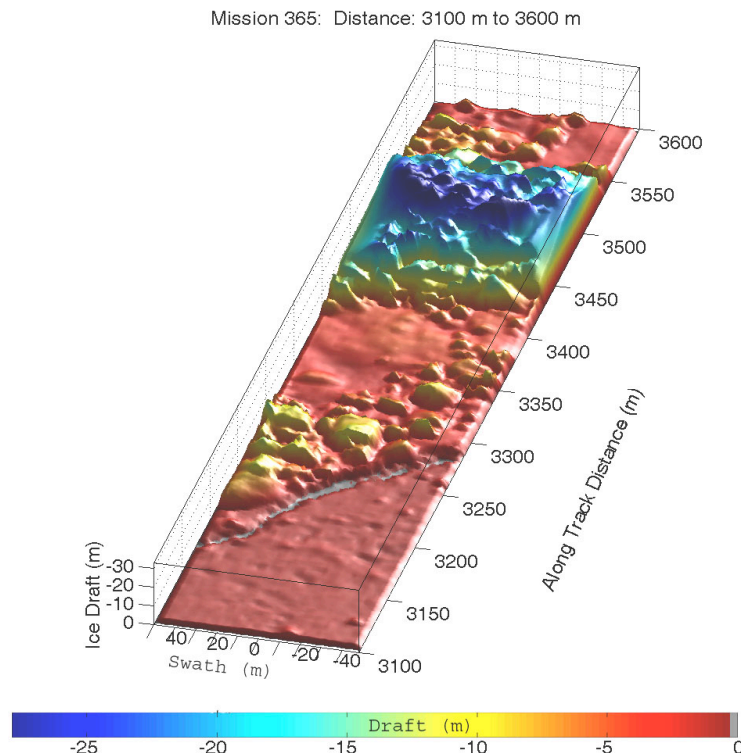


**Figure 6.4.** A 500 m section from the EM2000 multibeam (M365) showing a deep 33 m ridge on Belgica Bank, with shallower ridge (10+ m) in foreground ending in a small lead (grey). The undeformed ice surrounding the ridge is less than 2 m thick. This multibeam image is in perspective view, and is illuminated by a sun of elevation 20°. Data points fill 2 m x 2 m grid. Data aspect ratio is 1:1:1.

After this successful mission M366 was performed at the northern region of the NØIB. M367 and M368 were performed near to M365, the western edge of the NØIB, in order to perform an overlapping “lawnmower” survey of the region.

While the Autosub was active the sea ice team ran lines of drilled holes parallel and perpendicular to the vehicle’s track for ice and snow thickness measurements and obtained ice cores for salinity and ice fabric analysis. Further ice characterisation was performed during the “lawnmower” surveys (M367 and M368) in partnership with an ice team from the German research ship RV *Polarstern*. This involved drilling and coring by the UK team, and profiles by sledge, resistivity and ground penetrating radar systems by the German team. Unfortunately due to the heavy fog the coordinated helicopter-mounted EM, which was to give total ice + snow thickness, could not be run over the corresponding tracks of Autosub.

### 6.2.3 Data

The following figures shows some examples of the magnificent quality of data obtained from the Simrad EM-2000 swath sonar system. Each of the displayed images is a perspective view of the underside of ridged ice, obtained at 40 m depth. The scenes are shown illuminated by a sun of elevation 20°. Alongside each image is a probability density function (pdf) of ice draft for the image region compared with a pdf for the entire mission.



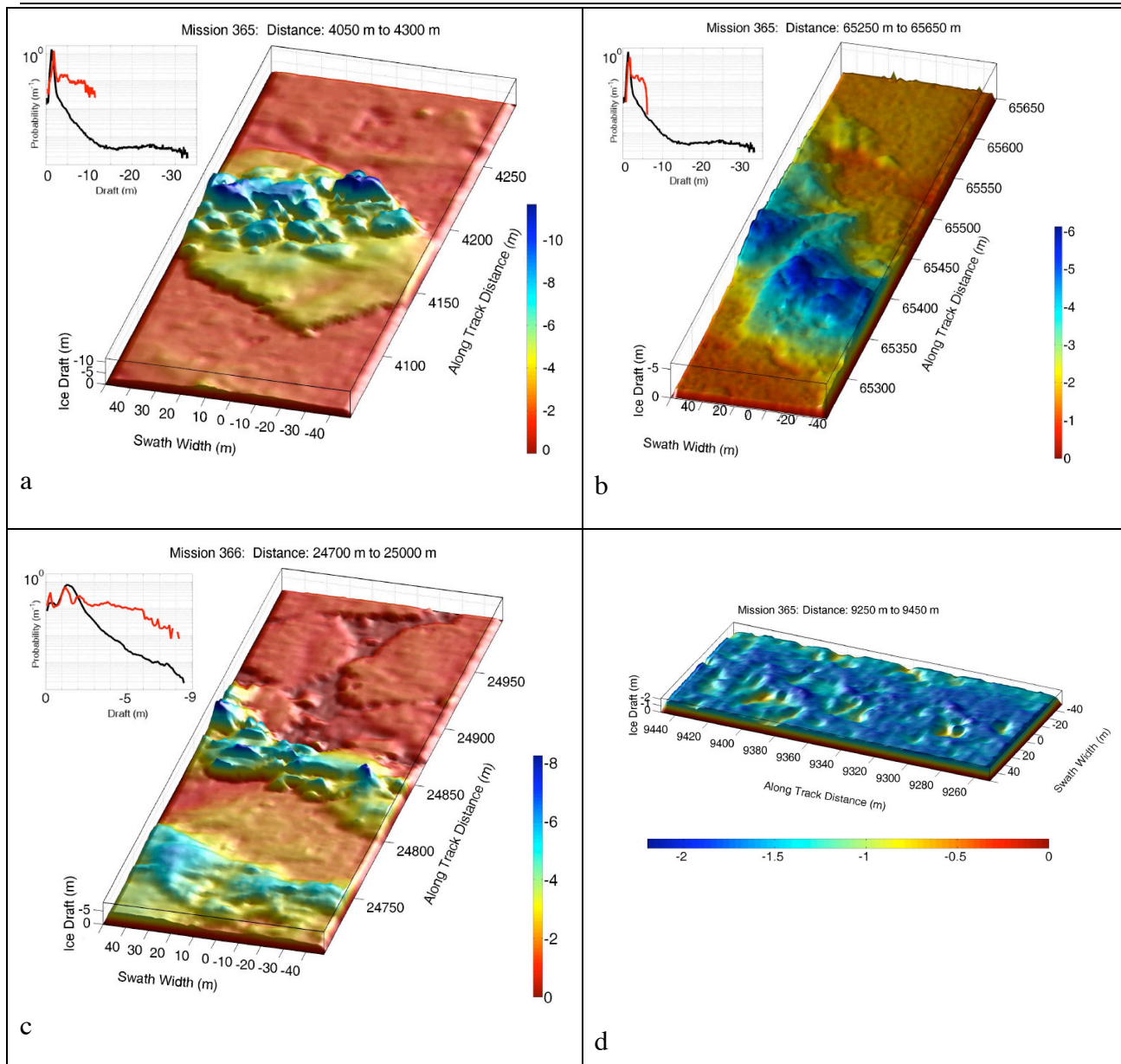


**Figure 6.5. Examples of results from the Simrad EM-2000 sonar system:**

(a) is a 100 x 250 m image also obtained over Belgica Bank. It shows an old multi-year ridged floe of thickness 3-5 m which is clearly embedded in younger fast ice of draft 1.8 m. The older, thicker floe resembles floes seen in the marginal ice zone (MIZ) of Fram Strait, where large sheets of advecting Arctic sea ice are fractured by wave action and turned into floes of typical diameter 100 m retaining fragments of their original pressure ridges. The edges of the floe are sharp and linear as would occur with a fracture which occurred just before embedding.

(b) is from the western limit of M365, near the coast of Greenland. It shows a pressure ridge of 6 m draft, the only pressure ridge in this region, after more than 30 km of undeformed fast ice. The ridge axis is oriented at 45° to the track of the AUV. The fast ice around the ridge has 1.7 m draft, while further to the east, across the trough and bank, it is only 1.0-1.3 m, indicating either that in this western part of Norske Trough, close to the continental influence of Greenland, the ice grows more rapidly, or that unbalanced isostasy in the ridge is affecting the draft of nearby ice.

(c) is from M366 into Westwind Trough, showing in the background broken first-year floes (1.2 m) glued together by very young ice (0.25 m), with a young (probably first-year) ridge in the centre of the image and an old worn-down hummock in the front. Between the two is a multi-year floe of



thickness 1.85-2.25 m containing the hummock. The young ridge is may be formed by motion or pressure between the first-year ice and the older floe. The contrast between the sharpness of topography in the two ridges is dramatic, showing the effect of a number of years of ageing and partial melt in rounding off the blocky topography of the older ridge.

(d) shows an example of a large undeformed multi-year floe which has developed a much deeper system of melt pool-associated depressions than the first-year ice of fig.(b). The contrast between very shallow pools (3(b)) and canyon-like craters on the upper surface is because each year the refrozen melt pools from the year before reopen and deepen, causing increased compensating melt on the underside. This image is vertically enhanced to 4:1 to show the crater-like nature of the features. We infer that the floe was multiyear despite a modal draft of only 1.7 m because it lay close to our validation line, where the modal draft was also 1.7 m and where the thickness-averaged salinity of the ice cores was only 0.96 PSU, characteristic of multiyear ice.

The accompanying pdfs are of particular interest. The advantage of having 111 beams is that good quality pdfs can be obtained over much shorter distances than the 50 km commonly employed for single-beam upward sonar. The pdfs yield wholly new information about ice draft distribution. Hitherto it was known from long upward sonar profiles that the pdf has a tail with a negative exponential form but now we see that this is created by the superposition of a series of top hat functions each due to a single ridge, which are flat as far as an ultimate drop-off depth, as would be expected from a basically triangular geometry. The overall pdf of M365 approaches a negative exponential from 3-10 m draft but then flattens out as the only contribution to deeper ice comes from the single ridge in figure 4. These results highlight the advantage of obtaining a high resolution 3-dimensional image of the underside of the ice compared to traditional single beam sonar.

#### 6.2.4 Conclusions

Autosub operated highly successfully under Arctic sea ice, obtaining 458 km of high quality upward looking swath sonar data and accompanying oceanographic data. It undertook necessary avoidance manoeuvres for obstacles, and the acoustic homing system ensured that the vehicle could be returned with confidence to an area covered with loose moving pack ice. The vehicle is clearly a rugged and useful measuring tool for studies under sea ice. The combination of an unmanned under-ice vehicle and a multibeam sonar gives, literally, a new dimension to under-ice studies, and is important for work on ice thickness changes, the disappearance of deep ridges from the Arctic, navigability in ice, the effects of oil and other pollutants, the interactions between sea ice and under-ice currents and water structure, the underside as biological habitat, and many other studies critical to the role of ice in polar climate change.

It is hoped that this successful ice profiling mission will be a precursor to larger-scale missions with AUVs which will develop into a major monitoring effort for Arctic sea ice changes. Also ice thickness results from future AUV runs can be used to validate freeboard estimates from the satellite altimeters, in order to allow mean ice thickness to be estimated throughout the Arctic.

The AUV has many advantages, notably the high resolution which is possible by sailing close to the ice bottom, a possibility which manned submarines cannot enjoy for safety reasons; and the possibility of a closely controlled tight or overlapping grid of imaging tracks. The main drawback of the present AUV is lack of range when compared to nuclear submarines.

## 7. Results from radar altimeter measurements

### 7.1 Introduction to radar altimetry for ice thickness retrieval

Satellite radar altimetry has the potential in providing estimates of sea ice thickness from direct measurement of ice freeboard. Preliminary results from the ERS radar altimeter show good agreement with in-situ submarine observations and reveal that Arctic ice thickness is highly variable and largely controlled by the length of the summer melt season [Laxon, et al., 2003]. The objective of our work in SITHOS is to develop techniques to carry out similar mapping using data from the Envisat RA-2 radar altimeter. This instrument has a number of new features compared with the altimeters on-board ERS-1/2 which should improve the retrievals of freeboard and hence thickness. Our starting point has been to adapt the ERS processing scheme and then investigate differences between the ERS and Envisat retrievals of ice freeboard and also sea surface topography. These comparisons have been delayed due to the lateness of data delivery from ESA but these problems are now fixed allowing us to show the first comparisons of retrievals from the two instruments and to identify areas for tuning of the Envisat algorithms.

Since September 2003 CPOM has been developing a processing system to extract sea ice thickness from Envisat altimetry data as part of the SITHOS project. The system can now produce ice freeboard and thickness maps within a short time of receiving the satellite data. As will be explained in the report, there remain some problems with the freeboard maps and addressing these will be the subject of further work. Rather than showing ice thickness, the results are presented here as freeboard so as not to complicate the matter with the further uncertainty of snow depth and density.

Unfortunately only one validation dataset suitable for comparison with the altimetry has been received. Further validation work will be carried out.

## 7.2 Data availability

Envisat SGDR altimetry data now arrives regularly in house about 3 months after collection and we now have a complete dataset running from September 2002 to August 2005. The results presented in this report are based on the three complete winters of data: 2002/2003, 2003/2004 and 2004/2005. The 2002/2003 winter is of particular importance because it is the only complete winter where Envisat results can be compared with those from ERS-2. After 23<sup>rd</sup> June 2003 a problem with the on board tape recorder drastically reduced the ERS-2 Arctic coverage making comparison with Envisat results difficult.

Although 3 complete winters are now available, the project was delayed in the early stages by late arrival of the SGDR data. Of particular importance was the data before mid January 2003 during the vital overlap period with ERS-2. This data was originally produced for the Cross Calibration and Validation Team (CCVT) and used different processing parameters to the more recent data, making a consistent comparison with ERS-2 difficult. The reprocessed data from the CCVT period has only arrived intermittently over the last year.

## 7.3 Method description

The method used to extract sea ice freeboard from Envisat altimetry data is heavily based on the already published method used for ERS-2 [Peacock and Laxon, 2004; Laxon et al., 2003]. Radar echoes returning from the leads and ice floes are identified by their shape, the leads causing the echo to have a peaky or specular appearance and the floes causing a more broad or diffuse echo shape. After filtering out bad echoes, a satellite to surface range is computed from the radar echo using a process called 'retracking'. This range is corrected for various propagation delays in the atmosphere and then deducted from the known altitude of the satellite above a reference surface to give the sea surface height in the leads and the height of the snow/ice interface on the floes.

The freeboard can then simply be computed by deducting the interpolated sea surface height at the floe location from the height of the floe.

Although the processing chain used for Envisat data is very similar to that used for ERS-2, differences between the two instruments mean that there are also some differences in the processing. The most important processing differences as listed below :

- 1) The filters applied to the radar echoes to remove bad data points have been specifically tuned for each instrument. This is an important processing step as bad data points can strongly influence the final freeboard results. Work is continuing to improve the filters applied to the Envisat data.
- 2) A pulse blurring correction was required when constructing the sea surface height in the leads from ERS-2 data. This pulse blurring correction is not required when using the more advanced Envisat instrument.
- 3) For a diffuse ERS-2 echo to be identified as coming from an ice floe, it has to be in a region where the SSIM ice concentration is above 40%. This threshold is now thought to be rather low and for the Envisat processing it has been raised to 75%.
- 4) Most importantly there are differences in the retracking algorithms applied to the returning echoes to extract lead or floe elevations from the echo shape. ERS-2 used a threshold retracking algorithm with an empirical extra correction for pulse peakiness to compute ocean surface height in the leads. This has been swapped for a Gaussian tracker on Envisat which studies over the Salar De Uyuni in Bolivia have shown to be highly accurate. To extract the height of the floes, an OCOG tracker is used in both cases. Envisat records twice as much of the returning echo as ERS-2 but this results in the echo tail being more influenced by the antenna response pattern. Because of this, the OCOG retracking technique measures the Envisat floe heights about 12 cm too high. Work is continuing to remove this bias by correcting the returning Envisat echo for the effect of the radar antenna response.

In spite of the differences between the two instruments and the processing methods used, freeboard results from ERS-2 and Envisat are now in reasonable agreement. Figure 7.1 shows a comparison of ice freeboard from the same 35 day cycle of both satellites. Note that the 12cm bias in the Envisat data mentioned above has been removed from the Envisat freeboard map.

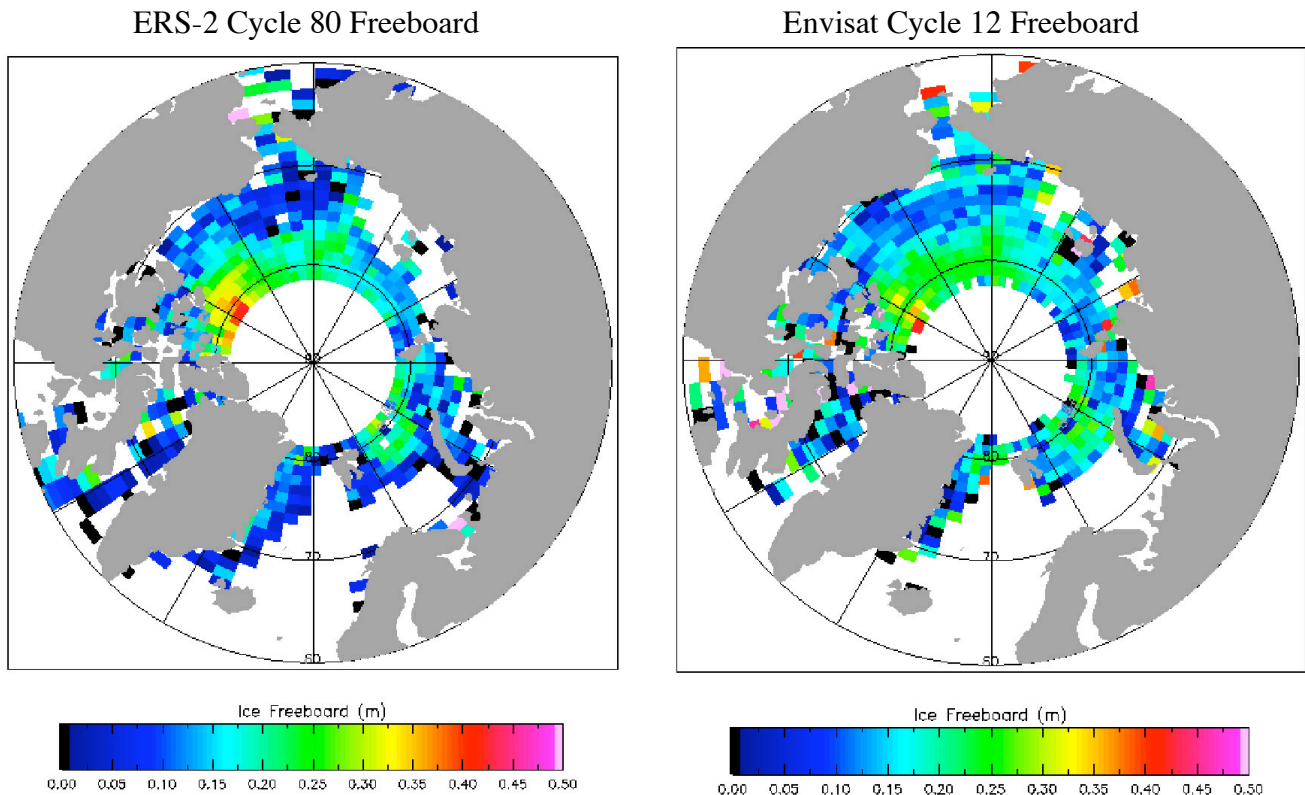


**Figure 7.1:** Comparison of Freeboard Maps from Envisat and ERS-2. A 12 cm bias has been removed from the Envisat freeboard map to match it to the ERS-2 map. The wider range gate of Envisat causes the return echo to be more influenced by the power pattern of the antenna, introducing a bias in the tracking of ice floe heights.

#### 7.4 Validation with in situ data

Figure 7.2 shows a preliminary comparison of freeboard (converted to ice thickness) retrieved from the Envisat radar altimeter, and EM helicopter ice thickness in the Fram Strait. There are clear differences between the altimeter and EM measurements with the altimeter data biased high. Additional differences may be due to the different sampling patterns of the two sensors. Further comparisons will be made once some remaining issues with the Envisat altimeter processing have been resolved. Submarine data was not available for comparison.

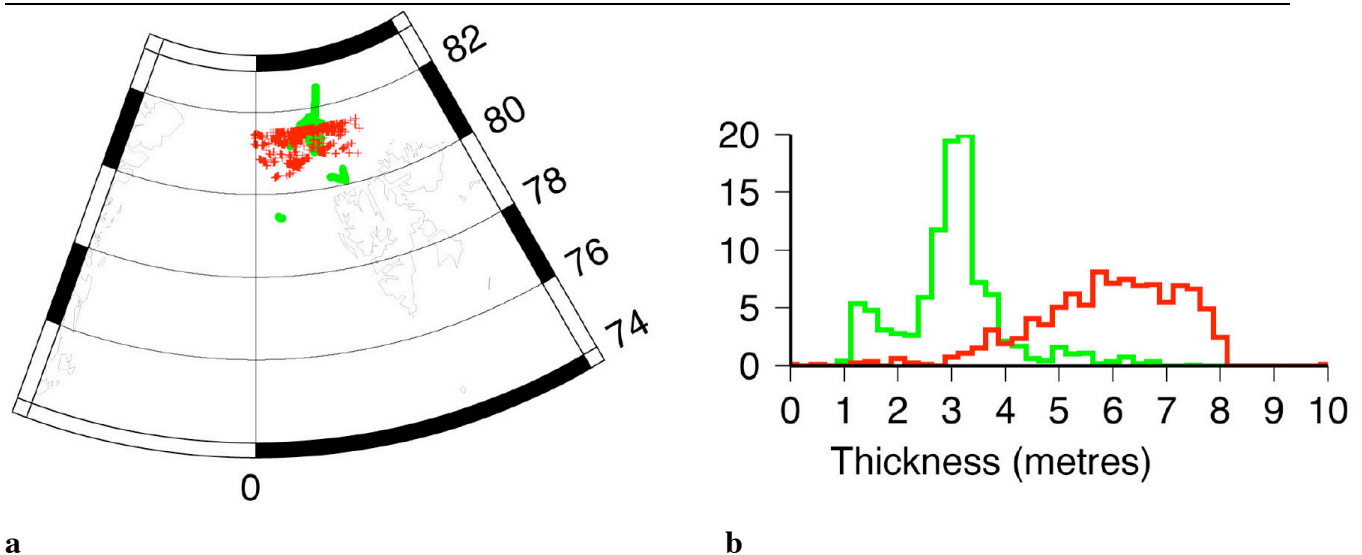


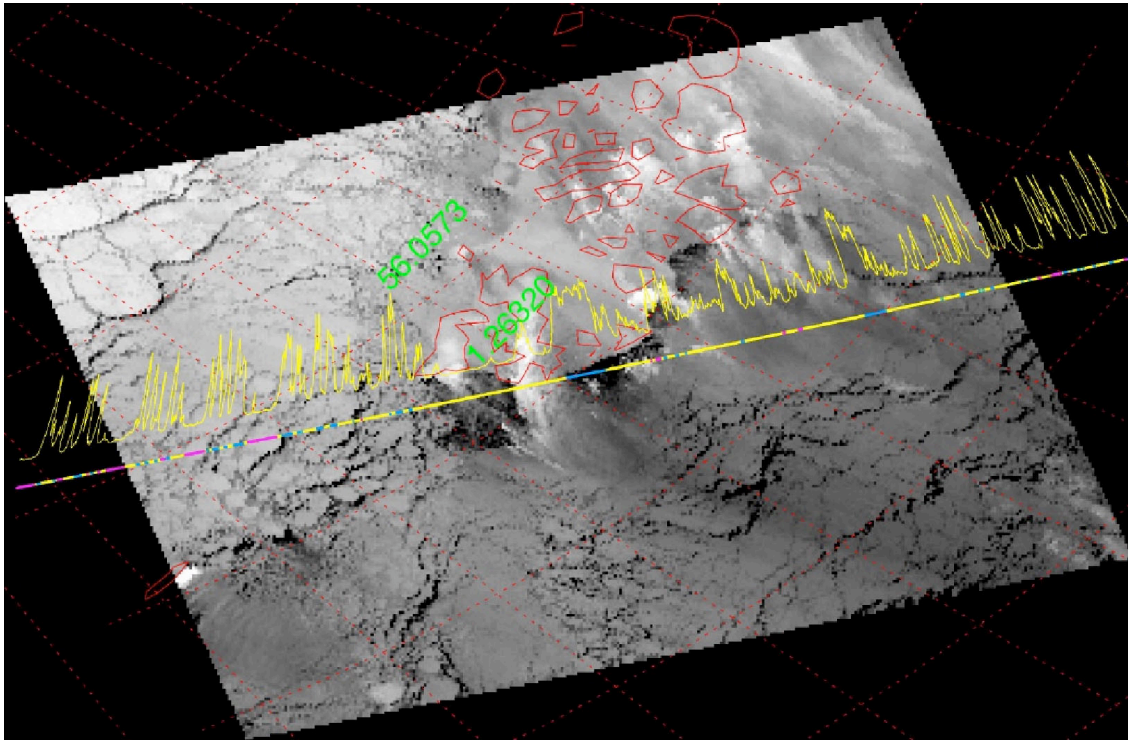
**Figure 7.2:** Comparison of Envisat ice thickness (red) and EM Helo measurements (green) in the Fram Strait during April 2003: (a) map showing the distribution of the EM data and altimeter data (left) and (b) probability distribution of ice thickness.

## 7.5. Discrimination checking with ATSR images

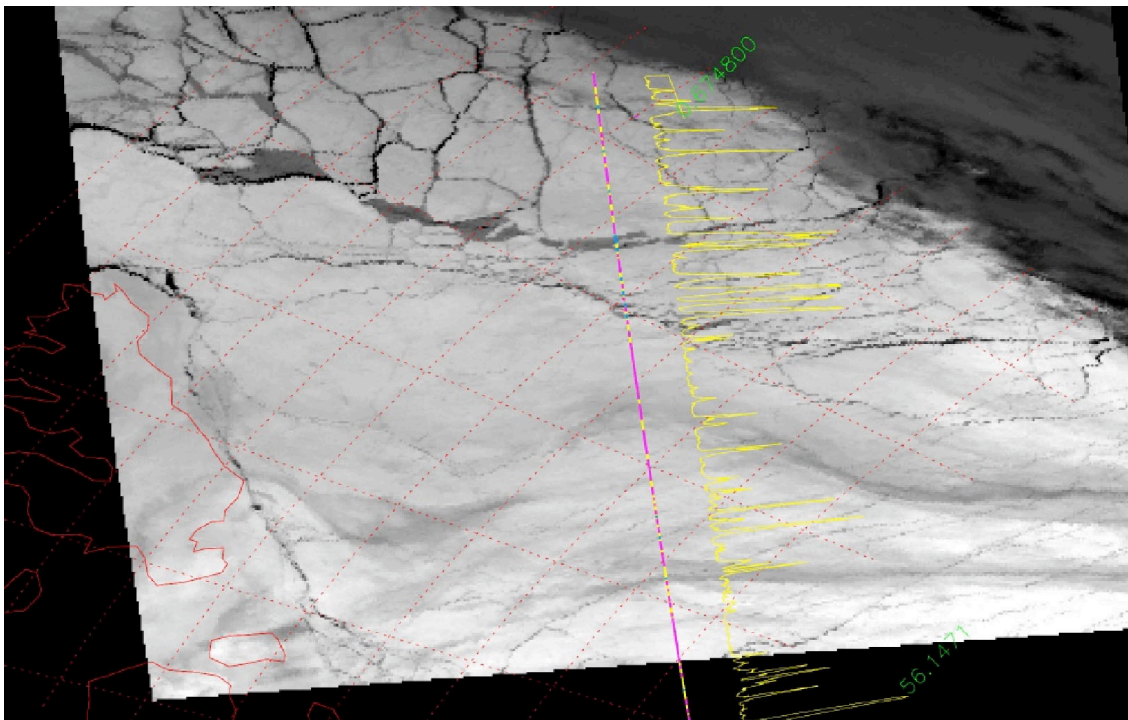
Correctly identifying leads and ice floes from the radar echo shape is a crucial step in the ice thickness processing. Several hundred AATSR quicklooks were searched for cloud free images coincident with the altimetry data. Software was then developed to overlay the altimeter echo type along the ground track to check the discrimination. Although the leads are correctly identified it is possible that some echoes from the ice floes are lost due to misclassification. Further comparisons will be performed to fine tune the discrimination.

In Fig. 7.3 the echo discrimination of ENVISAT altimeter data is compared with ice-open water signatures using simultaneous ATSR images. In the two examples an Envisat altimetry track has been superimposed on a cloud free ATSR image to check the echo discrimination. The track colour indicates how the processor categorised the radar echo. Purple = ice floe, Blue = open water or lead, Yellow = unknown. The yellow graph next to the tracks indicates pulse peakiness. The blue segments agree fairly well with the position of smaller leads, while the purple segments agree well with large ice floes. A large part of the refrozen polynya with thin and young ice to the south of Franz Josef Land (Fig. 7.3a) is classified as unknown.





a



b

**Figure 7.3.** Examples of comparison of altimeter echoes with ATSR image. The processor classifies the surface in three categories: purple = ice floe, blue = open water or lead, yellow = unknown.

## 7.6. Discussion of the results

The CCVT data has now been completely reprocessed and it was not used to produce any of the following results. A peakiness dependent bias seen when retracking specular echoes to construct the sea surface height in the leads. This has largely been solved by the new Gaussian retacker.

Figures 7.4a and 7.4b show the time series of freeboard maps from the winters of 2002/2003, 2003/2004 and 2004/2005. The freeboard values are averaged on a 1 degree latitude by 5 degree longitude grid and are uncorrected for the 12cm bias mentioned above. Only grid cells containing more than 6 input freeboard values are displayed. A high degree of variability can be seen from year to year in any particular month. The summer months are not shown because surface melting strongly influences the radar return making this method unsuitable for extracting freeboard at these times.

The maps shown in Figures 7.4a and 7.4b were used to get a single average winter freeboard map for all 3 winters. Only grid cells which were present in 4 out of the 6 winter month maps were included in the average map for that winter. Winter pairs were then selected and one deducted from the other to show interannual variability and the results from this are shown in Figure 7.5. Differences of up to 10cm can be seen from year to year, especially between the 2003/2004 and 2004/2005 winters where the freeboard in the Beaufort Sea near the Canadian Archipelago increases.

The 3 winter averaged maps mentioned above were then themselves averaged over the area of coverage in common to produce the short time series of average freeboard shown in Figure 7.6. The average freeboard values are also shown in the table below.

Winter	2002/2003	2003/2004	2004/2005
Freeboard (cm)	29.79	28.85	29.45

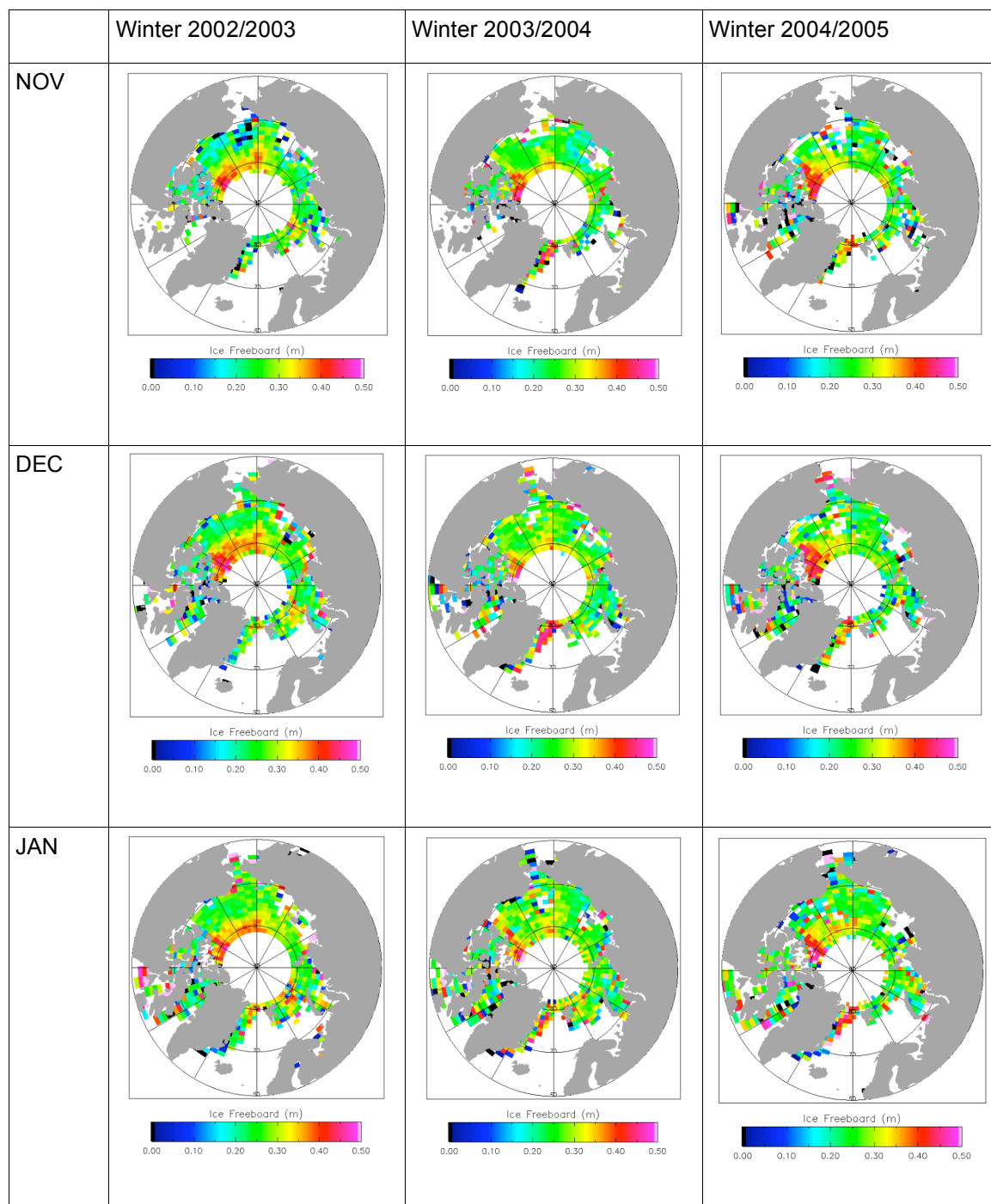


**Figure 7.4a :** Time Series of Envisat Winter Freeboard Maps. The panel shows the November to January freeboard maps for the first 3 winters of Envisat data.

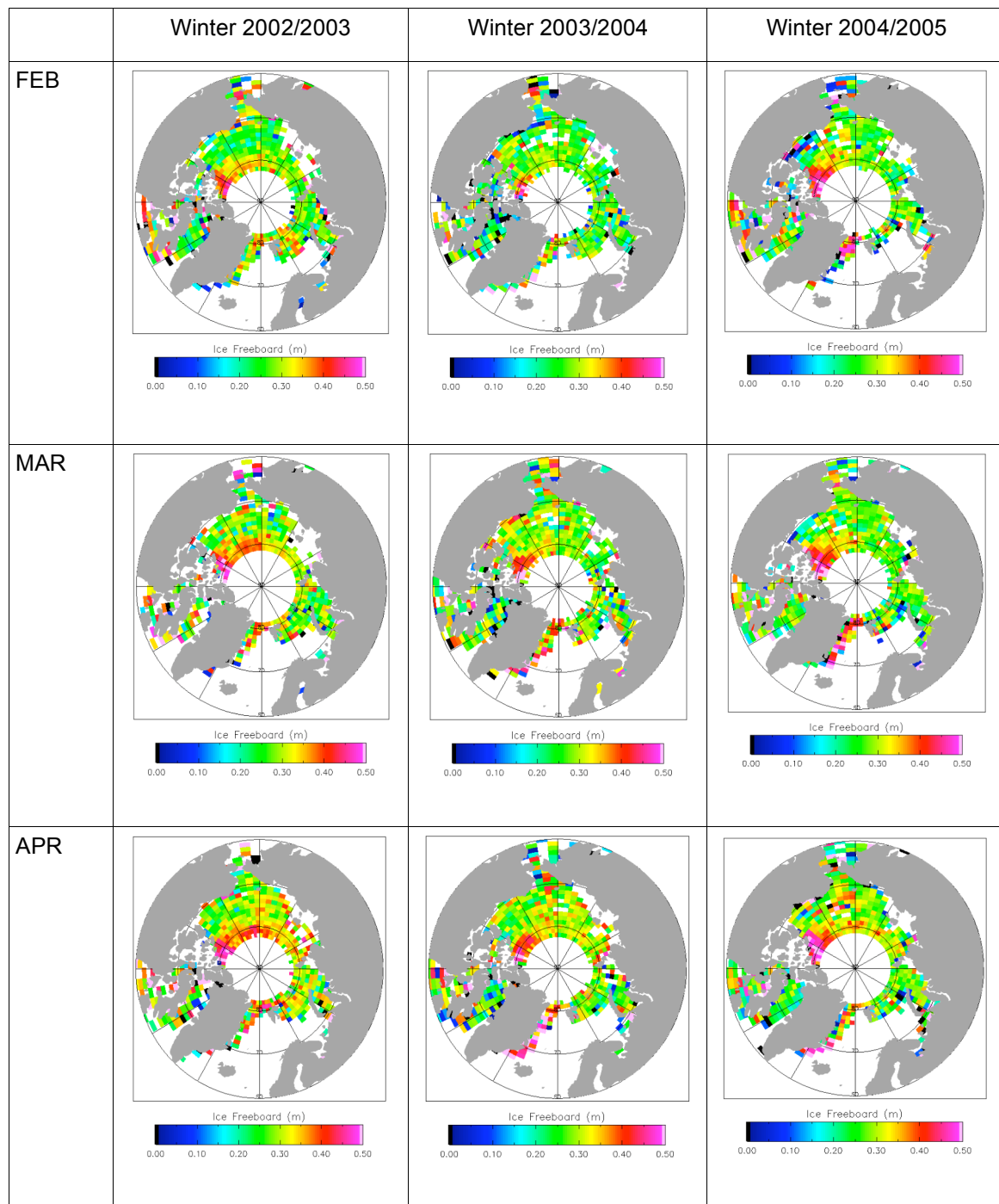


**Figure 7.4b :** Time Series of Envisat Winter Freeboard Maps. The panel shows the February to April freeboard maps for the first 3 winters of Envisat data.



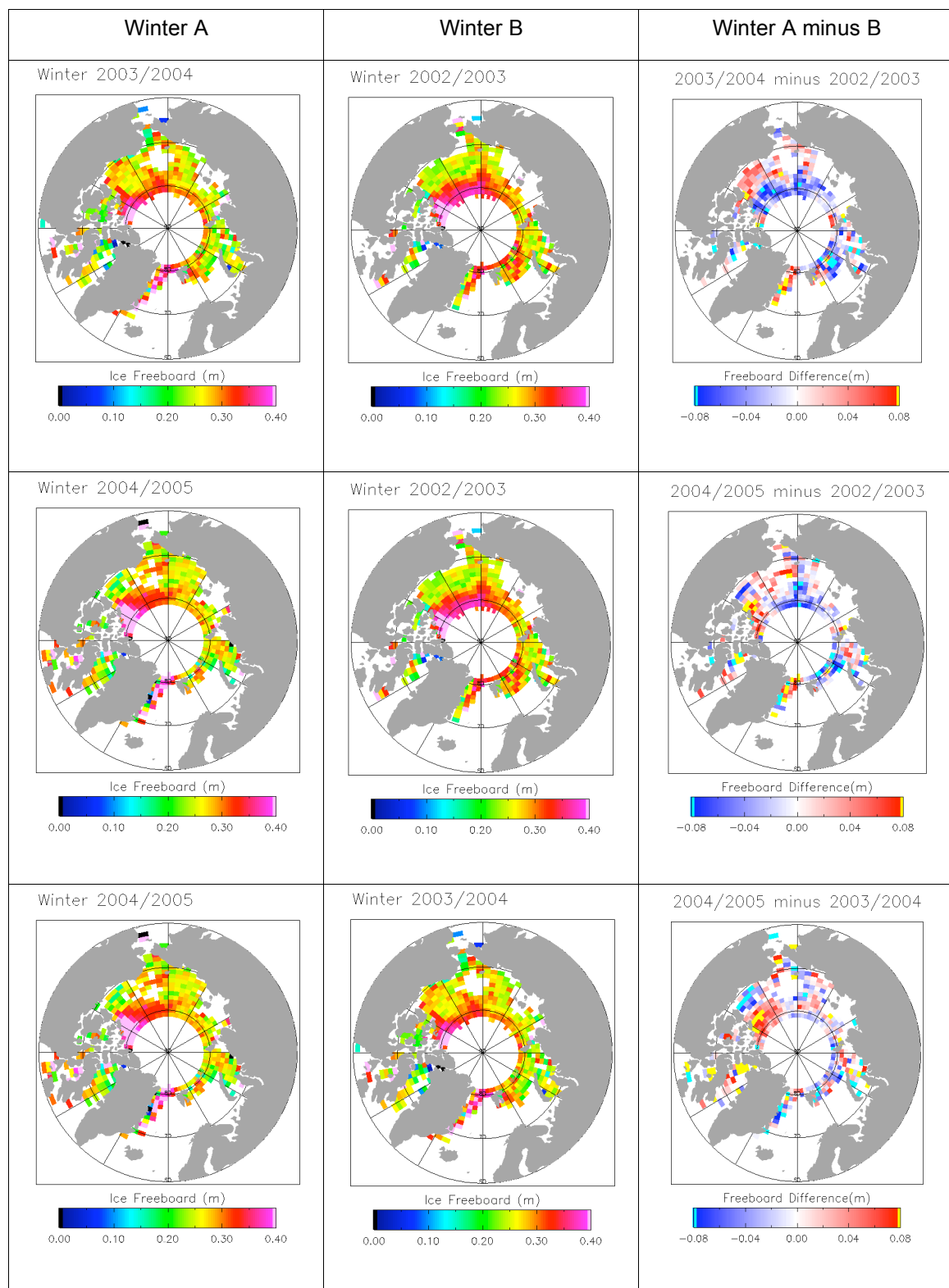


**Figure 7.5:** Changes in average winter freeboard. Freeboard maps for November to April are averaged to give an average winter map. Pairs of winters are then compared.



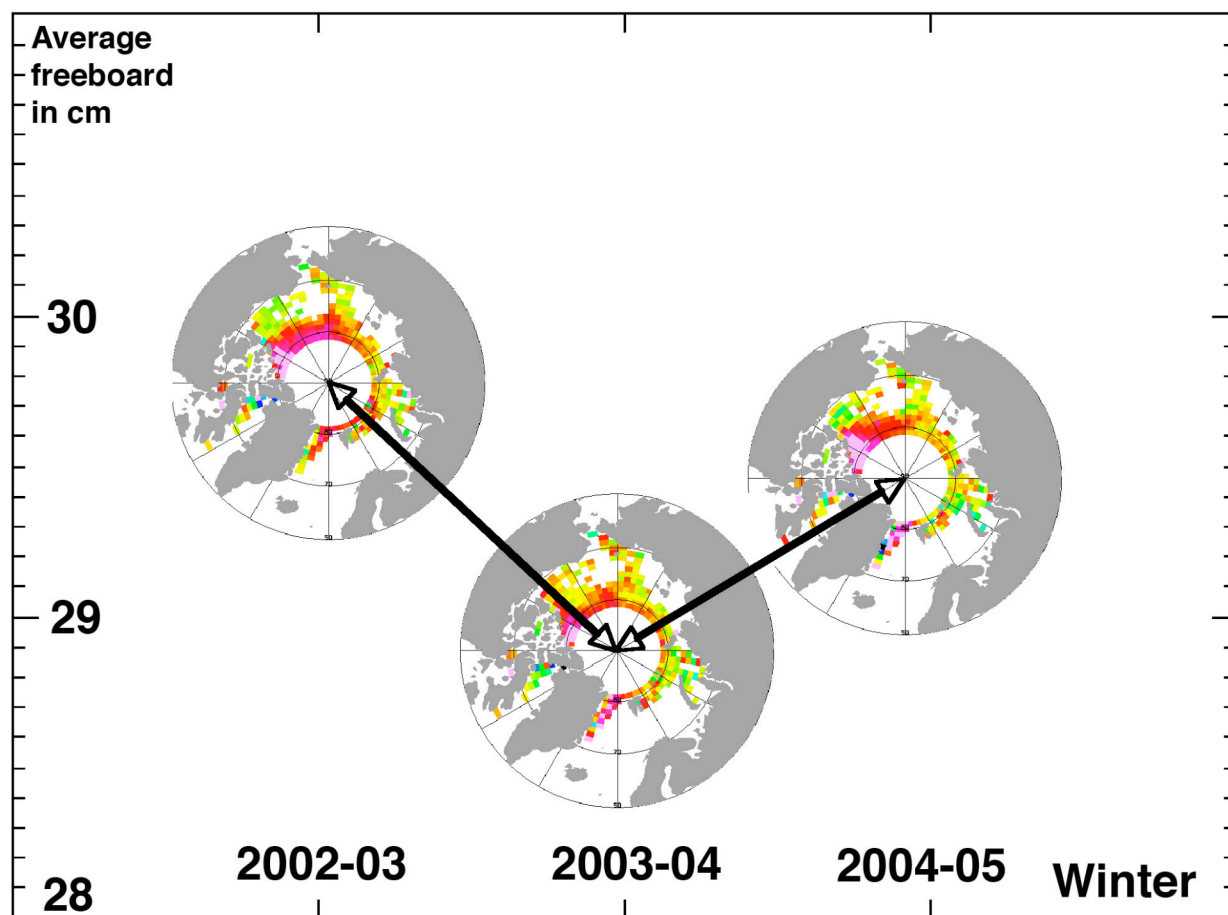


**Figure 7.6: Average Winter Freeboard Time Series.** Where freeboard measurements for all 3 winters are present, the average freeboard is computed to give a single freeboard value for the winter.

## 7.7 Concluding remarks

The failure of the Cryosat launch in October 2005 has increased the importance of the Envisat altimeter for monitoring sea ice thickness, and work will continue to try to improve on the current results. One of the highest priorities is to improve the performance of the retracking algorithms. It has already been mentioned above that waveforms should be properly corrected for the antenna response to remove the bias in the observed floe elevations. The tracking of the sea surface in leads is believed to be working well, but work is planned on developing a retracker specifically designed for this purpose which could make use of a larger number of the specular returns than can currently be used. Hand in hand with this, further work is planned on more accurately separating leads from floes and data filtering by looking at satellite imagery. Finally, further validation with in situ data is highly desirable.

## 8. Results from ice modelling

### 8.1 Introduction

The purpose of using sea ice models in SITHOS was to 1) compare modelled ice thickness with observed thickness using the different methods applied in the project, and 2) Define requirements for ice data from ice modelling point of view, addressing spatial and temporal scales of the data, measurement accuracy, and what ice parameters are need to be observed. In this chapter, results of various sea ice models at NERSC and AWI are presented. NERSC has focused on simulating long-term variabilities in ice thickness in five different thickness classes and comparison of modelled ice thickness with observed ice thickness from submarine data. AWI has focused on optimization of the thermodynamics and ridging treatment in numerical sea ice models. Furthermore, AWI has included a fast ice parameterization into the model, and implemented a ridging module into the stand-alone sea ice model. In addition, AWI has begun developing a finite-element coupled ice ocean model for the Arctic.

### 8.2 Ice models at NERSC

Several ice-ocean model systems are developed and used at NERSC for use both in climate studies and in operational oceanography (see Table 8.1 for a summary). The operational TOPAZ system (Bertino et al. 2004), the Global ice-ocean model and the North-Atlantic model are run under various EU and national projects.

All ice models, except the Global ice-ocean model, use Elastic Visco Plastic (EVP) rheology by Hunke and Dukowicz (1997). The Global ice-ocean model uses viscous-plastic rheology (Hibler III, 1979). A single category ice model is used in TOPAZ, Barents Sea model and the Global ice-ocean model, while a multi category ice model is used in the North-Atlantic model. The Barents Sea model will be upgraded to use multi-category ice model when the nesting routines have been upgraded to incorporate data from multi category models. In the following we describe each of the model systems and examples of results derived from them.

**Table 8.1.** Ice-ocean modelling systems at NERSC

<b>Ice-ocean model system</b>	<b>Model components</b>	<b>Ocean resolution &amp; layers</b>	<b>Assimilation</b>	<b>Modelling period</b>	<b>Geographical region</b>
<b>TOPAZ</b>	Ocean: HYCOM Ice: EVP rheology	20-22 km resolution; 22 layers in vertical	EnKF / 100 members	Start : 01.01.2003 Up to real time	Atlantic & Arctic regions
<b>North-Atlantic model</b>	Ocean: HYCOM Ice: EVP rheology, Multi-category ice thickness	40-70 km resolution; 26 layers in vertical	None, Free run, Single member	Start: 01.09.1958 Integrated up to 2002	North Atlantic & Arctic regions
<b>Global ice-ocean model</b>	Ocean: MICOM Ice: Viscous-plastic rheology	40 km resolution; 26 layers in vertical	None, Free run, Single member	Start: 01.01.1948 Current end 01.01.2003	Global
<b>Barents Sea model</b>	Ocean: HYCOM Ice: EVP rheology	5 km resolution; 22 layers	None, Single member	Start from 01.01.2003.	Barents Sea, Kara Sea

The most relevant model for relevant for SITHOS is the North Atlantic model. This model has been run from 1958 to 2002, and provides monthly maps of the main sea ice parameters for the Arctic and peripheral seas (Fig. 8.1a). The North-Atlantic ice-ocean model is based on the HYCOM ocean model and the dynamic part of the ice model is based on the Elastic Viscous Plastic (EVP) rheology by Hunke and Dukowicz (1997). For the thermodynamics a more complex ice representation, that discretizes ice into several ice thickness classes within each grid cell is used. Multi-Category ice models see the ice cover as a collection of ice floes in different thickness categories. This ice model also describes the redistribution of ice thickness through ridging and rafting within the grid cell. This makes it possible to model the ice thickness probability density function for each grid cell. Example of such thickness distribution is shown in Figure 8.1 b, which shows the total ice concentration in one grid cell in the Barents Sea along with the fraction of ice in the intervals 0-0.5m, 0.5-1.0m and so on. The seasonal cycle of total ice concentration is shown, and the figure illustrates how, during the course of a season, the fraction of thick ice increases from October to July (green yellow and red lines). A lot of this thicker ice is due to ice import from the central Arctic Ocean.

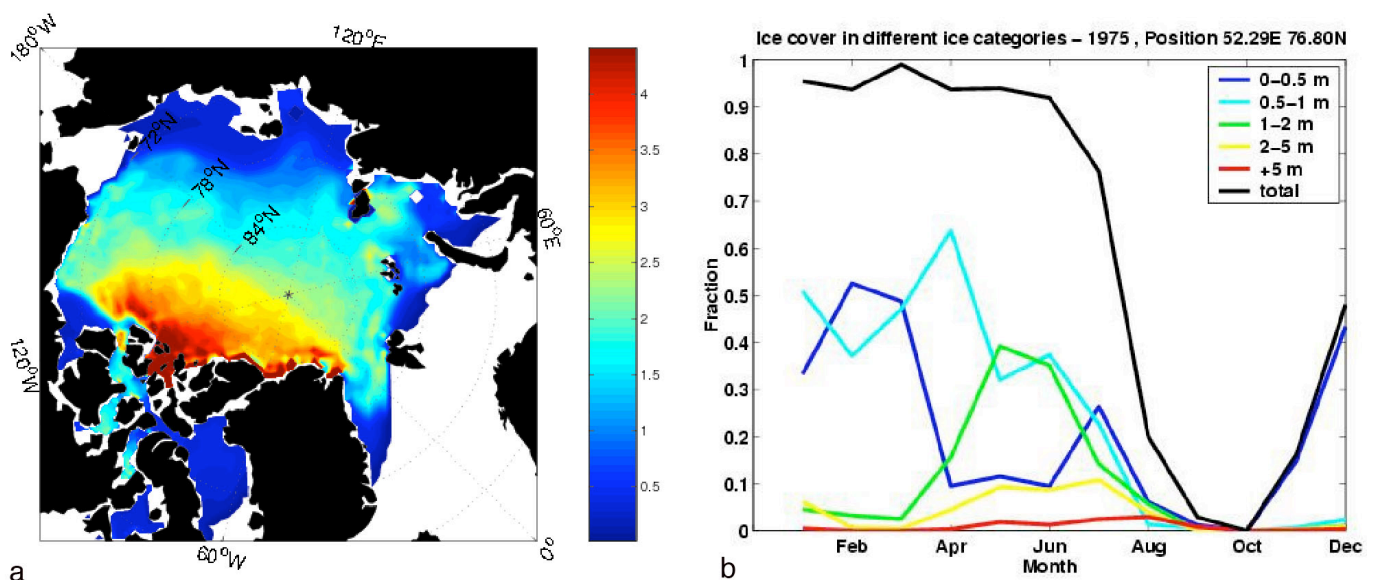


**Figure 8.1** a) Example of ice thickness map from the North Atlantic model, produced for day 304 in 1990; b) example of seasonal ice thickness distribution for 1975 for a given grid cell in the Barents Sea.

It provides a complement to the TOPAZ and Barents Sea simulations, since the North Atlantic model has a description of the sub-grid scale features of the Arctic Sea ice cover. Where the TOPAZ model and the Barents Sea model describe the ice cover using a single ice thickness, the North Atlantic model describes the ice cover with five ice thickness categories. This makes it possible to describe the ice thickness distribution, which is important for climate research as well as for risk assessment of sea ice operations.

Both TOPAZ and the North Atlantic model cover the entire Arctic Ocean, but the TOPAZ system is focusing on real-time operations, which means that important historical ice information is not available from TOPAZ. The North-Atlantic model is therefore useful for the historical ice thickness information in the Arctic. In the following we will demonstrate the annual variability of the sea ice cover in the Arctic from the model, as well as a validation against observations.

### 8.3 Ice Thickness variability from the North Atlantic Model

The ice thickness varies significantly seasonally as well as from year to year. To illustrate this variability, the seasonal cycle of ice thickness along a section from Greenland to the Siberian coast is shown in Figure 8.2. This Hovmuller diagramme shows that the thickest ice in the section is found on the Greenland side, and that the seasonal variability is not very strong. The thickness varies typically between 3.5m and 4.5 m. The rest of the section, from the North Pole area towards the Siberian coast, there is a decreasing trend in the thickness and the seasonal variability is much stronger. In the Laptev Sea there is no ice in most summers and the winter ice is not very thick, typically less than 1.5 m.

The time period from 1990 up to 1996 is a period of strong decline in the total sea ice mass in the Arctic. This can be inferred from the plots of sea ice thickness from the model as well. And even though the sea ice volume has recovered somewhat towards the mid 1990s, it remains a lot lower than in the beginning of the 1990s, up until the end of the simulations in 2002. The decline in ice thickness are also supported by observations and other model studies (Yu et al., 2004).

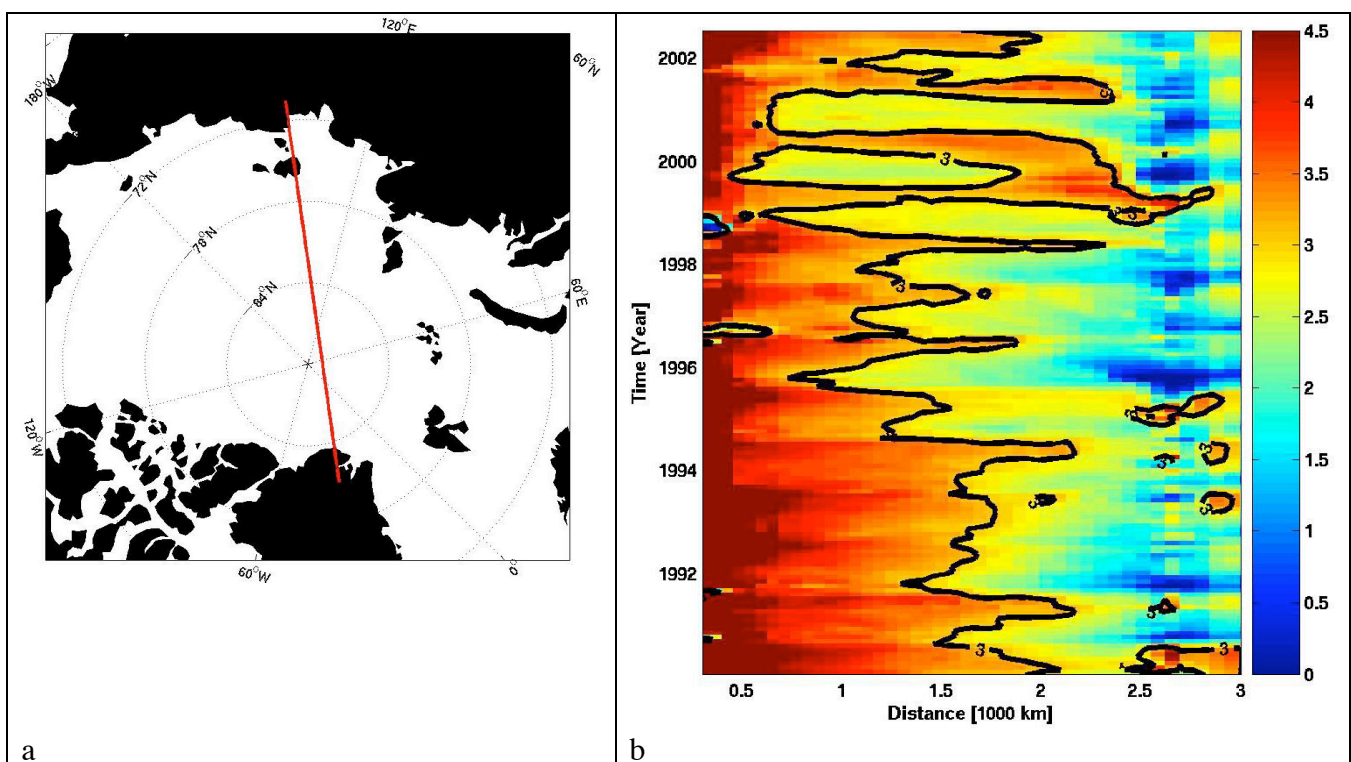


**Figure 8.2.** a) section from Greenland to Laptev Sea, where b) a Hovmuller diagramme (time-distance plot) of ice thickness for the section is presented for the period 1990 – 2002.

The mechanisms causing the decline seems to be a combination of dynamic (wind-driven) and thermodynamic effects. Based on satellite observations the export of sea ice from the Arctic to the Greenland Sea, for instance, was relatively high in the time period 1990-1996 (Kwok, 2004). Fram Strait is the section where most of the ice export from the Arctic takes place, although the export to other regions (such as the Barents sea) can be relatively high at times. However, the ice export alone is not enough to explain the decline in Arctic Sea ice volume, pointing to thermodynamical effects as well.

## 8.4 Comparison between modeled and observed ice thickness

During the last decades, American and British submarines have conducted surveys in the Arctic, where they used upward-looking sonar to measure the ice draft (the amount of ice below the sea surface). Comparisons between the model and these data has been performed, showing that the model does a relatively good job of describing the sea ice draft. When viewing these comparisons, it should be remembered that the sea ice model is relatively coarse (approximately 50-80 km in the Arctic), so that the model results will tend to be much smoother than the data retrieved from the measurements (approximate resolution of 10 km).

Figures 8.3 – 8.5 show the modeled ice thickness and corresponding profiles of submarine ULS data. The comparisons show that for the observations used here, stretching from 1976 to 1998, the large-scale features of the Arctic ice thickness are well represented. The major discrepancy appears to be at the end of the simulation (1997-1998). However, given uncertainties in the forcing fields used to drive the sea ice model (these are generally larger for the Arctic, due to sparse data coverage), the results are show that overall the model does a good job in describing the sea ice cover.



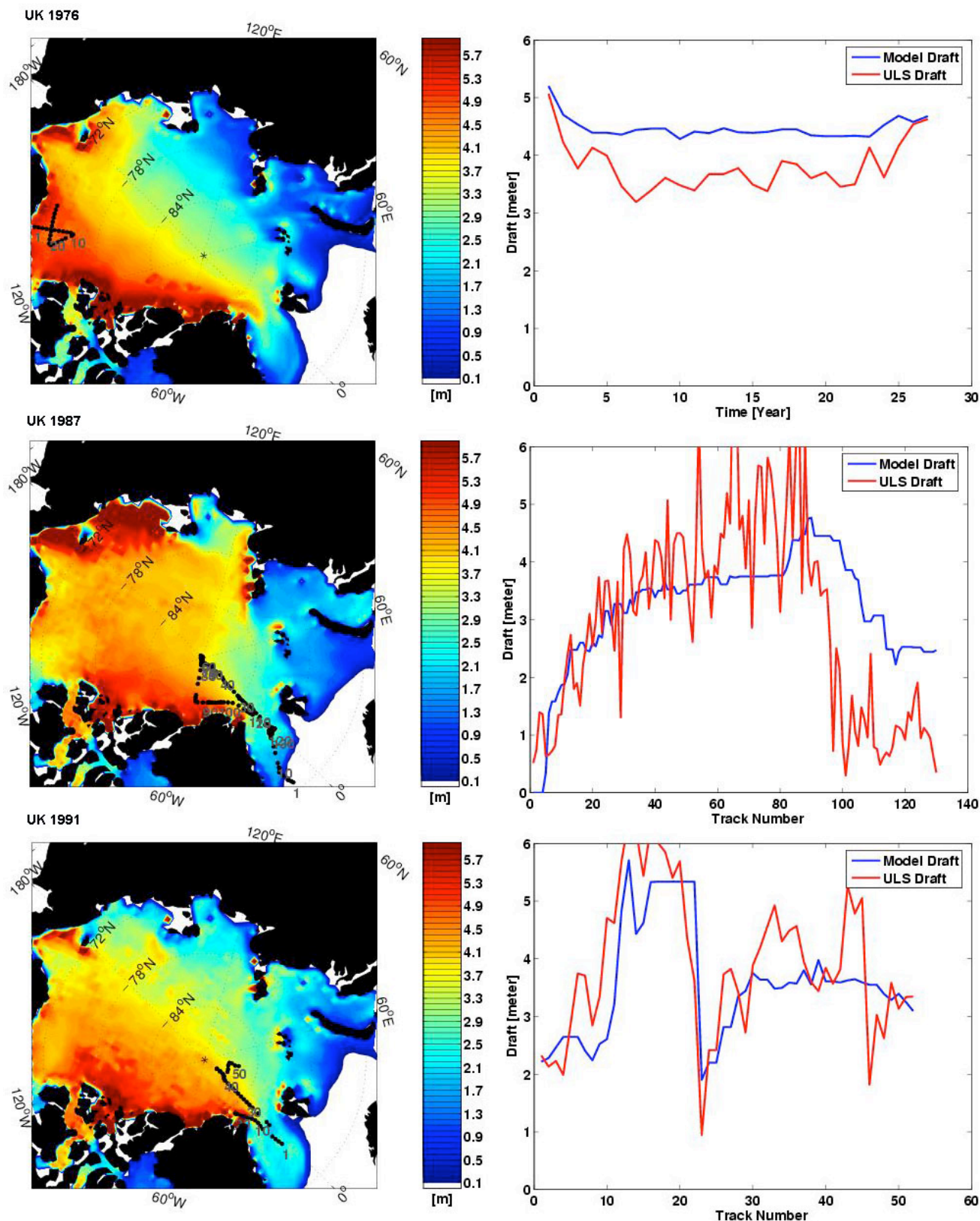


**Figure 8.3** Comparison between ULS and model data for 1976, 1987 and 1991

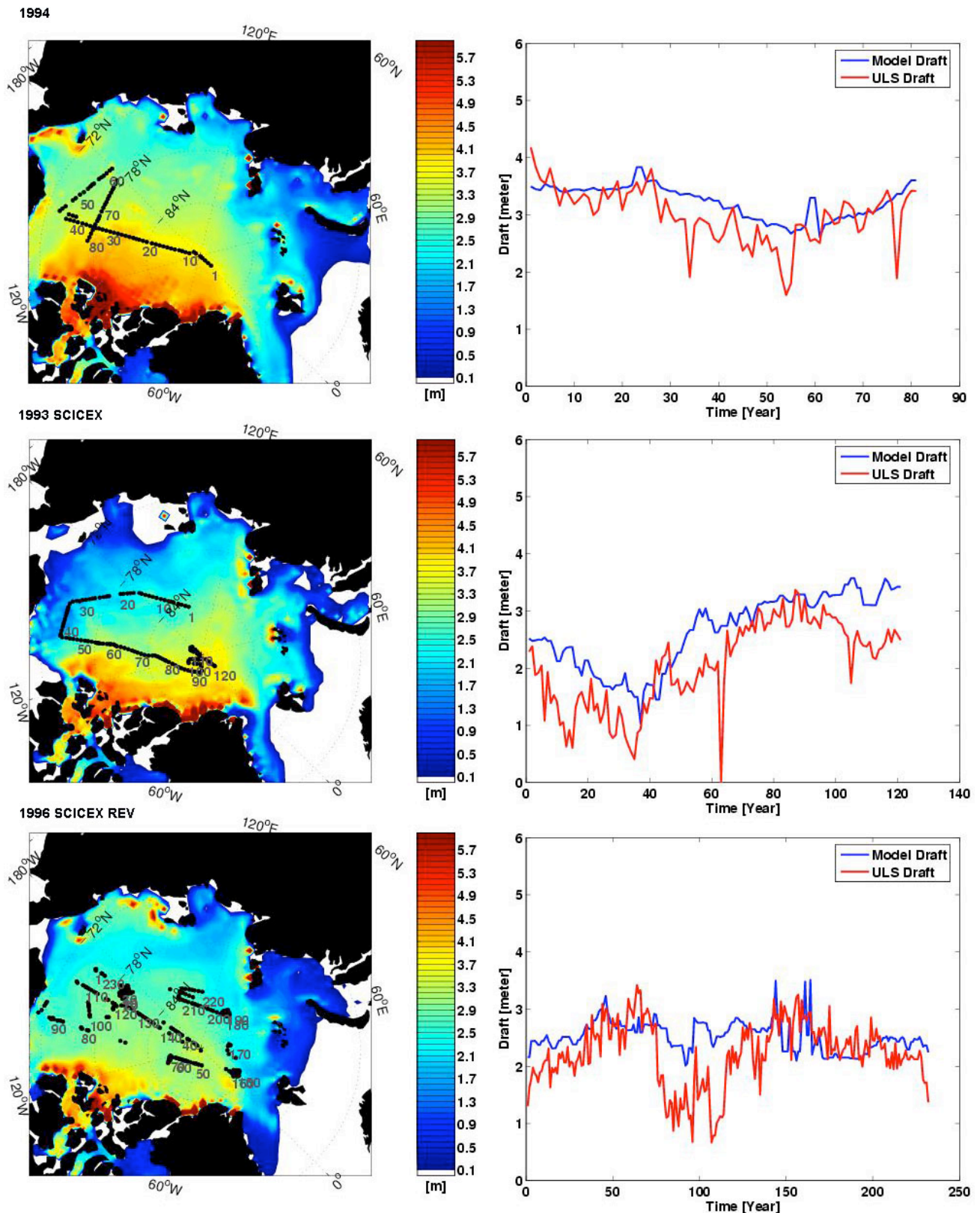


**Figure 8.4.** Comparison between model and submarine sea ice draft for 1993, 1994 and 1996



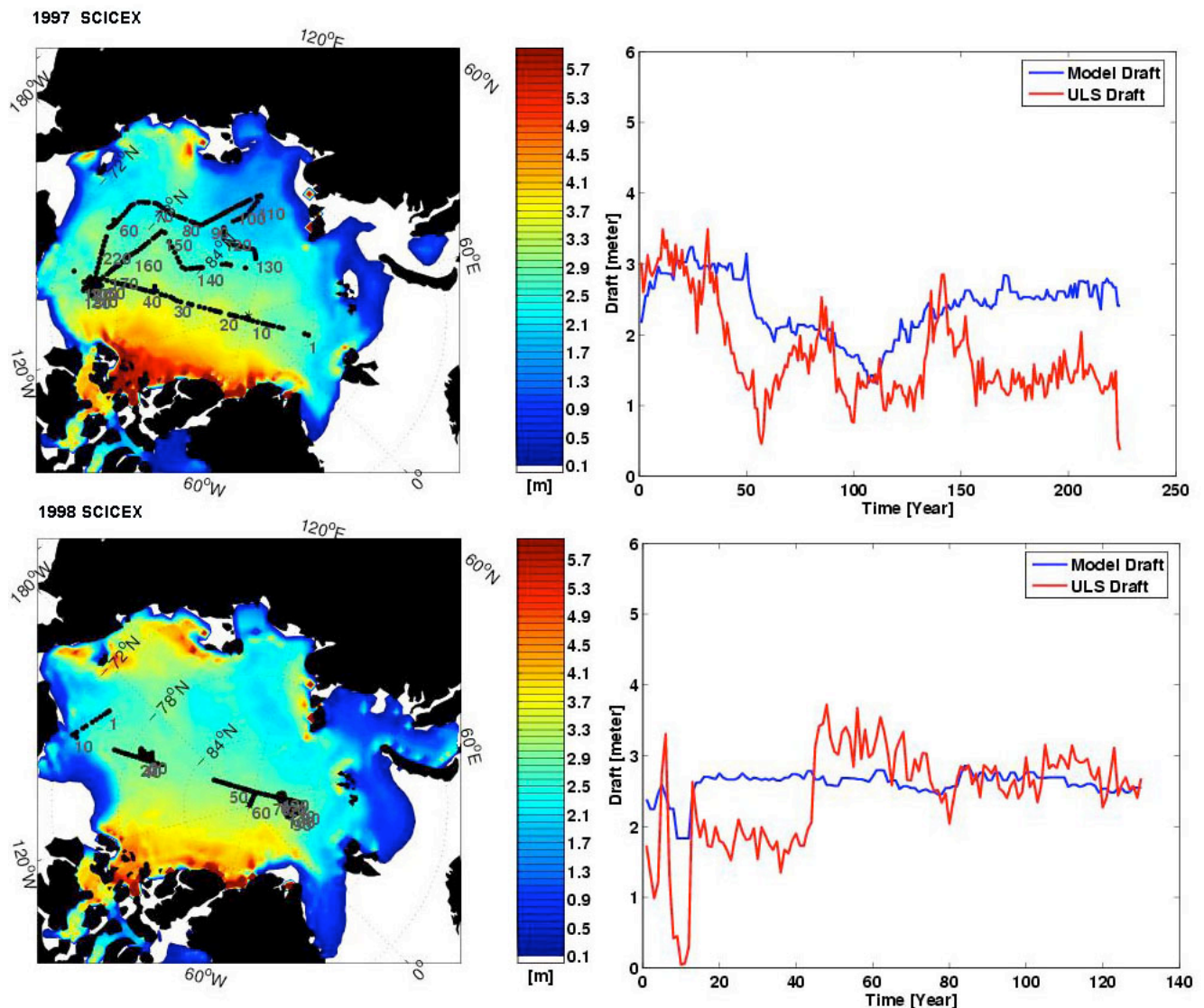


**Figure 8.5.** Comparison between submarine and model ice draft 1997 to 1998

## 8.5 Comparison with airborne laser data north of Greenland

The monthly model results are compared to airborne laser estimates of ice thickness in the areas north of Greenland for 1998, 2001 and 2002. The comparisons are shown in Figure 8.7. There is general agreement between the two data sets, where the thickest ice is found along the north coast of Greenland west of Station Nord. In the Fram Strait and along the east coast of Greenland there is thinner ice. Local variabilities in ice thickness observed in the laser data are not captured by the model because the model resolution is much coarser than the laser surveys.

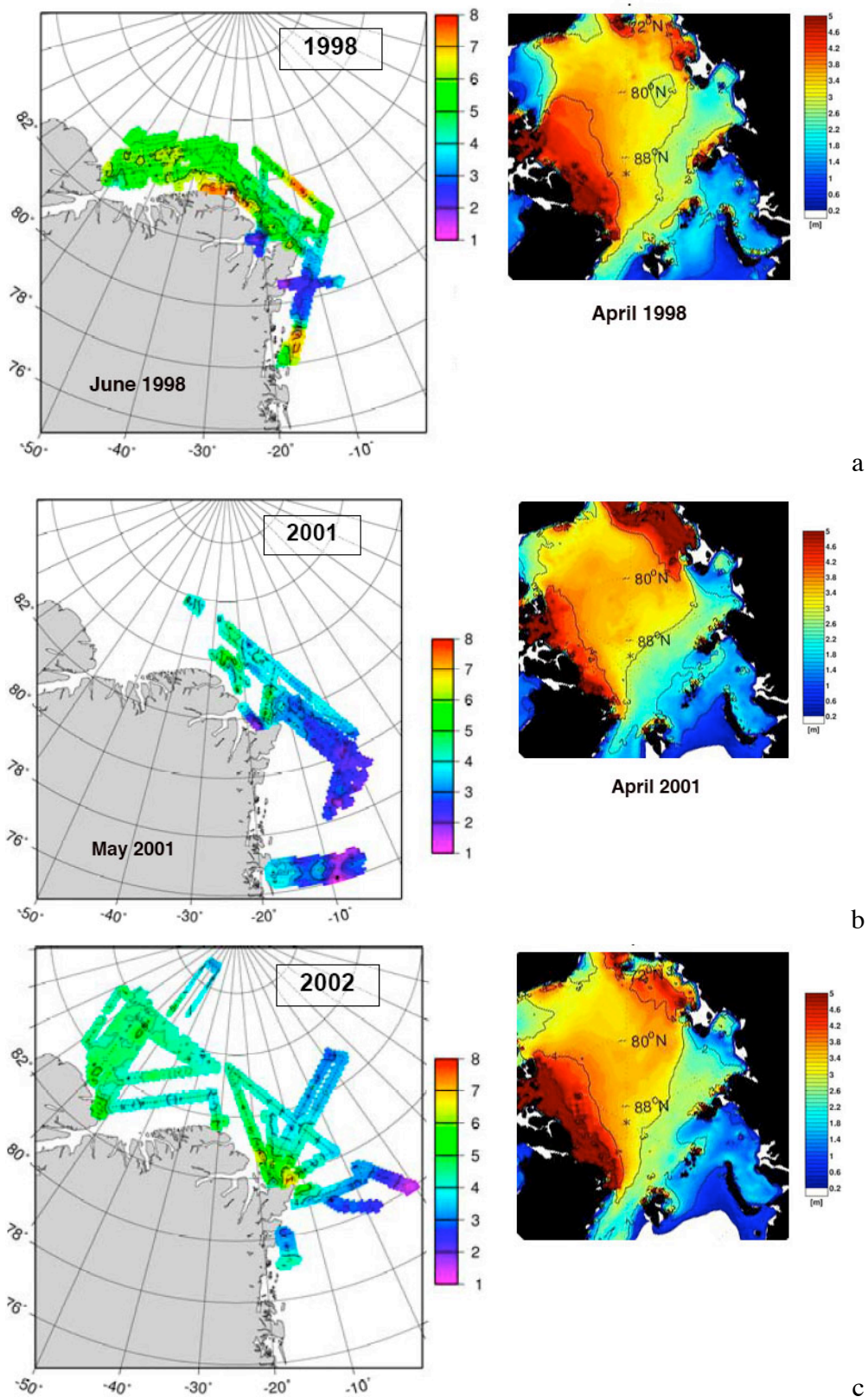


**Figure 8.7.** Comparison of ice thickness between airborne laser data (left side) and model simulations (right side) for a) 1998, b) 2001, and c) 2002. Note: the colour scale is different for the two data sets.

## 8.6 AWI sea ice model with fast ice parameterization

The sea ice model used for SITHOS is a further development and combination of different versions of the fundamental work of Hibler III. (1979) and Parkinson and Washington (1979) for the formulations of the dynamic and thermodynamic processes, respectively. This new realization is based on the work done by Harder (1996) improving the dynamics of the numerical model and introducing sea ice roughness and age as prognostic variables. Kreyscher (1998) tested different rheology schemes with respect to the sea ice dynamics and found that the viscous-plastic parameterization including shear strain gives the most realistic estimates of sea ice conditions. A new description for sea ice roughness and pressure ridges was included by Steiner (1998) leading to a statistical prediction of pressure ridge distribution. Hilmer (2001) studied the modelled long-term sea ice variability and found that, in addition to good reproduction of the mean quantities, the model is also able to describe observed features of inter-annual fluctuations of the Arctic sea ice cover. This includes the response of e.g. sea ice thickness to atmospheric variations such as the Arctic Oscillation (AO) or North Atlantic Oscillation (NAO).

The model operates with a time step of six hours ( $t = 21600$  s). This allows the local influence of atmospheric pressure systems to be taken into account. The horizontal grid resolution is  $1/4^\circ$  (27 km). Some of the passages that are critical to ship routing, e.g. the Kara Gate at the southern tip of the island Novaya Zemlya connecting the Barents Sea and the Kara Sea, or the Vilkitsky Strait between the southern island of Severnaya Zemlya and the northern tip of the Taymyr Peninsula connecting the Kara Sea and the Laptev Sea are resolved with several grid points.

In the SITHOS model version a fast ice parameterization has been implemented. If sea ice exceeds a certain thickness over a defined ocean depth it is assumed to be steadily connected to the adjacent coast line. From observations in the Russian Arctic Seas, the limiting water depth for this assumption in shelf areas has been set to 30 m. The fast ice is released as soon as thermodynamic processes melt the ice and dynamical processes push it offshore.

As can be seen from Figures 8.8 and 8.9 the parameterization works well in early summer situations. The so-called Western New Siberian Polynya reaches from Kotuy estuary to the New Siberian Islands with a landfast ice area between the coastline and the southern boundary of the polynya. The image in Figure 8.8 was taken from satellite NOAA-14 of the National Oceanic and Atmospheric Administration (NOAA) in late June 1995 with the Advanced Very High Resolution Radiometer (AVHRR) channel 1 (visible spectrum), which has a horizontal resolution of approximately 1.2 km. Dark values represent low albedos (open water and snow-free land), light values indicate high albedos (snow cover, sea ice and clouds). A model simulation for the same date (Figure 8.9) produces an ice-free area very similar in shape and dimension to that seen in the AVHRR image. Even smaller features like the ice tongue between the Lena delta and the Kotuy estuary are well represented. The ice conditions around the New Siberian Islands appear to be realistic as well.



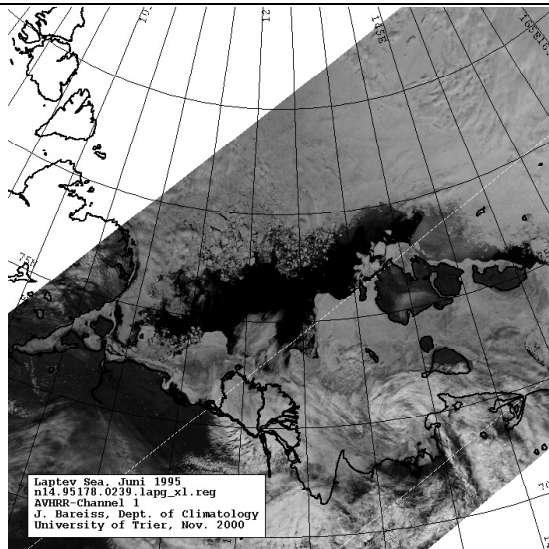


**Figure 8.8:** Satellite image of the Laptev Sea taken by the NOAA-14 satellite with AVHRR Channel 1 on 27 June 1995. (J. Bareiss, 2003, pers. comm.)

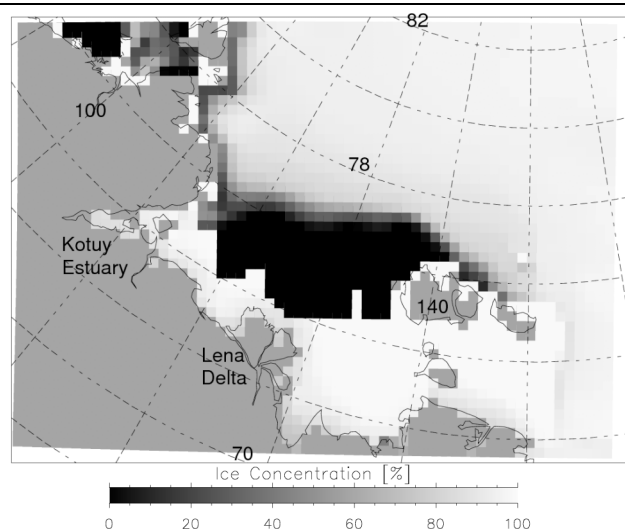


**Figure 8.9:** Model result of sea ice concentration from a simulation for 27 June 1995 showing the Laptev Sea region with fast ice and a polynya.

## 8.7. Modelling of sea ice ridging

The ridge model is based on the work of M. Lensu (2003) and contains evolution equations for ridge density and ridge height separately. Ridge evolution is described with parameters derived from laser measurements in the Arctic (Kara and Barents Sea as well as Fram Strait) and the Baltic. The cross-section of a ridge is assumed to be of triangular shape, one for the sail and one for the keel, where the draft of the latter is taken as equal to 3.8 times the sail height. The decrease in cross-sectional volume due to clustering – ridges grow that close to each other that they cannot develop their full triangular shape – is calculated as a function of ridge density and height from a one-dimensional Monte-Carlo like model.

Figures 8.10 and 8.11 show first examples of simulated ridge parameters density and sail height, respectively. Although the ridge height shows the highest values around Greenland and at the northern Canadian Archipelago, the ridges are widely spread within the model domain with a spacing usually lesser than 1 per km.

During the time span of the project the ridging algorithm was further developed and is now able to simulate realistic ridge quantities for the whole Arctic. Figures 8.12 a) and b) display examples of the distribution of monthly mean level and ridged sea ice thickness for late winter, respectively. The Arctic sea ice is at a maximum extent and the different portions of the two different ice classes are clearly visible from the modelled data. Transformation of level ice into ridged ice results in thickest ridged ice around Greenland and off the Canadian Archipelago. The thickest level ice can be found in the western Arctic.

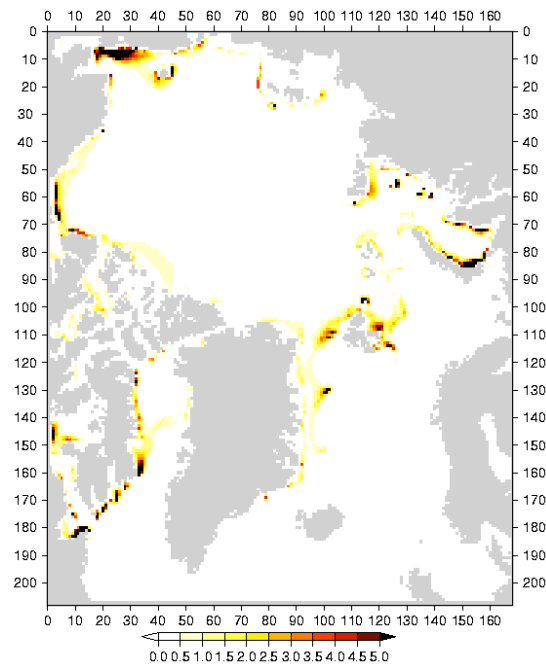


**Figure 8.10** First results of simulated ridge density [ $\text{km}^{-1}$ ] for the Arctic basin.

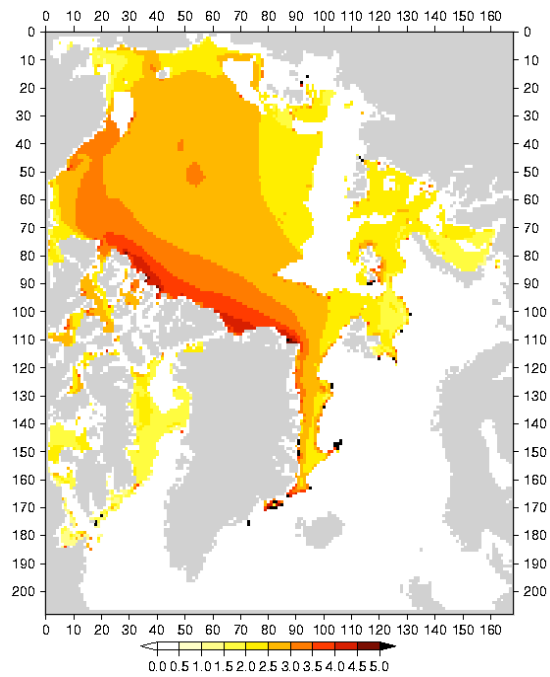


**Figure 8.11** First results of simulated ridge sail height [m] (corresponding to Figure 3) for the Arctic basin.

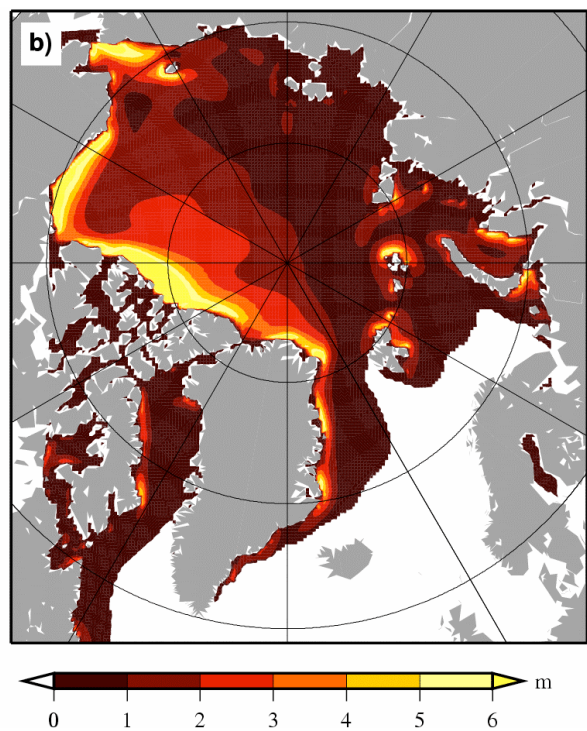
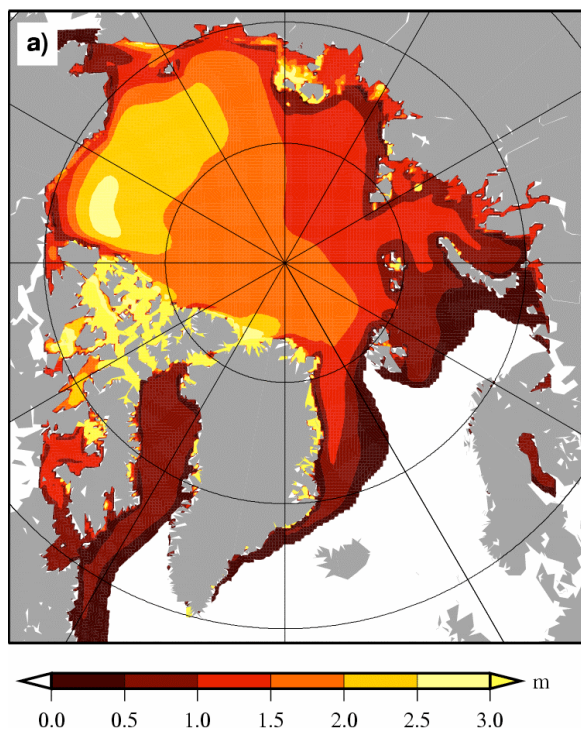


**Figure 8.12** a) Simulated monthly mean late winter level ice thickness and b) corresponding simulated monthly mean ridged ice thickness.

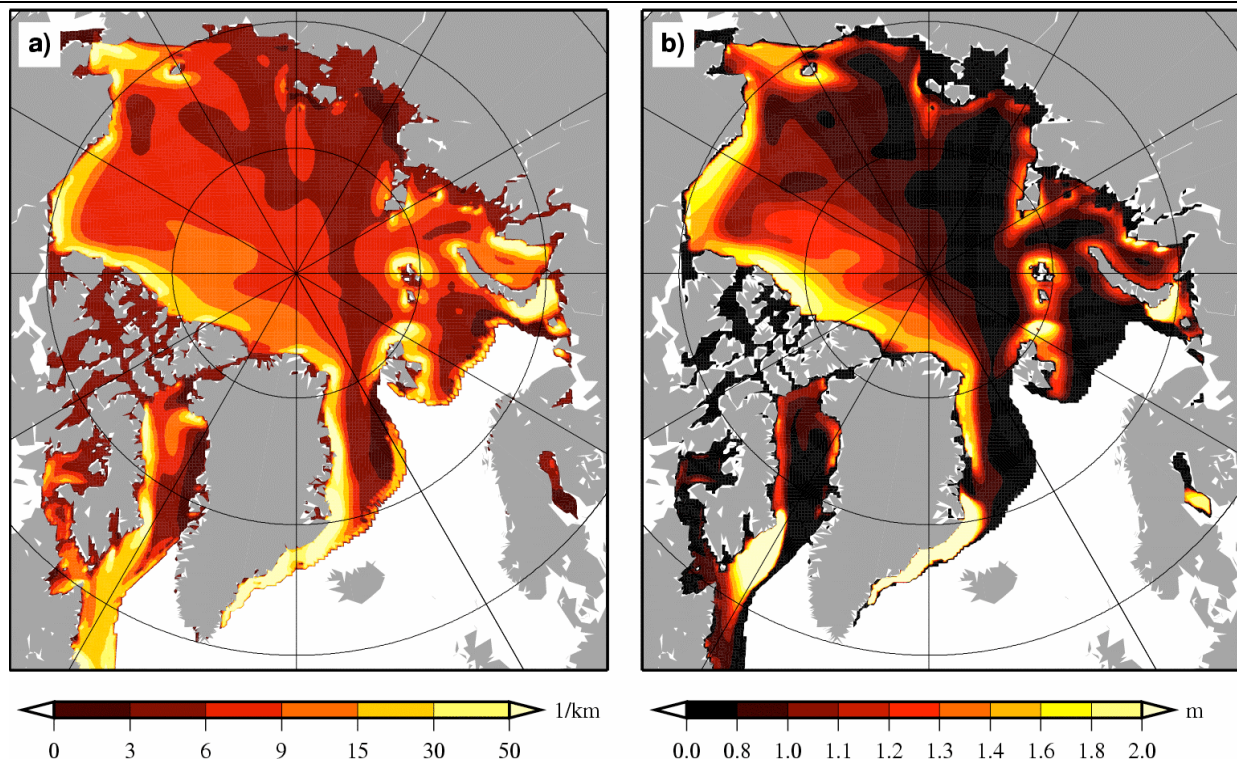


**Figure 8.13** a) Simulated monthly mean late winter ridge density and b) corresponding simulated ridge sail height.

Monthly mean ridge parameters ridge density and ridge sail height are shown in Figures 8.13 a) and b), respectively. Along the Transpolar Drift the lowest ridge densities are simulated corresponding with the lowest sail heights in this region. On the other hand, the highest values of ridge density and sail height are simulated north of the Canadian Archipelago and along the east coast of Greenland, thus representing the regions with the most heavily ridged sea ice (see Figure 8.12 for comparison). The low values of both ridge density and sail height along the Russian coast can be attributed to the fast ice parameterization. Here sea ice forms and is locked at the shoreline and therefore not subject to wind driven deformation events. However, off the fast ice edge, sea ice is newly formed in the maintained polynya and deformation occurs according to the parameterization.

A more detailed comparison of modelled and observed sea ice deformation features is depicted in Figure 8.14. The number of ridges per km as well as the typical ridge height are deduced from helicopter borne laser altimeter data obtained during a field experiment in March and April 2003 in SITHOS WP3. Mean values are calculated for 25 km long lags for the comparability with modelled values (which are available with a 25 km grid spacing) and displayed in colour coded circles at their appropriate location. In the central Fram Strait region the observed ridge density is in close agreement with the modelled. Whereas the simulated ridge density is slightly overestimated close to the north eastern part of Greenland. A relatively uniform distribution of ridge sail heights was observed during the expedition. Though the modelled values show a clear gradient from coastal areas towards the central part of Fram Strait (which can be attributed to model setup) the two datasets are in general in good agreement.



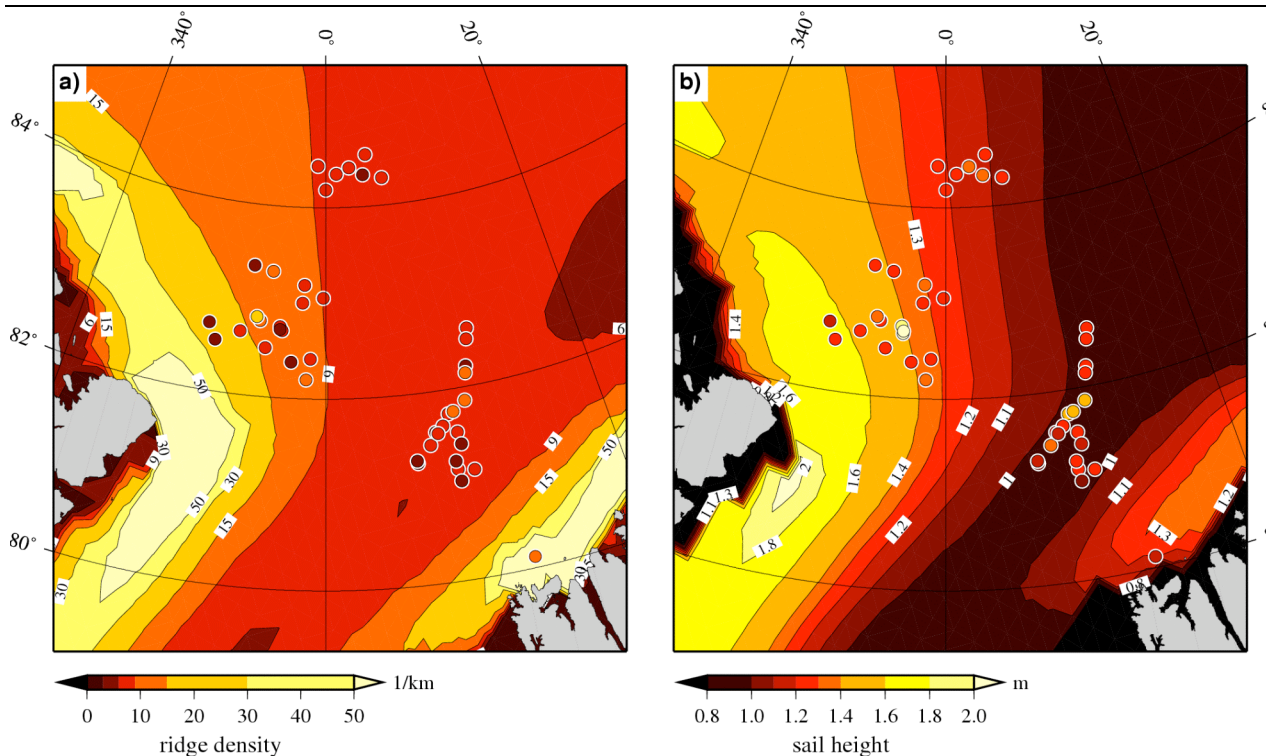


**Figure 8.14** a) Simulated ridge density (background colour code) and observed ridge density from laser altimeter measurements (colour coded circles) and b) corresponding simulated ridge sail height (background colour code) and observed ridge sail height from laser altimeter measurements (colour coded circles).

## 8.8 Finite element model

The first version of the model was designed as a stand-alone model. It uses ocean and atmosphere forcing to predict ice velocity, mass, compactness and freshwater flux. It shares the names and mesh structure with the Finite-Element Ocean Model (FEOM) and assumes that the mesh is triangular and unstructured. Such a mesh is described by the lists of nodal coordinates and triangles (triplets of nodes). Any existing regular (finite-difference) mesh could be easily triangulated by dividing every cell into two triangles, numbering the nodes and constructing the two lists with information on nodes and triangles (Figure 8.15).

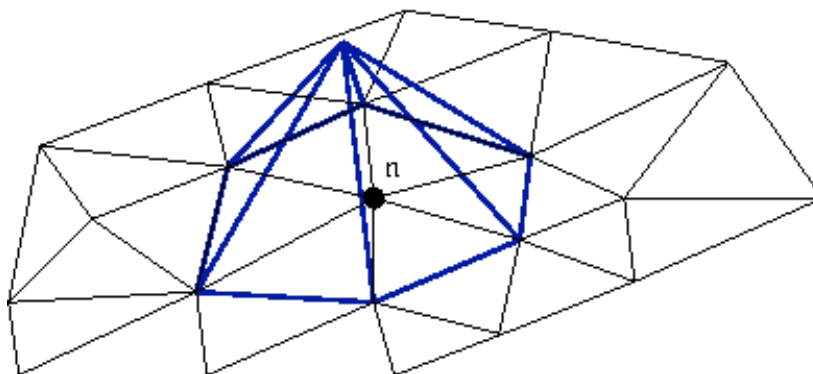


**Figure 8.15:** Illustration of mesh structure of finite element model.

Using such meshes does not require re-interpolating data, but only reordering them according to

numbering of nodes. The potential of finite element approach, however, lies in one's ability to refine the mesh where it is necessary. The current version of the model uses a fixed mesh, but in principle, the refinement could be done adaptively in time. Clearly, coupling the finite-element ice model based on an unstructured mesh to regular-grid ocean models would require data interpolation between different meshes.

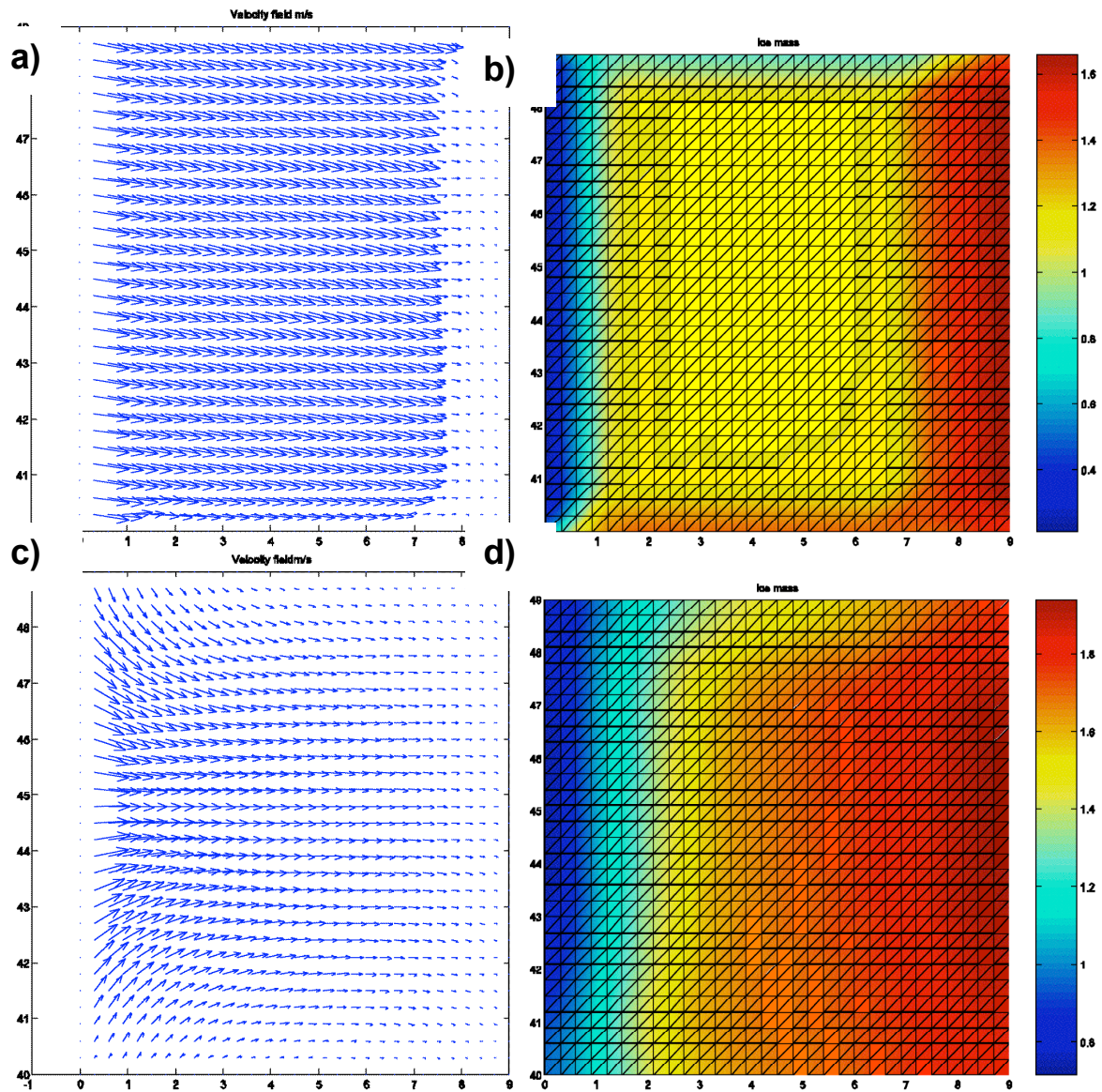


**Figure 8.16:** Result of a simple set-up of the FE sea ice model with a square domain. Wind is blowing permanently from the left. The panels show ice velocity and distribution of ice thickness after 5 days (a, b) and 30 days of integration (c, d).

The model could be run with both visco-plastic (VP) and elastic-visco-plastic (EVP) rheologies, although the first choice is on the slow side and less reliable. The one-dimensional sea ice thermodynamic model is modification of the AWI ice model and is similar to the simplest model of Parkinson and Washington (1979). This model has been intensively used for many years both for the ice-mixed layer and ice-general ocean studies of the Arctic and Southern oceans. The initial



code is courtesy to Prof. P. Lemke (AWI, Bremerhaven). This code was reprogrammed in a form suitable for further coupling with the FEOM. The ice transport uses a backward Euler implicit stabilized advection scheme. The PILUT solver of FOSSI library (S. Frikenhaus, AWI RZ) is employed for solving systems of linear equations of ice transport. The solver library is ported to all main platforms available at AWI.

Parallelization of the model is straightforward, as the solver interface is already parallelized (requires MPI). The current version of the model was tested on Origin-2000 and SUN-Fire.

As a first test, the model was set up in a square domain, and a permanent wind from the west (left) was applied on the sea ice cover. Figure 8.16 shows the ice velocity field and regional ice thickness distribution after 5 and 30 days of integration. All the ice is moved to the south eastern corner of the domain, and in the west a large polynya opens. Ice velocity decreases with increasing ice thickness.

## 8.9 Conclusion on the modelling work

The AWI modeling activities show interesting results of ridge simulations and ice age simulations. This is complementary to the results provided by the NERSC models. The modelling systems are producing large-scale sea ice thickness fields which need to be validated on similar scales. This is a real challenge because most ice thickness measurements are obtained on regional and local scale.

The main purpose of demonstrating sea ice modeling results, using the available models at NERSC and AWI, is to compare observed ice thickness by the different methods used in the other SITHOS tasks with modeled field. The observations can be used to validate the model results, but the validation is of limited value when the observations are on a different scale compared to the models. The comparison can also be used to define scales of observations that are needed in the future for model validation.

The large-scale observations by radar altimetry provide interesting data for comparison with large-scale model results. But the radar altimeter method needs further validation before it can be a useful tool for model validation. Sea ice models can only be expected to be as good as the atmospheric forcing fields and the ocean models coupled to the ice models. It is therefore important to provide improved atmospheric fields in the Arctic where the observation network is sparse.

## 9. Synthesis of results and conclusions

The results of the ice thickness measurements obtained in SITHOS can broadly be synthesized on two different scales: local and regional scale where most of the data collection takes place, and the large scale where modelling and satellite remote sensing are the main methods.

### 9.1 Local and regional scale

The six field experiments conducted in the period March 2003 to May 2005 collected ice thickness and related snow and ice measurements on local and regional scale using different methods which could be compared to each other. The use of airborne laser and helicopter electromagnetic induction (EM-method) measurements were the two most important methods covering scales up to 100 km. There was general agreement between these two methods within 10 – 20 % in retrieved thickness. The airborne laser measurements of freeboard had to be translated into thickness by assuming an appropriate K-factor. The EM-method observed ice thickness directly because it could measure the distance to the underside of the ice. In situ measurements of snow and ice properties were conducted on local scale, i.e. within a few hundred meters. This gives another scale of observation compared to airborne and helicopter measurements. The local measurements of ridges, ice keels, leads, etc. could resolve variability on meter scale, but could not areas beyond a scale of one km. The in situ measurements, using drilling, ground penetrating radar and EM measurements from a sledge, give the best estimates of the true ice thickness, snow thickness as well as density and freeboard. But there is always a question of the representativeness of local measurements on regional (100 – 1000 km) and large scale (above 1000 km). The in situ measurements are also essential for validation of the measurements on regional and large scales. The EM method is considered to be the best method on regional scale, because it has been validated in several experiments over the last decade. However, the EM-method under estimates the ridges, which means that the probability density function for ice thickness from EM data has too little ice in the thickest category. The airborne laser method is very good for covering regions of several hundred km, but the method needs calibration from in situ observations and/or from EM-data. The ice thickness measurements on regional scale are important for many users, including offshore operators, regional scale modellers and operational services. But the regional data are not necessarily useful for global scale and climate research. The variability in ice thickness in one region, for example the European sector of the Arctic, is not necessarily correlated with other regions. Therefore, global ice thickness data is a requirement for studying total ice masses and their seasonal and interannual variability.

### 9.2 Large scale

To provide global scale data on ice thickness is the most difficult task, because there are lack of methods to obtain such data. It is difficult to translate regional data into large scale fields, because there is general lack of synoptic data covering large parts of the Arctic Ocean. Satellite altimetry is the most promising method to make synoptic maps covering the whole Arctic region. The present results from ERS and ENVISAT are promising, showing that the thickest ice is found in the Canadian sector of the Arctic and thinner ice is found in the Russian sector of the Arctic. However, there is practically very little data available for validating the altimeter results. Furthermore, the capability to resolve the thickness by altimetry is so far documented for the thickest ice only, i.e. for the multiyear ice, but large parts of the Arctic has firstyear ice with thickness of 1 – 2 m. To resolve the firstyear thickness it is necessary to measure freeboard with an accuracy better than 10 cm, assuming that data are averaged in space and time. CryoSat will make an important contribution to this, but we have to wait a few more years for CryoSat-2 to be launched. The most useful data sets on ice thickness covering large parts of the Arctic Ocean is the submarine data which has

recently been published. As discussed in chapter 8, the submarine data are used to validate the ice models. This comparison shows that the ice models is in reasonable good agreement with observations if the local and regional variability is filtered out. But there are also many examples of disagreement between observations and model simulations, showing that models in the Arctic needs to better in order to simulate regional variability. One of the problems with the ice models is the quality of the atmospheric forcing fields, which is not very good in the Arctic.

### 9.3 Overall results of the thickness measurements

The main results of the thickness measurements in the CryoVex experiment was that in the multiyear floe near Polarstern the mean thickness derived from drilling holes was about 2.6 m with 10 % std. The airborne scanning laser measurements showed a mean thickness of about 3.2 m with up to 20 % std. The laser measurements depend very much on the R-factor which translates freeboard in to thickness. The overestimation by the laser data suggests that the k-factor was too high. In the two 100 km long flight tracks, the scanning laser measurements were compared with helicopter EM data. The track in southwesterly direction showed a mean thickness of about 2.1 m for both systems. The std was up to 71 %, indicating that the variability in ice thickness was much larger for a 100 km long track compared to the measurements on a single floe near the Polarstern.

The northward track showed a mean thickness of about 3.7 m in the laser data (std = 46 %) and 3.4 m in the helicopter EM data (std = 42%). The overall result was that the most reliable methods (drilling and EM data) showed a general increase in the mean thickness from south to north over a 200 km distance. The scanning laser data showed larger variability and a tendency to overestimate the thickness in the middle and northern part of the study area. This shows that a constant k-factor for the laser data should not be applied over the whole study area. In future use of laser data, the R-factor should be adapted to the local ice conditions, taking into account that ice density and snow depth vary within a distance of 200 km.

The thickness observed north of Greenland in May 2005 showed mean values from 2.90 to 5.20 m.

Data from summer expeditions with Polarstern between 1991 and 2004 shows that the ice thickness in the European sector of the Arctic has declined from a mean of 2.5 m to about 2.0 m, but we do not know the effect of regional differences in the thickness data,

### 9.4 Basic physical measurements of snow and ice

This study has analysed in situ snow and ice measurements from the Fram Strait area and compared them with previous measurements in other parts of the Arctic. First, the effect of snow cover on freeboard was studied, showing that the maximum effect is in the period April – June when the mean ice freeboard is reduced by an average of 10 – 12 cm for the whole Arctic. The strongest effect is found north of Greenland where the freeboard reduction is up to 18 cm. This is quite significant since the mean freeboard for 2 m thick MY is 20 – 30 cm.

To retrieve thickness from freeboard require good estimates of the freeboard error. For example, an error in freeboard of 10 cm is magnified to an error of 50 – 80 cm in the ice thickness estimates. Other important problems to investigate are ice density and snow thickness. The ice density is the most critical factor for the thickness determination. Another hypothesis to be further investigated is the isostatic equilibrium for ice floating on water, and the scale where this assumption can be applied.

Furthermore, studies were done to compare retrieved ice thickness from airborne laser freeboard measurements with in situ measurements of snow and ice parameters in the Fram Strait area. The retrieved ice thickness from a 100 km long profile, providing a mean snow plus ice freeboard of 0.55 m, was 3.5 m using ice density of 910 kg/m<sup>3</sup>, and 2.2 m using a density of 836 kg/m<sup>3</sup>. The high density of 910 kg/m<sup>3</sup> is typically found for MY floes with considerable refrozen melt ponds. The value of 836 kg/m<sup>3</sup> was the mean value measured directly from a few ice cores in the study area. The density decreases to 810 – 820 kg/m<sup>3</sup> in areas with ridges and hummocks. Another survey covering a specific MY floe, showed that the mean snow plus ice freeboard was 0.65 m, resulting in a retrieved thickness of 4.4 m using a density of 910 kg/m<sup>3</sup> and 2.7 m using a density of 836 kg/m<sup>3</sup>. This ice floe was also surveyed by helicopter EM measurements, showing a mean thickness of 2.0 m. These examples illustrate the sensitivity of ice thickness retrievals from freeboard measurements to snow depth and ice density (Sandven et al., 2005). It is important to obtain improved statistics on snow and ice density as part of the CryoSat ice thickness validation.

Statistics of snow and ice parameters for the whole Arctic has been compiled by Russian surveys over many years, and have been published in various reports and in the atlas by Romanov (1995). Ice density is one of the most sensitive parameters in calculation of thickness from freeboard measurements. This is illustrated in Table 9.1, where typical range in ice densities shows the impact on the thickness calculation. For multiyear ice, the density varies typically between 820 kg/m<sup>3</sup> to 920 kg/m<sup>3</sup>, giving a range in ice thickness between 1.76 m to 3.39 m. The lower densities are found in MY ice with hummocks where more air pockets are embedded in the ice. The higher values are found in MY ice with melt ponds, where the freshwater content brings up the density. Direct measurements of ice density in the CryoVex area showed values of 833 kg/m<sup>3</sup> and 836 kg/m<sup>3</sup>.

The snow distribution on sea ice is very variable and existing data and statistics of snow on ice are scattered in space and time. The most extensive analysis on snow climatology in the Arctic is produced by Warren et al (1999), but Warren's study which is based on data from all the North Pole drifting stations has no data for the area north of Svalbard. Romanov (1995) has produced statistics of snow parameters for the whole Arctic including the Fram Strait area based on aircraft surveys and landings over many years.

*Table 9.1. Ice thickness as function of ice density (from Romanov, 1995).*

Ice density kg/m <sup>3</sup> x 10 <sup>-3</sup>	0.78	0.80	0.82	0.84	0.86	0.88	0.90	0.92	0.94
Hi (m)	1.48	1.60	1.76	1.95	2.18	2.47	2.86	3.39	4.16

A major challenge is to obtain validation data covering different areas and seasons. The studies in SITHOS could only provide data from very limited areas, and it is evident that more data on basic physical properties of snow and ice is needed in different parts of the Arctic. This should be taken into account in future field experiments in the Arctic. The International Polar Year 2007 – 2008 will offer good possibilities to carry out more extensive field investigations across the Arctic Ocean.

## 9.5 Further work

Since focus of the SITHOS has been to perform field experiments and collect new data sets, analysis of the data and publication of results have not been completed by the end of the SITHOS project. Therefore, the efforts to work up and disseminate results will continue in 2006 and 2007. During the International Polar Year from 2007 – 2009 there will increased focus on the Arctic and the observing systems from SITHOS will be implemented and enhanced through DAMOCLES integrated project and in the context of national projects.

## 10. References

- Belchansky, G. I., D. C. Douglas, I. V. Apastsky, and N. G. Platonov, 2004. Spatial and temporal multi-year sea ice distributions in the Arctic: A neural network analysis of SSM/I data, 1998-2001. *J. Geophys. Res.*, 109, C10017, doi:10.1029/2004JC002388.
- Belchansky, G. I., D. C. Douglas, I. V. Apastsky, and N. G. Platonov, 2005. Variations in the Arctic's multi-year sea ice cover: A neural network analysis of SMMR-SSM/I data, 1979-2004. *Geophys. Res. Lett.*, 32, L09605, doi:10.1029/2005GL022395.
- Bertino (2004), Lisæter, Sagen, Counillon, Winther, Stette, Natvik, G. Evensen, Morel, Brankart, Testut, Birol, Brasseur, Verron, Schartau, Schröter, Dombrowsky, Burillo, Gilles Larnicol, Schaeffer & Weller. Towards an Operational Prediction system for the North Atlantic and European coastal Zones – TOPAZ Final report, NERSC Technical Report, 251
- Bourke R.H., Paquette R.G. – Estimating the thickness of sea ice//J. Of Geophys. Res., 1989, vol. 94, N C-1, pp. 919-923.
- Bjørge, E., O. M. Johannessen and M. W. Miles, 1997. Analysis of merged SMMR-SSM/I time series of Arctic and Antarctic sea ice. *Geophys. Res. Lett.*, 24, 413–416.
- Cavalieri, D., J. Crawford, M. Drinkwater, D. Eppler, L. Farmer, R. Jentz and C. Wackerman, 1991. Aircraft active and passive-microwave validation of sea ice concentration from the DMSP SSM/I, *J. Geophys. Res.*, 96, 21,989–22,008.
- Cavalieri, D. J., P. Gloersen, C. L. Parkinson, H. J. Zwally and J. C. Comiso, 1997. Observed hemispheric asymmetry in global sea ice changes, *Science*, 278, 1104–1106.
- Cavanié, A., 1998. An empirical C-band backscatter melt over arctic sea ice from ERS-1 AMI-wind data, *Proc., Joint ESA-EUMETSAT Workshop on Emerging Scatterometer Applications – From Research to Operations*, 5-7 October 1998, ESTEC, Noordwijk, Netherlands (ESA SP-424), 99–106.
- Chapman, W. L. and J. E. Walsh, 1993. Recent variations of sea ice and air temperature in high latitudes, *Bull. Amer. Meteor. Soc.*, 74, 33–47.
- Comiso, J., 1990. Arctic multiyear ice classification and summer ice cover using passive-microwave satellite data, *J. Geophys. Res.*, 95, 13,411–13,422.
- Comiso, J. 2002. A rapidly declining perennial ice cover in the Arctic, *Geophys. Res. Lett.* 29, 1956, doi:10.1029/2002GL015650.
- Comiso J. C., D. J. Cavalieri, C. L. Parkinson and P. Gloersen. 1997. Passive microwave algorithms for sea ice concentration: A comparison of two techniques, *Remote Sens. Environ.*, 60, 357–384.
- Czipott, P. V. and W. N. Podney (1989). Measurement of fluctuations in the tilt of Arctic Ice at the CEAREX oceanography camp. La Jolla, Physical Dynamics Inc: 53.
- Dalå, N. S., R. Forsberg, K. Keller, H. Skourup, L. Stenseng, and S. M. Hvidegaard: *Airborne Lidar Measurements of Sea Ice North of Greenland and Ellesmere Island 2004. GreenICE/SITHOS/CryoGreen/A76 Projects. Final Report*, DNSC Technical Report, No. 1, 69 pp., 2005.
- Deser, C., J. E. Walsh, and M. S. Timlin, 2000. Arctic sea ice variability in the context of recent atmospheric trends, *J. Clim.*, 13, 617–633.
- Duckworth, R. and P. H. Westermann (1989). "Stress and strain measurements developed for field measurements of ice." *IEEE J. of Oceanic Eng.* 14(2): 159-165.
- Emery, W. J. and R. E. Thomson (1998). *Data Analysis Methods in Physical Oceanography*. Oxford, Pergamon.
- Ezraty R. and A. Cavanie, 1999. Intercomparison of backscatter maps over Arctic sea ice from NSCAT and ERS scatterometer, *J. Geophys. Res.*, 104, 11,471–11,483.
- Ezraty R. and J.-C. Gascard, 2003. Arctic perennial sea-ice seasonal and interannual variability. *Geophysical Research Abstracts*, 5, 05383, European Geophysical Society (Abstract).
- Gloersen, P. and J. Yu, 1997. Oscillatory behavior in Arctic sea ice concentrations, *J. Geophys. Res.* 101, 6641–6650.
- Haas, C., *et al.* (2006). "Comparison of the sea ice thickness distribution in the Lincoln Sea and adjacent Arctic Ocean in 2004 and 2005." *Ann. Glaciol.* 44.
- Haas, C., and H. Eicken (2001) Interannual variability of summer sea ice thickness in the Siberian and Central Arctic under different atmospheric circulation regimes, *J. Geophys. Res.*, 106(C3), 4449-4462.
- Harder, M., 1996: *Dynamik, Rauigkeit und Alter des Meereises in der Arktis - Numerische Untersuchungen mit einem großskaligen Modell*, Ph.D. thesis, Universität Bremen, Bremen, Germany, published by Alfred Wegener Institute: Berichte zur



- Polarforschung, **203**, 1996.
- Haskell, T. G. and W. H. Robinson (1994). "A sensitive and robust strain-meter for ice studies." *Cold Reg. Sci. Tech.* **23**: 99-104.
- Hibler III (1979). A dynamic thermodynamic sea ice model. *J. Phys. Oceanogr.*, **9**, 815-845).
- Hilmer, M., 2001: *A model study of Arctic sea ice variability*, Ph.D. thesis, Christian-Albrechts-Universität, Kiel, Germany.
- Holloway, G. and T. Sau, 2002. Has arctic sea ice rapidly thinned? *J. Clim.*, **15**, 1691–1698.
- Hunke & Dukowicz (1997). An Elastic-Viscous-Plastic Model for Sea Ice Dynamics, *Journal of Physical Oceanography*, **27**, Pg. 1849-1867.
- Hunkins, K. (1962). "Waves on the Arctic Ocean." *J. Geophys. Res.* **67**(C?): 2477-2489.
- Hvidegaard, S. M. and R. Forsberg. Sea-ice thickness from airborne laser altimetry over the Arctic Ocean north of Greenland. *Geophys. Res. Letter*. Vol. 29n No. 20, pp. 1952, 2002.
- Hvidegaard, S. M. Airborne ice altimetry methods for calibration and validation of CryoSat results. Ph D thesis, Niels Bohr Institute, University of Copenhagen and Danish National Space Center, 2005.
- Hvidegaard, S. M., A. V. Olesen, R. Forsberg, and N. S. Dalå: *Airborne Lidar Measurements of Sea Ice Thickness North of Greenland 2005*. DNSC Technical Report, No. 3, 2006.
- Intergovernmental Panel on Climate Change (IPCC), 2001. *Climate Change 2000 – Third Assessment Report*, Cambridge University Press.
- Johannessen, O. M., M. W. Miles and E. Bjørge, 1995. The Arctic's shrinking sea ice, *Nature* **376**, 126–127.
- Johannessen, O. M., E. V. Shalina and M. W. Miles, 1999. Satellite evidence for an arctic sea ice cover in transformation, *Science* **286**, 1937–1939.
- Johannessen, O. M., L. Bengtsson, M. W. Miles, S. I. Kuzmina, V. A. Semenov, G. Alekseev, V. F. Zakharov, A. P. Nagurnyi, L. P. Bobylev, K. Hasselmann and H. Cattle, 2004. Arctic climate change – observed and modeled temperature and sea ice. *Tellus* **56A** 4, 328–341.
- Kauker, F., R. Gerdes, M. Karcher, C. Köberle and J. Lieser, 2003: Variability of Arctic and North Atlantic sea ice: A combined analysis of model results and observations from 1978 to 2001, *Journal of Geophysical Research*, **108** (C6), 3182, doi:10.1029/2002JC001573.
- Keller, K., S. M. Hvidegaard, R. Forsberg, N. S. Dalå, H. Skourup and L. Stenseng: *Airborne lidar and radar measurements over sea-ice and inland ice for CryoSat validation: CRYOVEX-2003 final report*. KMS Technical Report, No. 25, 58 pp., 2004.
- Kreyscher, M., 1998: *Dynamik des arktischen Meereises - Validierung verschiedener Rheologieansätze für die Anwendung in Klimamodellen*, Ph.D. thesis, Universität Bremen, Bremen, Germany, published by Alfred Wegener Institute: Berichte zur Polarforschung, **291**, 1998.
- Kreyscher (2000), Harder, Lemke, and Flato. Results from sea ice model inter-comparison project: Evaluation of sea ice rheology schemes for use in climate simulations, *J. Geophys. Res.*, **105**, C5), 11299 – 11320,
- Kwok, R. Annual cycles of multiyear sea ice coverage of the Arctic Ocean: 1999-2003. *J. Geophys. Res.* Vol. **109**, C11004, 2004.
- Laxon, S. W., Peacock, N. R. & Smith, D. M. High interannual variability of sea ice thickness in the Arctic region. *Nature*, doi:10.1038/nature2050, 947-950, 2003.
- Lensu, M., 2003: *The evolution of ridged ice fields*, Ph.D. thesis, Helsinki University of Technology, Espoo, Finland, M-280
- Maslanik, J. A. 1991. Effects of weather on the retrieval of sea ice concentration and ice type from passive microwave data. *Int. J. Remote Sens.*, **13**, 37–54.
- Maslanik, J., M. C. Serreze and R. G. Barry, 1996. Recent decreases in Arctic summer ice cover and linkages to atmospheric circulation anomalies. *Geophys. Res. Lett.*, **23**, 1677–1680.
- Maslanik, J. A., M. C. Serreze, and T. Agnew, 1999. On the record reduction in western Arctic sea-ice cover in 1998, *Geophys. Res. Lett.*, **26**, 1905–1908.
- McPhee, M. G., T. P. Stanton, J. H. Morison and D. G. Martinson, 1998. Freshening of the upper ocean in the Arctic: Is perennial sea ice disappearing? *Geophys. Res. Lett.*, **25**, 1729–1732.
- Menemenlis, D., *et al.* (1995). "A note on infragravity waves in the Arctic Ocean." *J. Geophys. Res.* **100**(C4): 7089-7093.

- Moore, S. C. and P. Wadhams (1981). Recent developments in strainmeter design. *Proc. Workshop on Sea Ice Field Measurement*, St. John's, 29 April - 1 May 1980 (eds. A. J. Allan, D. P. Bazeley). Memorial Univ. of Nfld., St. John's, 97-125.
- Moritz, R., C. M. Bitz and E. J. Steig, 2002. Dynamics of recent climate change in the Arctic. *Science*, 297, 1497–1502.
- Nagurny, A. P., *et al.* (1994). "A method for determination of effective sea ice thickness in the Arctic basin for climate monitoring." *Bull. Russian Acad. Sci., Phys./Suppl.* **58**: 168.
- Parkinson, C. L., D. J. Cavalieri, P. Gloersen, H. J. Zwally and J. C. Comiso, 1999. Spatial distribution of trends and seasonality in the hemispheric sea ice covers: 1978-1996, *J. Geophys. Res.* **104**, 20,827–20,856.
- Parkinson, C. and W. Washington, 1979: A large-scale numerical model of sea ice, *Journal of Geophysical Research*, **84** (C1).
- Peacock, N. R. & Laxon, S. W. Sea surface height determination in the Arctic Ocean from ERS altimetry. *Journal of Geophysical Research*, Vol. 109, No. C7, C07001 10.1029/2001JC001026, 2004.
- Rigor, I. G., J. M. Wallace and R. L. Colony, 2002. Response of sea ice to the Arctic Oscillation. *J. Clim.*, **15**, 2648–2663.
- Romanov, I.P.: "Atlas of Ice and Snow of the Arctic Basin and Siberian Shelf Seas". Edited by A. Tunik, Backbone Publ. Comp., 277 pp., 1995.
- Rothrock, D.A., Y.Yu and G.A. Maykut, 1999. Thinning of the Arctic sea-ice cover. *Geophys. Res. Lett.* **26**(23), 3469-72
- Serreze, M. C., J. A. Maslanik, T. A. Scambos, F. Fetterer, J. Stroeve, K. Knowles, C. Fowler, S. Drobot, R. G. Barry and T. M. Haran. 2003. Record minimum sea ice cover in the Arctic Ocean for summer 2002. *Geophys. Res. Lett.*, **30**, 1110–1113.
- Serreze, M. C., J. E. Walsh, F. S. Chapin, T. Osterkamp, M. Dyurgerov, V. Romanovsky, W. C. Oechel, J. Morison, T. Zhang and R. G. Barry, 2000. Observational evidence of recent changes in the northern high-latitude environment. *Clim. Change*, **46**, 159–207.
- Shalina, E. V., O. M. Johannessen and M. W. Miles, 1999. Arctic ice transformations: multiyear ice changes in comparison with summer minima. *Proc., International Geosciences and Remote Sensing Symposium, IGARSS99*, 28 June–2 July 1999, Hamburg, Germany, 2023–2026.
- Smith, D. M., 1998. Recent increase in the length of the melt season of perennial Arctic sea ice. *Geophys. Res. Lett.*, **25**, 655–658.
- Stroeve, J. C., M. C. Serreze, F. Fetterer, T. Arbetter, W. Meier, J. Maslanik and K. Knowles (2005): Tracking the Arctic's shrinking ice cover: another extreme September minimum in 2004. *Geophys. Res. Lett.* **32**, L04501, doi:10.1029/2004GL02810.
- Sandven, S., K. Kloster, H. Sagen and V. Alexandrov. CryoSat pre-launch cal-val studies of sea ice thickness. NERSC Tech. Report no. 257, September 2005, 47 pp.
- Squire, V. A. (1978). "An investigation into the use of strain rosettes for the measurement of propagating cyclic strains." *J. Glaciol.* **20**(83).
- Squire, V. A. and A. J. Allan (1978). Twillingate 1977 field report. Cambridge, Scott Polar Research Institute: 26.
- Steiner, N., 1998: *Nutzung der Meereisrauhigkeit zur Validierung und Optimierung eines großskaligen Meereismodells für die Arktis*, Ph.D. thesis, Christian-Albrechts-Universität, Kiel, Germany.
- Svendsen, E., K. Kloster, B. Farrelly, O. M. Johannessen, J. Johannessen, W. Campbell, P. Gloersen, D. Cavalieri and C. Matzler, 1983. Norwegian Remote Sensing Experiment: Evaluation of the Nimbus-7 SMMR for sea ice research, *J. Geophys. Res.*, **88**, 2781–2791
- Thompson, D. & J.M. Wallace, 1998. The Arctic Oscillation signature in the wintertime geopotential height and temperature fields. *Geophys. Res. Lett.*, **25**(9), 1297-1300
- Vinnikov, K. Ya., A. Robock, R. J. Stouffer, J. E. Walsh, C. L. Parkinson, D. J. Cavalieri, J. F. B. Mitchell, D. Garrett and V. F. Zakharov, 1999. Global warming and the northern hemisphere sea ice extent, *Science*, **286**, 1934–1937.
- Wadhams, P. 1990 Evidence for thinning of the Arctic ice cover north of Greenland. *Nature, Lond.*, **345**, 795-797.
- Wadhams, P. 1992. Sea ice thickness distribution in the Greenland Sea and Eurasian Basin, May 1987. *J. Geophys. Res.*, **97**, 5331-5348.
- Wadhams, P., 2000. *Ice in the Ocean*. Taylor and Francis, 368pp.
- Wadhams, P. and N.R. Davis, 2000. Further evidence of ice thinning in the Arctic Ocean. *Geophys. Res. Letters*, **27**(24), 3973-3976.
- Wadhams, P. and N.R. Davis, 2001. Arctic sea-ice morphological characteristics in summer 1996. *Ann.*

- 
- Glaciol.*, 33, 165-170.
- Wadhams, P., W.B. Tucker III, W.B. Krabill, R.N. Swift, J.C. Comiso, and N.R. Davis,. (1992), Relationship Between Sea Ice Freeboard and Draft in the Arctic Basin, and Implications for Ice Thickness monitoring, *J. Geophys. Res.*, 97, 20325-20334.
- Walsh, J. E. and H. J. Zwally, 1990. Multiyear sea ice in the Arctic: Model- and satellite-derived, *J. Geophys. Res.*, 95, 11,613–11,629.
- Warren, S. G., I. G. Rigor, N. Untersteiner, V. F. Radionov, N. N. Bryazgin and Y. I. Alexandrov. Snow depth on Arctic Sea Ice. *Jour. Climate*, Vol. 12, pp. 1814 – 11829, 1999
- Yu, Y., G.A. Maykut, and D.A. Rothrock, "Changes in the thickness distribution of Arctic sea ice between 1958-1970 and 1993-1997," *J. Geophys. Res.*, 109, 10.1029/2003JC001982, 2004.